Technical solutions for low-temperature heat emission in buildings

Abstract

The European Union is planning to greatly decrease energy consumption during the coming decades. The ultimate goal is to create sustainable communities that are energy neutral. One way of achieving this challenging goal may be to use efficient hydronic (water-based) heating systems supported by heat pumps.

The main objective of the research reported in this work was to improve the thermal performance of wall-mounted hydronic space heaters (radiators). By improving the thermal efficiency of the radiators, their operating temperatures can be lowered without decreasing their thermal outputs. This would significantly improve efficiency of the heat pumps, and thereby most probably also reduce the emissions of greenhouse gases. Thus, by improving the efficiency of radiators, energy sustainability of our society would also increase. The objective was also to investigate how much the temperature of the supply water to the radiators could be lowered without decreasing human thermal comfort.

Both numerical and analytical modeling was used to map and improve the thermal efficiency of the analyzed radiator system. Analyses have shown that it is possible to cover space heat losses at low outdoor temperatures with the proposed heating-ventilation systems using low-temperature supplies. The proposed systems were able to give the same heat output as conventional radiator systems but at considerably lower supply water temperature. Accordingly, the heat pump efficiency in the proposed systems was in the same proportion higher than in conventional radiator systems.

The human thermal comfort could also be maintained at acceptable level at low-temperature supplies with the proposed systems. In order to avoid possible draught discomfort in spaces served by these systems, it was suggested to direct the pre-heated ventilation air towards cold glazed areas. By doing so the draught discomfort could be efficiently neutralized.

Results presented in this work clearly highlight the advantage of forced convection and high temperature gradients inside and alongside radiators - especially for low-temperature supplies. Thus by a proper combination of incoming air supply and existing radiators a significant decrease in supply water temperature could be achieved without decreasing the thermal output from the system. This was confirmed in several studies in this work. It was also shown that existing radiator systems could successfully be combined with efficient air heaters. This would also allow a considerable reduction in supply water temperature without lowering the heat output of the systems. Thus, by employing the proposed methods, a significant improvement of thermal efficiency of existing radiator systems could be accomplished. A wider use of such combined systems in our society would reduce the distribution heat losses from district heating networks, improve heat pump efficiency and thereby most probably also lower carbon dioxide emissions.

Keywords: Analytical and numerical modeling, baseboard (skirting) heating, building energy performance, computational fluid dynamics (CFD), heat transfer, low-temperature heating, thermal comfort

Sammanfattning

Europeiska unionen planerar att kraftigt minska energiförbrukningen under de närmaste decennierna. Målet är att skapa hållbara samhällen som på nära sikt blir energineutrala. För att bidra till att uppnå detta utmanande mål föreslås här effektivta värmesystem (rumsvärmare) tillsammans med värmepumpar.

Huvudsyftet med forskningen och detta arbete var att förbättra termiska effektiviteten hos vattenburna rumsvärmare. Målet var att förbättra den befintliga värmöverföringen i rumsvärmarna så att lägre framledingstemperaturer kan användas. Detta resulterar i förbättrad värmefaktorn hos värmepumpar och även i minskat utsläpp av växthusgaser. Syftet var även att undersöka hur mycket framledningstemperaturen kunde sänkas utan att minska den upplevda termiska komforten.

Både numeriska och analytiska beräkningar har används i arbetet. Beräkningar och simuleringar har visat att det är fullt möjligt att täcka värmeförluster från byggnader med föreslagna lågtemperatursystem. Vidare framgår att föreslagna lågtemperatursystem kan avge samma värmeeffekt som konventionella radiatorsystem, men vid en betydligt lägre framledningstemperatur. Följaktligen blir värmefaktorn högre i motsvarande grad hos värmepumparna i föreslagna system.

Studier har även visat att termiska komforten är god trots lägre framledningstemperaturer. För att undvika eventuella dragproblem i rum föreslås att förvärmd tilluft riktas mot kalla glasytor. Detta neutraliserar effektivt eventuella dragproblem.

Resultat som presenteras i detta arbete belyser tydligt vikten av påtvingad konvektion och höga temperaturgradienter vid värmeöverföring. Stora insatser i detta arbete har därför lagts på att hitta metoder för att effektivt utnyttja detta. Resultaten visar att värmeavgivningen från radiatorer avsevärt förbättras genom en väl genomtänkt forcering av tilluften över radiatorytor. Det visas också att det är fullt möjligt att kombinera befintliga radiatorsystemen med effektiva luftvärmare. En betydlig sänkning av framledningstemperaturen kan även åstadkommas i denna kombination utan att värmeavgivningen från systemen minskar. Man kan av detta dra slutsatsen att termiska verkningsgraden avsevärt förbättras genom att använda förslagen lågtemperaturteknik jämfört med befintliga värmesystem.

Slutligen kan man också konstatera att en bredare användning av föreslagna värmesystemen i vårt samhälle skulle minska värmeförluster i fjärrvärmenät, förbättra värmefaktorn hos värmepumpar och därmed sannolikt också minska koldioxidutsläppen.

Acknowledgement

I wish first and foremost to thank my supervisor Professor Sture Holmberg for giving me the opportunity to be his student. I especially acknowledge his consistent confidence in me from the day I started my doctoral studies. And, of course, also for all the time and inspiration he has given me during our many spontaneous meetings. The major part of my research was founded by the Swedish Energy Agency (Energimyndigheten) and the Swedish Construction Development Fund (Svenska Byggbranschens Utvecklingsfond). Their financial support is gratefully acknowledged. I would like to thank Heather Robertson and Christina Hörnell for language correction and for improving my English. Their corrections and suggestions have not only improved my language, but also helped me to create new ways of writing and structuring my work. Special thanks go to my colleague Jonn Are Myhren for all discussions we have shared, especially in the beginning of my doctoral studies. His knowledge concerning heat transfer in buildings has greatly influenced me and contributed to the direction of my research. I want also to thank Armin Halilović for his utter willingness and preparedness to help me with mathematics whenever I needed. I would like to express my sincere gratitude to Stephan Pitsch and Sven Alenius for introducing me to CFD and for their help with my CFD modeling. My thanks go to Jan-Erik Nowacki for all his help in making me understand heat pump technology. Gratitude goes also to Shia-Hui Peng for his help with turbulence modeling and for all his explanations about this difficult area. I would also like to thank my colleagues at Fluid and Climate Technology, Arefeh Hesaraki and Sasan Sadrizadeh, for teamwork and many inspiring ideas. Especially Sasan for all the discussions we have had during working hours as well as during our daily walks toward our homes.

I particularly wish to thank my wife Aida for her patience and the encouragement she has given me during the whole of this demanding time. Her support has greatly helped me during the difficult periods. Many great thanks go to my parents and sister for the unreserved love, support and understanding they have given me for as long as I can remember. I also want to thank the rest of my extensive family for their support during all these years. Finally, I would like to express my deep gratitude to my dear cousin Ismar Karčić and friend Mustafa Šetkić who have helped me when I mostly needed.

Contents

List of papers

This doctoral thesis is a summary of the following papers, appended at the end of the text.

Paper 1 Ploskić A, Holmberg S. Heat emission from thermal skirting boards. Building and Environment 45 (2010) 1123-1133.

Paper 2 Ploskić A, Holmberg S. Low-temperature baseboard heaters with integrated air supply - An analytical and numerical investigation. Building and Environment 46 (2011) 176-186.

Paper 3 Ploskić A, Holmberg S. Low-temperature ventilation pre-heater in combination with conventional room heaters. Energy and Buildings 65 (2013) 248-259.

Paper 4 Ploskić A, Holmberg S. Performance evaluation of radiant baseboards (skirtings) for room heating - An analytical and experimental approach. Applied Thermal Engineering 62 (2014) 382-389

Paper 5 Holmberg S, Myhren J A, Ploskić A. Proceedings of International Conference Clima 2010. 10th Rehva World Congress on Sustainable Energy Use in Buildings, Antalya - Turkey 2010.

Paper 6 Ploskić A, Holmberg S. Heat emission from skirting boards - An analytical investigation. Proceedings of the 3rd International Conference on Built Environment and Public Health, EERB-BEPH 2009, Guilin - China 2009.

The work presented this doctoral thesis began in January 2008 and ended in November 2013. Professor Sture Holmberg has supervised all work reported in Papers 1-6.

Nomenclature

Latin letters

A	Heat transferring area	m^2
c_p	Specific heat capacity	J/(kg °C)
CO_2	Carbon dioxide	mass/unit time
COP	Coefficient of performance	-
Gr	$\equiv g \beta_{air} (\theta_{wall} - \theta_{room}) y^3 \upsilon_{air}^{-2}$, Grashof number	-
GSHP	Ground-source heat pump	-
g	Gravitational acceleration	m/s^2
H	Plate and radiator heights	m
HSPF	Heating seasonal performance factor	-
n	Number of plates	number
Nu	$\equiv \alpha_{air} y / \lambda_{air}$, Nusselt number	-
$\dot{m}$	Water mass flow	kg/s
P	Heat output / thermal power	W
Pr	$\equiv c_{p_{air}} \rho_{air} \upsilon_{air} \lambda_{air}^{-1}$, Prandtl number	-
Re	$\equiv v y \upsilon_{air}^{-1}$, Reynolds number	-
v	mean air velocity	m/s
x	Horizontal coordinate	m
y	Vertical coordinate	m

Greek letters

α	Heat transfer coefficient	$W/(m^2 °C)$
β	Thermal expansion	°C
Δ	Difference	°C
δ	Plate or layer thickness	m

$\Delta\theta$	Excess temperature = mean temperature difference between heater and surrounding air	°C
θ	Temperature	°C
λ	Thermal conductivity	W/(m °C)
υ	Kinematic viscosity	m^2/s
ρ	Density	kg/m^3

Subscripts

air	$\equiv (\theta_{wall} + \theta_{room})/2$, Air film temperature
conv.	Convection
eq	Equivalent
free	Free (convection)
forced	Forced (convection)
mixed	Mixed (convection)
layer	Layer (thermal boundary layer)
return	Return water temperature
room	Room temperature
supply	Supply water temperature
wall	Plate wall or radiator wall
water	Water

1. Introduction

The building sector stands for a large proportion of the energy usage and carbon dioxide (CO_2) emission in most countries. A usual estimation is that buildings consume about 20 to 40 % of primary energy, and are currently responsible for nearly 14 % of global CO_2 emissions [1, 2]. Presently the overwhelming majority of scientists believe that the prevailing Earth warming is unnatural, and can be attributed to the increased CO_2 emissions. The majority of scientists also believe that current climate changes are much more rapid and forced than the natural changes that took place before industrialization. Despite all appeals for reductions of the world-wide CO_2 emissions, the emissions have not yet started to decline. On the contrary, the global greenhouse gas emissions have increased by 75 % between 1970 and 2004 [3]. Even in Europe CO_2 emissions have continuously risen since 1990, reaching an all-time high in 2006 [4]. Since then, the emissions have declined. In order to create a more energy-sustainable society the governments of the European Union agreed to implement the so-called 20-20-20 plan in March 2007. Compared to levels in 1990 this means:

- 20 % reduction of greenhouse gas emissions,
- 20 % reduction of energy consumption through improved energy efficiency,
- 20 % increase of the renewable energy use by 2020.

Yet these targets should only be considered a first step toward a sustainable and low-carbon future. According to the Intergovernmental Panel on Climate Change (IPCC), the concentration of greenhouse gases in the atmosphere should not exceed 450 ppm CO_{2eq} to limit Earth warming to a maximum of 2 °C [4]. To achieve this, scientists believe that global CO_2 emissions need to be cut by 50 to 60 % by 2050. This requires a cut in industrialized countries by at least 80 % compared to 1990 levels [4]. In order to meet these challenges, investment in improvements in all sectors, including the building sector, is a must.

By 2009 residential buildings stood for 11 % of global CO_2 emissions and consumed nearly 27 % of the produced energy in European Union in 2010 [5, 6]. In the same year these buildings generated 6 % of global CO_2 emissions and were responsible for 14 % of world-wide energy consumption in 2012 [7, 8]. These facts clearly indicate that CO_2 emissions generated by residential buildings are connected to their energy consumption. Therefore, by increasing the energy efficiency of these buildings their CO_2 footprint can correspondingly be decreased. In order to meet some parts of the 20-20-20 targets in residential buildings:

- their thermal insulation should be improved,
- the efficiency of their heating, cooling and ventilation systems should be increased,
- usage of efficient heat pumps should be increased.

1.1 Potential of thermal insulation

Several studies from various countries with different climate conditions have shown that increased thermal insulation decreases the energy consumption of buildings [9-12]. An illustration of how additional wall insulation may decrease the annual energy consumption and specific heat loss of a building is given in Fig. 1. According to the figure an increase of

wall insulation from 3 to 30 cm would reduce the annual heating consumption by about 6.9 times. Although this is a large saving potential it should be remembered that this is only one of many possibilities.

According to recent statistics by the Swedish Energy Agency, an average Swedish single-family dwelling of 149 m^2 floor area consumed in total about 21.3 MWh of energy in 2011. Of this amount, approximately 4 MWh was used for household electricity [13], 3 MWh for domestic hot water (DHW) [14] and 14.3 MWh for heating [13]. This implies that transmission and ventilation heat losses stood for approximately two thirds of the total energy consumption. Eriksson[1] [15] and the Swedish Energy Agency[2] [16], respectively, found that the building envelope alone was responsible for 32 and 36 % of annual energy use in an average Swedish single-family dwelling built between 1940 and 1989. This implies that about one third of the energy use in these building types could be saved by improving thermal insulation of the envelope.

It should be noted that proportions of different energy needs vary greatly from one household to another. The amount of consumed electricity and hot water is strongly influenced by the habits and the number of persons living in the building. The distribution between transmission and ventilation heat losses is highly controlled by the thermal properties of the building and its ventilation system. Thus, the presented percentages in Fig. 2 should only be viewed as general guideline values. Nevertheless, the figure demonstrates a typical distribution between different energy needs for an average Swedish single-family dwelling built in the second half of the 20th century.

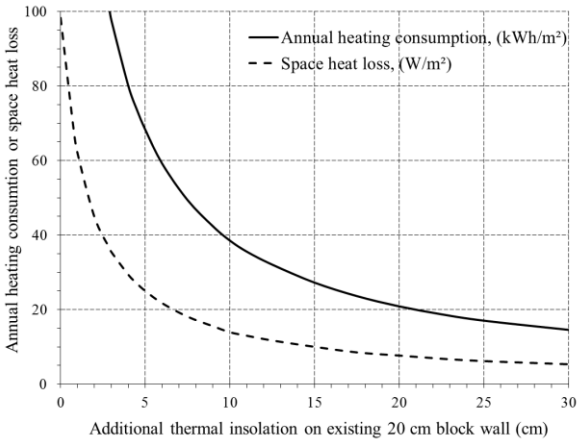

Fig. 1. The decrease of annual heating consumption and specific heat loss per square meter floor area as function of increased wall insulation are shown [12].

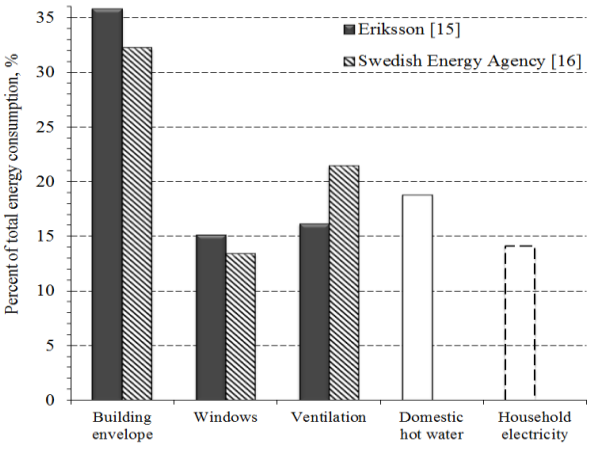

Fig. 2. The shares of the energy needs for an average Swedish single-family dwelling built in the second half of the 20th century. The needs for domestic hot water and household electricity were adopted from [14] and [13], respectively.

[1] Average heat losses from single-family dwellings built between 1940 and 1980.
[2] Average heat losses from a single-family dwelling built in 1970.

1.2 Potential of heat pumps

Unlike transmission heat losses that can be reduced by static measures such as improved thermal insulation, the thermal needs of domestic hot water and air supply must be met by an active heat supply. One method for meeting these needs is to use sustainable energy supplies by means of efficient heat pumps. A heat pump is a heat engine that moves free heat from a cold reservoir (heat source) to a reservoir of higher temperature such as domestic hot water and/or heating system (heat sink). To perform this refining process, additional mechanical work must be supplied to the system. This additional work is often done by a compressor which usually is driven by electricity. The heat source can be of various types. The free heat stored in the ground, rock, groundwater, lakes, rivers and outdoor air can be effectively extracted by heat pumps and converted to useful heat. The heat from exhaust air and waste heat can also be recovered by heat pumps. Due to these possibilities heat pumps can be/are used as heat-supplying system in buildings. A simple sketch showing components and flowchart of a ground source heat pump connected to domestic hot water and heating system is given by Fig. 3.

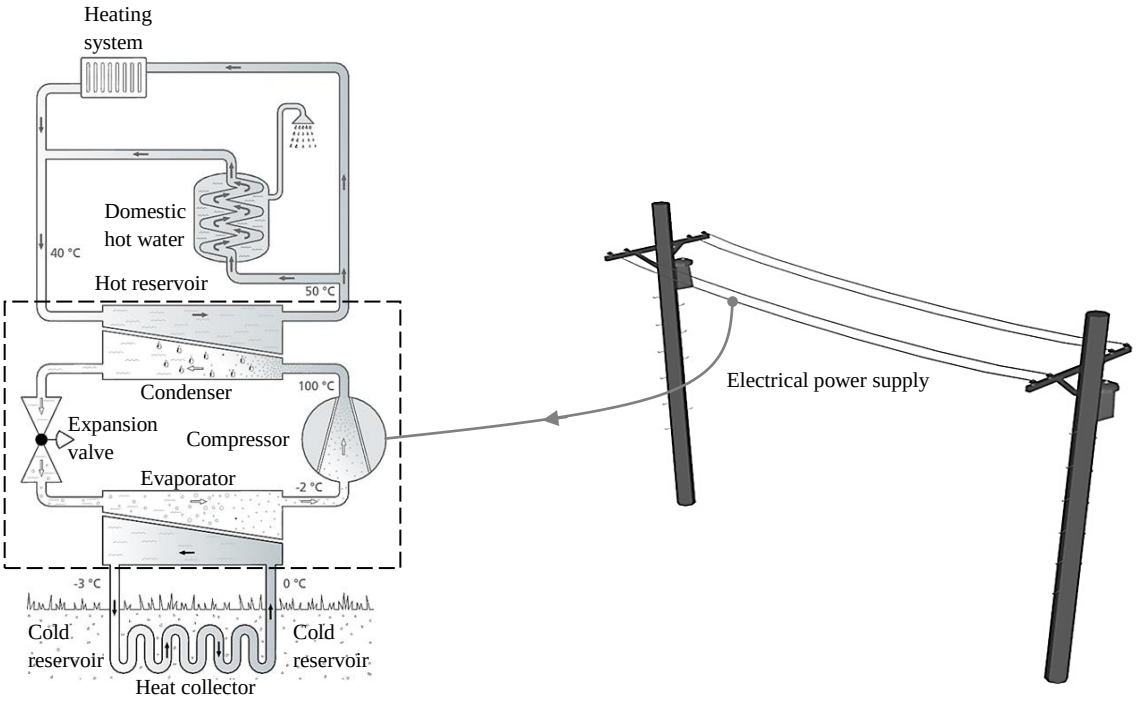

Fig. 3. The sketch and flowchart of a ground source heat pump (GSHP) with working temperatures. The dashed lines show the boundaries of the heat pump.

The efficiency of the heat pump is manly affected by the temperatures of the cold and the hot reservoirs. The higher the temperature of the cold reservoir and the lower the temperature of the hot reservoir the less the compressor work needed, and thereby the higher the heat pump efficiency. The efficiency of a heat pump is defined by the ratio between the useful heat energy produced and the energy consumed by the compressor. This ratio is known as the Coefficient of Performance (COP) of a heat pump. The higher the COP the higher the efficiency. Thus, a common goal of current researchers and operating engineers is to find methods to increase the COP value of heat pumps.

Different types of heat pumps have different COP levels. Currently COPs are ranging from 2 to 4.5. This means that heat pumps are able to generate 2-4.5 kWh heat from 1 kWh of electricity. This makes heat pumps more environmentally friendly than most traditional heating options. Of course, this also largely depends on the cleanness of the consumed electricity. Heat pumps are commonly designed to cover 50 to 90 % of annual heat demand in residential buildings. They alone, however, are often incapable of overcoming the heating peak loads during the coldest days. In these situations an auxiliary heat source is often needed. It should also be remembered that the COP value varies during a heating season. The value is highly dependent on building heat demand, which may oscillate greatly from day to day. Therefore a Heating Seasonal Performance Factor (HSPF), which is an average COP value taken over the whole heating season, is usually used to rate the system performance.

1.2.1 Heat pumps in Europe and Sweden

The installation of heat pumps in Europe has increased greatly during the last two decades. Since the beginning of 1980s, Sweden and Switzerland were leading in using this technology for heating. However, some other countries like Austria, Germany and France have lately also shown a rapid increase in the number of installed units (Fig. 4) [17]. The International Energy Agency Heat Pump Centre have found that if 80 % of the households in the OECD (Organisation for Economic Co-operation and Development) countries replaced their oil boilers with heat pumps of HSPF = 4, approximately 2.4 Tkg CO_2 emissions could be saved. This would reduce the global CO_2 emission by nearly 10 % annually [18]. Also, according to a recent report by the Swedish National Board of Housing, Building and Planning, the CO_2 emissions from a single-family dwelling could be considerably reduced if the dwelling were served by a heat pump of HSPF = 4 [19], as shown by Fig. 5. The question is; how to achieve a HSPF value of 4?

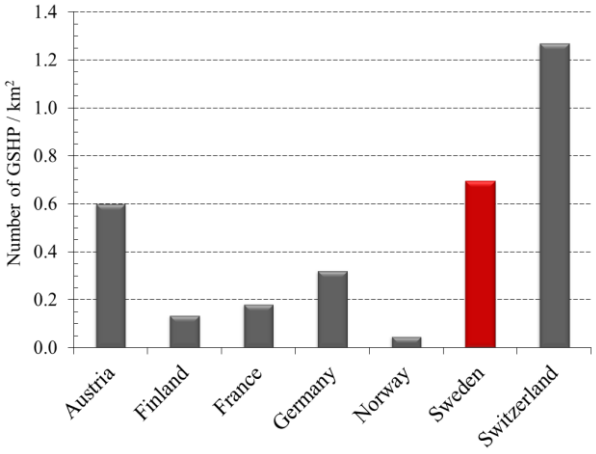

Fig. 4. The number of installed ground source heat pumps per square kilometer land area in some European countries in 2007 [17].

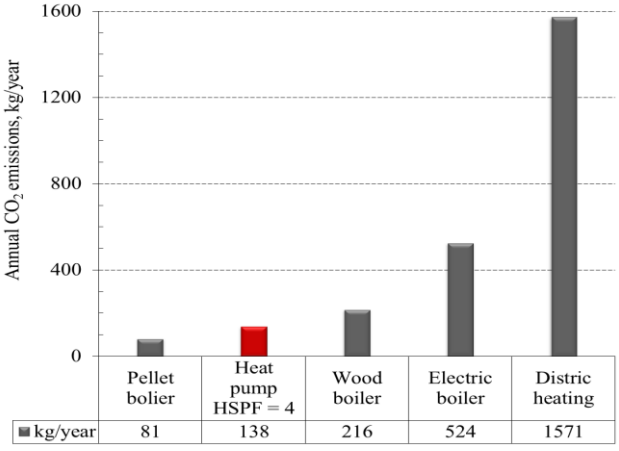

Fig. 5. The CO_2 emissions[3] from five heating options currently used in Swedish single-family dwellings [19].

[3]The CO_2 emissions from district heating and for electricity generation were based on the average Swedish fuel mix in 2008. The emission from a heat pump was recalculated to apply for HSPF = 4, instead of 2.5. The original emissions were also based on a total annual heat need of 20 MWh. These were reduced by factor 1.16 to apply for a need of 17.3 MWh/year according to [13, 14].

According to Table 1, a supply water temperature of approximately 40 °C is needed to achieve a HSPF value of about 4 for a ground source heat pump installed in an average Swedish family house. The table also shows that water supplies of lower temperatures generate higher HSPF values and lower CO_2 emission rates. This implies that low-temperature heating systems are both energy efficient and environmentally friendly options. More detailed explanations what is meant by a low-temperature heating system will be given in the following section.

Table 1. The variation of HSPF values for a ground-source heat pump at different supply and return water temperatures. The pump serves a single-family dwelling with a time constant of 72 h, placed in the central part of the Sweden. The temperature change of refrigerant in the vertical heat collector was set to 3 °C. The calculations were performed using the commercial code Vitocalc [20].

Total energy and power need		**Temperatures**					**Efficiency and sustainability**	
Heat demand	Heat pump power	Design outdoor	Annual outdoor	Indoor	Supply water	Return water	HSPF value	CO_2 emission
[4]MWh/year	[5]kW	°C	°C	°C	°C	°C	–	[6]kg/year
17.3	6.8	-16	6.6	20	75	65	2.0	262
17.3	6.8	-16	6.6	20	55	45	3.1	169
17.3	6.8	-16	6.6	20	45	35	3.5	142
17.3	6.8	-16	6.6	20	35	25	4.1	128

1.3 Current classification of hydronic heating systems

The total heat output from a hydronic heating system is mainly controlled by three parameters. Namely by operating water flow, size of room heaters and temperature difference between the room heaters and surrounding air. It should also be noted that the surface temperature of the room heaters is controlled by supply and return temperatures and operating water flow. Since the size of the room heaters is constant, their heat output can either be controlled by the flow or the temperature control. Accordingly, the hydronics can be divided into two sub-systems according to their operating conditions as shown in Table 2.

Table 2. Subdivision of current hydronic systems with corresponding water flows and temperature drops. The approximate operating conditions for four hydronic systems are given, i.e. low-flow, high-temperature, high-flow and low-temperature systems.

	Water flow through room heaters	**Temperature drop across room heaters**
Hydronic system	kg/s (l/h)	°C
Low-flow ≈ high-temperature	≈ 0.011-0.004 (41-15)	≈ 15-40
High-flow ≈ low-temperature	≈ 0.034-0.017 (124-61)	≈ 5-10

The low-flow systems are presently characterized by high supply water temperatures and large temperature drops across room heaters. Due to this the low-flow systems are also

[4] Total annual heat demand according to [13, 14]. The heating need = 14.3 MWh. The domestic hot water need = 3 MWh.
[5] Also, design heat power need of the selected single-family dwelling at an outdoor temperature of -16 °C.
[6] The CO_2 emission was adopted from [19], and was recalculated to apply for different HSPF values.

commonly high-temperature systems. On the contrary, in high-flow systems the supply water temperatures and temperature drops are considerably lower. The high-flow systems are thus also commonly low-temperature systems. This, however, must not always be the case. For example, in buildings with low-to-moderate heating demands the hydronic systems can simultaneously operate in both low-flow and low-temperature regime. Therefore, although common, the subdivision given in Table 2 is not strict.

Approximately in the middle of the 20th century, the process of switching from what was then considered high-temperature systems (130/60/20 °C, 120/100/20 °C)[7] to then considered low-temperature system (90/70/20 °C) started in Europe [21, 22]. As heating demands of the European buildings have constantly decreased since the 1950s, the old 90/70 system was replaced by new 75/65 system in 1997 [23]. Also in Sweden the old high-temperature 80/60 system was replaced by new low-temperature 55/45 system in 1980 [24]. Since this system has been the Swedish standard for more than two decades, Fahlén [25] proposed classifying it as a medium-temperature system in 2003. He recommended the following classification:

- high-temperature system for supply temperatures > 55 °C
- medium-temperature system for 45 °C < supply temperatures < 55 °C
- low-temperature system for supply temperatures < 45 °C

A somewhat more detailed classification was also proposed by Boerstra et al. [26] in 2001, as shown in Table 3.

Table 3. Classification of hydronic systems according to Boerstra et al. [26].

	Water temperatures	
Hydronic system	Supply/°C	Return/°C
High-temperature	90	70
Medium-temperature	55	40-35
Low-temperature	45	35-25
Very low-temperature	35	25

In conclusion, it is obvious that system classification of hydronics is arbitrary and has been constantly changing with time. In this work the hydronic system that could cover a given space heat loss with supply water temperatures ≤ 45 °C has been regarded as a low-temperature system, which is in line with both recommendations described above.

1.4 Motivation for research work

By 2007, single-family dwellings stood for about 45 % of the total heated area in Sweden [27]. Of these 1.91 million building units around 25 % were heated by electric hydronic systems in 2011 [13]. In this share both air-to-water and exhaust-air heat pumps are included. In addition to these 25 %, an additional 11.5 % were served by closed-loop heat pump systems [13]. This implies that approximately 36.5 % (= 697 880) of the country's single-family dwellings were served by different types of hydronic systems supported by heat pumps

[7] Supply/return/room temperature.

at the time. Due to this, many studies during the recent past have been made to rate and increase HSPF values of the heat pumps in Sweden.

SP Technical Research Institute of Sweden has measured HSPF values of entire systems in five single-family houses served by ground source heat pumps and hot-water radiators[8] [28]. It was found that all five HSPFs were in close agreement, having an average value of 2.6 ± 0.3[9]. In her doctoral thesis Kjellsson [29] showed that HSPF value of a ground source heat pump could increase by 7.5 %[10] by doubling the depth of borehole. She also showed that an additional increase of about 3 % could be achieved by combining the heat pump with a solar collector of 10 m^2. Moreover, according to a recent report by Swedish Energy Agency the HSPF values of heat pumps in Sweden have increased by approximately 2 % annually between 1995 and 2009 [30]. This was mainly a result of long-term, continuous and goal-oriented research on heat pump technology in the country.

Facts presented in this section and in section 1.2 suggest that heat pumps have a large saving potential in Sweden, as the number of the installed units is quite large. Also, until now the research and development was mostly focused on the cold side of the heat pumps and improvement of their components. Data presented in sections 1.2 and 1.3 also show that supply temperatures in hydronic systems supported by heat pumps must be much lower than currently required by prevailing norms in order to achieve high HSPF values. According to Table 1, about 32 % of annual CO_2 emissions from a single-family dwelling could be saved if supply temperature were to be reduced from 55 to 35 °C. Accordingly, approximately 19 Mkg of annual Swedish CO_2 emissions would be cut if every fourth single-family house would switch from a 55/45 to a 35/25 system. This would reduce the total CO_{2eq} emissions from the country's housing stock by nearly 1.5 % [31].

1.5 Research objectives

Methods for increasing the heat outputs from different types of hydronic room heaters has therefore been a main objective of research at KTH Royal Institute of Technology at the Division of Fluid and Climate Technology between 2006 and 2013.

This research work is part of that endeavor. The main focus of this work was directed towards finding methods to improve the thermal efficiency of low-temperature radiators. The goal was to lay the ground for robust and efficient radiator systems capable of operating with low-temperature water supplies without compromising the perceived thermal comfort. From an engineering point of view there is a need for design requirements for such systems.

[8] Here, as in the rest of this work, radiators mean vertical wall-mounted heat-emitters used for space heating in a room.
[9] The houses were built between 1955 and 1970. The installed nominal power of the heat pumps ranged from 6.6 to 11 kW, and the deepness of boreholes varied from 92 to 170 m with an average depth of 140 m.
[10] Calculation was based on: total heat need of 29.4 MWh/year, a heat pump power of 7 kW and borehole depth increase from 80 to 160 m.

1.6 Hypothesis

"By decreasing the height and increasing the length of the radiators, their thermal efficiency can be increased. By forcing the supply air to pass through room heaters, the supply temperature to heaters can be decreased without decreasing their heat outputs. These two actions will lead to improved system efficiency without compromising the perceived thermal comfort".

2. Methods

To test the hypothesis two main methods have been applied - numerical and analytical calculations. The numerical calculations were performed using Computational Fluid Dynamics (CFD) commercial tools, and analytical calculations were performed using well-known mathematical and semi-empirical relations. It should be noted that in each paper the used methods were described in detail. In addition to that a relevant literature review was also given in each paper. Therefore, in following sections only a brief presentation of the main methods used will be given. Beside that, a short theoretical background regarding the systems investigated in this work is also given in the following section.

2.1 Theoretical background

In this section a brief review of mechanisms that control heat transfer from wall-mounted radiators is given. The goal here is not to repeat the well-known theories regarding heat transfer from vertical heaters. The goal is rather to present the most relevant parts of these theories to explain reasons for the research work reported in this thesis, and to partly support the hypothesis.

As mentioned earlier, the total heat output from a hydronic room heater is mainly controlled by three parameters: operating water flow, size of heater and temperature difference between heater and surrounding air. The joint influence of these three parameters is normally summarized by a global energy balance as illustrated by Eq. 1.

$$P = \dot{m}\, c_p\, (\theta_{supply} - \theta_{return}) = \overbrace{\left(\alpha_{water}^{-1} + \sum_{i=1}^{n} \delta_i \lambda_i^{-1} + \alpha_{air}^{-1} \right)^{-1}}^{\text{U-value of room heater}} A \overbrace{\frac{\theta_{supply} - \theta_{return}}{\ln\left[(\theta_{supply} - \theta_{room}) / (\theta_{return} - \theta_{room}) \right]}}^{\Delta\theta = \text{excess temperature}} \qquad (1)$$

Typically in water-to-air heat exchangers, the water-side heat transfer coefficient α_{water} is of the order of several thousand, and the thermal conductivity λ of the metal plates ranges from several tens to hundreds. In addition, the thicknesses of the plates δ are also often less than 1 mm. As the inverse of large numbers is small, the $\alpha_{water}^{-1} + \sum_{i=1}^{n} \delta_i \lambda_i^{-1}$ part usually ranges from about 10^{-3} to approximately 10^{-4} and can thus be neglected without significantly decreasing the calculation accuracy. Accordingly, the total heat transfer rate is therefore mainly controlled by the α_{air} value, as this parameter is the smallest in the series. For simplicity in coming explanations, the logarithmic excess temperature $\Delta\theta$ is also here approximated as

$(\theta_{wall} - \theta_{room})$. θ_{wall} represents the mean temperature of all heat-emitting walls of the radiator, and θ_{room} stands for the surrounding (room) air temperature adjacent to all heat-emitting surfaces. By doing so Eq. 1 can then be reduced to a more manageable expression as illustrated by Eq. 1*.

$$P = \dot{m}\, c_p\, (\theta_{supply} - \theta_{return}) \cong \alpha_{air}\, A\, (\theta_{wall} - \theta_{room}) \qquad (1^*)$$

The left part of Eq. 1 and Eq. 1* is known as a steady-flow energy equation and shows the enthalpy change of a given system, in this case a radiator. The right part of Eq. 1* is known as Newton's Law of Cooling and refers to the ability of a system to exchange heat with its surrounding. It should also be noted that the heat transfer coefficient α_{air} consists of two parts, a convective $\alpha_{conv.}$ and a radiative part α_{rad}. Since the radiative part (coefficient) is approximately constant (≈ 6.0-5.4 W/m^2·°C) for supply temperatures 55-35 °C, focus in this section is directed on the convective part as this part varies strongly in this temperature range.

According to Eq. 1 and Eq. 1* the heat output P can be incased by increasing the water mass flow $\dot{m}$. In practice, when $\dot{m}$ increases the temperature difference $(\theta_{supply} - \theta_{return})$ across the radiator correspondingly decreases. Therefore by increasing $\dot{m}$, the mean wall temperature of the radiator $\overline{\theta}_{wall}$ will also increase. This will generate a higher $\alpha_{conv.}$ value and thereby a higher heat output, as $\alpha_{conv.}$ is proportional to $(\theta_{wall} - \theta_{room})$ in natural (free) convection.

This enhancing method, however, is not very energy efficient. As shown in Paper 4, a doubling of the mass flow through a baseboard radiator would increase its heat output by approximately 4.5 %. Donjerković [32] has also found that the output from a water-to-air heater would be increased by 10 % by tripling the mass flow. Since for internal turbulent flows the hydraulic power loss is proportional to $\dot{m}^3$, it is obvious that heat transfer enhancement by a large increase of mass flow is inefficient. The methods for improvements must therefore be sought elsewhere.

2.2 Convective heat transfer from a vertical hot plate

In Fig. 6a, typical air movement behavior around a heat-emitting two-panel radiator is shown. As can be seen, the temperature and velocity distribution across the adjacent layers is identical in all there parts. Due to this symmetry the illustrated radiator can be approximated by a hot vertical plate, as shown by Fig. 6b.

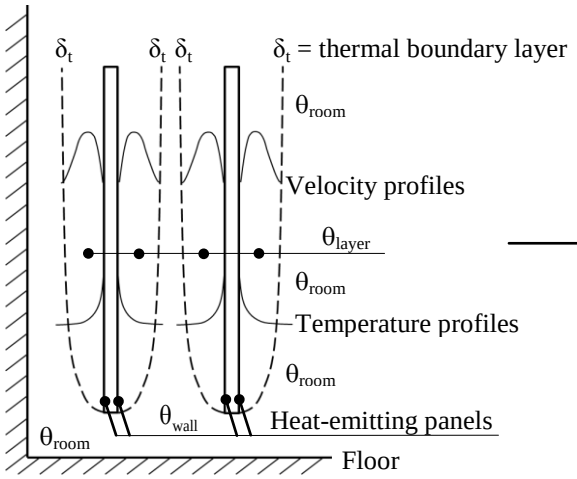

Fig. 6a. A sketch of propagation of thermal boundary layers, velocity and temperature changes along four sides of a two-panel radiator.

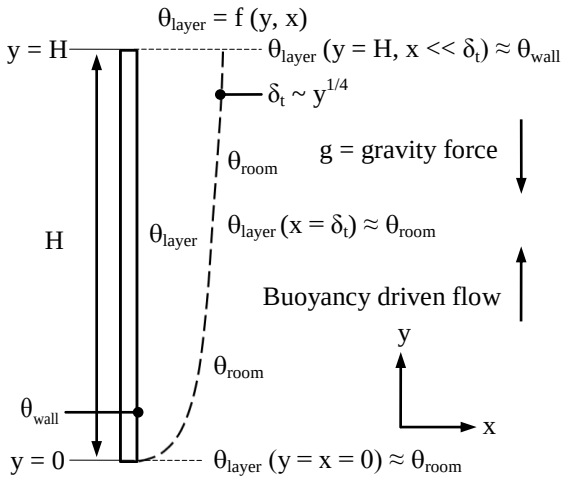

Fig. 6b. A sketch of the thermal boundary layer alongside a hot vertical wall together with associated temperatures and governing forces.

At the very moment the wall temperature of a plate is higher than that of the surrounding air, a thin air film next to the entire plate height is established. This film is the thermal boundary layer and it is normally only a few millimeters thick. Despite its relatively low thickness it plays a vital role for the convective heat transfer - especially in free convection. This is mainly due to the thermal property of the layer, i.e. air. Owing to its relatively low thermal conductivity, the temperature drop across the adjacent layer is steep. This implies that the thermal boundary layer behaves like an invisible insulating air film, blocking the heat transfer to surrounding air. Therefore by reducing the height and/or thickness of a thermal boundary layer, a higher convective heat flow to the surrounding air can be achieved.

The characteristics of a thermal boundary layer vary along a hot wall, and are mostly determined by its height and wall-to-air temperature difference. For $(\theta_{wall} - \theta_{room}) = 50$ °C, the transition from laminar-to-turbulent layer is likely to start at a height of 0.67 m [33]. Thus, in this section, the maximum plate height was set to 0.6 m, in order to stay within the laminar regime. It should also be stressed that the heights of most current conventional radiators are lower or around 0.6 m. This reference height is thereby also reasonable from an engineering point of view.

From Fig. 6a and 6b, it can be observed that boundary layer thickness grows rapidly alongside a hot vertical wall. It can also be noticed that the thickness at the starting edge is much smaller compared to the upper edge. As a result this, the layer temperature θ_{layer} at the starting edge ($y = 0$) is close to room temperature θ_{room}, i.e. $\theta_{layer} \approx \theta_{room}$. Consequently the convective heat transfer at the lower part of the plate is high, since $(\theta_{wall} - \theta_{layer}) \approx (\theta_{wall} - \theta_{room})$ and $\theta_{wall} > \theta_{room}$. On the other hand at the upper edge at $y = H$ and for $x << \delta_t$, the layer

temperature is close to the wall temperature θ_{wall}, i.e. $\theta_{layer} \approx \theta_{wall}$. Accordingly, the convective heat transfer in upper the part of the plate is quite low as the temperature difference between the wall and the surrounding air is small. This shows that the $\alpha_{conv.}$ value varies strongly alongside a hot vertical wall, and follows the change of air temperature inside the thermal boundary layer.

2.2.1 Free, mixed and forced convection

In Fig. 7a, the variation of the free convective heat transfer coefficient $\alpha_{free,\ conv.}$ along a 0.6 m high hot vertical wall is shown. The graphs in the figure were constructed using the well-known Nusselt relation for laminar free convection, i.e. Eq. 2 [34].

$$Nu_{y,\ free} = \frac{\alpha_{free\ conv.}\ y}{\lambda_{air}} = 0.68 + \frac{0.67 \cdot (Gr_y Pr)^{1/4}}{\left[1+(0.492/Pr)^{9/16}\right]^{4/9}} \qquad Gr_y < 10^9,\ 10^{-3} \leq Pr \leq 10^3 \qquad (2)$$

The graphs show that the $\alpha_{free,\ conv.}$ value declines exponentially up to about y/H = 0.35, independently of excess temperature. After that the decline is constant and approaches an asymptotic value. The drop of the $\alpha_{free,\ conv.}$ value is also considerably lower for a reduction of excess temperature from 50 to 30 °C, compared with reduction from 30 to 10 °C. This demonstrates that the heating power from free convection at low-temperature supply is much weaker compared to medium and high-temperature supplies. This explains why low-temperature radiators at standard operating conditions are not as powerful as medium and high-temperature radiators. Data in Fig. 7a also suggest that radiators should be low and long in order to have a high thermal efficiency. This finding partly supports the first part of the hypothesis of this work.

In Fig. 7b the effect of a forced airflow of 0.2 m/s on convection rate is shown. The plots were created using Nusselt relations for laminar forced and mixed convection, as shown by Eqs. 3 and 4 [35].

$$Nu_{y,\ forced} = \frac{\alpha_{forced\ conv.}\ y}{\lambda_{air}} = 0.664 \cdot Re_y^{1/2}\ Pr^{1/3} \qquad Re_y < 5 \cdot 10^5,\ Pr > 0.6 \qquad (3)$$

$$Nu_{y,\ mixed} = \frac{\alpha_{mixed\ conv.}\ y}{\lambda_{air}}\ \left(Nu_{y,\ free}^3 + Nu_{y,\ forced}^3\right)^{1/3} \qquad (4)$$

The criteria for forced, mixed and natural convection were determined by generally accepted Gr_y-to-Re_y ratios as follows:

- $\frac{Gr_y}{Re_y^2} \ll 1$ forced convection
- $1 \approx \frac{Gr_y}{Re_y^2} < 10$ mixed convection

- $\frac{Gr_y}{Re_y^2} \geq 10$ free convection

It was observed that for an excess temperature of 10 °C forced convection dominated up to y/H ≈ 0.08, and mixed convection for the rest of the plate. At an excess temperature of 30 °C, the mixed convection started to dominated from y/H ≈ 0.03, and a strong presence of natural convection was only observed at the y = H. It was also noted that the heat transfer coefficient in mixed convection is noticeably higher than in both natural and forced convection. It therefore seems reasonable to utilize this potential, and create the right conditions for radiators to operate within this mode.

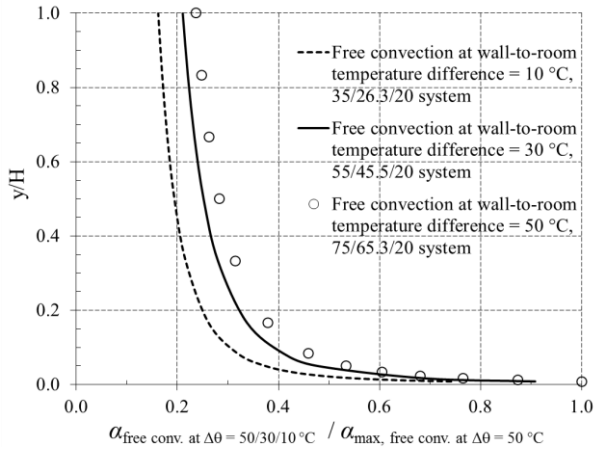

Fig. 7a. Variation of the laminar free convective heat transfer coefficient along a hot vertical wall for excess temperatures of 10, 30 and 50 °C is shown. The values on the x-axis were normalized with maximum $\alpha_{free,\ conv.}$ value at Δθ = 50 °C and y/H ≈ 0.01.

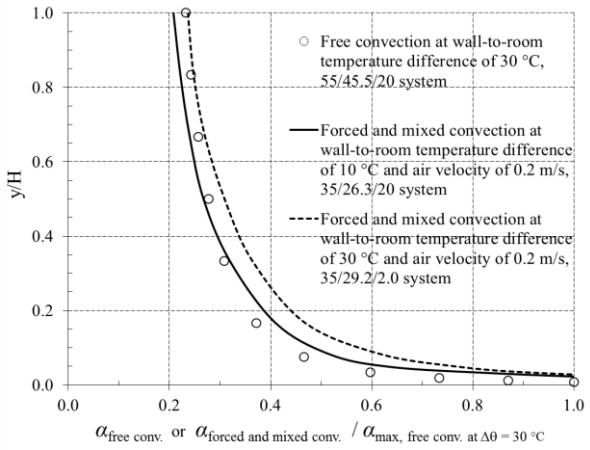

Fig. 7b. Variation of laminar free, forced and mixed convective heat transfer coefficients along a hot vertical wall for excess temperatures 10 and 30 °C is shown. The values on the x-axis were normalized with maximum $\alpha_{free,\ conv.}$ value at Δθ = 30 °C and y/H ≈ 0.01.

The plots in Fig. 7b suggest that the excess temperature could be lowered from 30 to 10 °C without decreasing the $\alpha_{conv.}$ value, by using a forced airflow of 0.2 m/s. The $\alpha_{conv.}$ value could be additionally enhanced by about 13 % if temperature difference (gradient) would be increased from 20 to 2 °C. This means that by a proper combination of existing radiator systems with add-on fans and/or cold supply air, the supply water temperature to the radiators could be decreased from 55 to 35 °C without decreasing their thermal power. Having this in mind, it becomes more understandable why Myhren and Holmberg [36, 37] have found that a forced airflow of 7 l/s through a double-panel radiator would increase its output twice. Similarly, Johansson and Wollerstrand [38] have also found that add-on fans of 3 W would enable lowering of the supply water temperature from 55 to 45 °C without reducing the heat output from a single-panel and column radiator.

The results presented in this section together with previous findings by others clearly demonstrate the potential of forced airflow through and alongside radiators. It seems that to additionally decrease the supply water temperatures in radiator systems the advantage of forced convection and high thermal gradients should be utilized. It is obvious that large improvements in convective heat transfer could be gained by relatively low air speeds of low

entering temperatures. This is especially favorable for Nordic countries where temperature differences between outdoors and indoors are large, and where the heating need is the dominant part of energy consumption in buildings. The results presented in Fig. 7b also partly support the second part of the hypothesis of this research work. Thus the goal of this work was also to give some practical design requirements for radiator systems in order to utilize the above-presented potentials.

2.3 Computational Fluid Dynamics

The results presented in Papers 1-3 were mainly obtained using Computational Fluid Dynamics (CFD). CFD in Papers 1-3 was used to analyze fluid movement and heat transfer inside considered domains. CFD in general can be used for simulation of both internal and external flows, in two or three dimensions. The simulations can be performed in transient of steady-state regime. In this work the CFD was used to analyze internal airflows together with heat transfer predictions. In all three studies the air and the thermal flows were simulated at steady-state. The comprehensive possibility to visualize simulation results was utilized to adjust the geometry and other design parameters to achieve the most favorable solution in all three studies. In general, the results in CFD are obtained by numerical solutions of Navier-Stokes equations including the continuity and energy equations. The turbulence is currently predicted by various turbulence models, available in CFD codes. In Papers 1-3 the turbulence was predicted by the Re-Normalization Group (RNG) k-ϵ turbulence model. This model is a further development of the standard k-ϵ model, and it has improved ability to account for the effects of smaller scales of fluid motion. Therefore this model is also suitable for simulations of airflows in indoor environments. The discretization of governing equations can be handled by finite-volume or finite-element based solvers. CFD codes used in this work had finite-volume based solvers. The solvers also solved the governing equations in their time-averaged and conservative form.

It was decided not to present the mathematical equations for continuity, momentum, energy and turbulence model here - as these equations are presently well-known and available in most handbooks of fluid mechanics. For readers interested in becoming familiar with the derivation of these governing equations it is suggested to consult the recent book by Tu et al. [39]. An example of the distribution of the unstructured and structured volume elements used in Paper 3 is shown in Fig. 8.

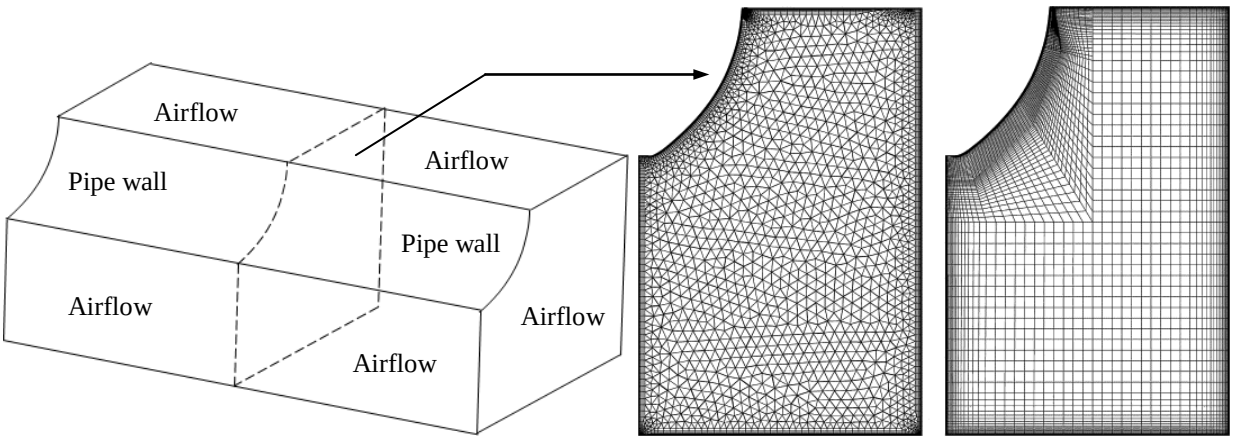

Fig. 8. At left a sketch of the computational domain around a pipe wall surrounded by an airflow is shown (Paper 3). The vertical and horizontal distribution of the unstructured and structured volume elements is shown in the middle and at the right, respectively.

Simulations in Papers 1-2 were performed using commercial CFD-codes Gambit and Fluent 6.3 while in Paper 3 the code Ansys 13 was used. Gambit is a pre-processing tool and was used for geometry and computational grid (mesh) generation. After geometry and mesh were constructed, the mesh file was manually imported to Fluent 6.3. In Fluent 6.3 the boundary conditions were specified and the governing equations solved. After obtaining convergence, solution results were post-processed either by Fluent 6.3 or by some other data-handling code. In Ansys 13, unlike in Gambit and Fluent 6.3, the pre, processing and post-processing were included in same code.

Although CFD simulations have a large design potential the proper selection of numerical methods, turbulence model and boundary conditions play a decisive role for correct of results. By numerical methods is here meant quality of mesh generation, selection of near-wall treatment, pressure-velocity coupling and order of discretization scheme. The correct selection of these parameters is not always obvious. On the other hand, an incorrect employment of the parameters can lead to large errors in simulation results. Therefore it is always desirable to validate CFD results with experimental data or analytical calculations. This helps the CFD user to estimate the reliability of simulation results.

2.3.1 Validation work

A large effort was put on validation work in Papers 1-3. The main focus of the validation work in these papers was to ensure the ability of CFD codes and the user to correctly predict air movement and heat transfer. A key publication used as guideline in this process was “How to Verify, Validate and Report Indoor Environment Modelling CFD Analyses” by Chen and Srebrić [40]. Here a detailed validation procedure, including the judgment of CFD results, was presented in several steps. The same validation modus was also applied in this work.

A room model previously used by Omori et al. [41, 42] was used for validation in Paper 1. The room geometries and boundary conditions reported by Omori et al. were reproduced in detail by Gambit and Fluent 6.3. The obtained CFD results were then compared with both numerical and experimental findings reported by the above-mentioned authors. In addition to this, the CFD-predicted mean room and inner glazing temperatures were also matched with those analytically calculated. Detailed results of the validation work in Paper 1 can be found in Fig. 4a-4d and Table 5 in the same article.

In Paper 2 well-known semi-empirical relations were used to validate results obtain by CFD simulations. The objective of the validation work was to determine which model most accurately predicted convective heat transfer inside a narrow heat-emitting channel. This model was then used to represent the heat variation along the channel, and to demonstrate the required channel surface temperatures to pre-heat different supply airflow rates to room temperature. The results of the validation work were summarized in Fig. 2a-2d in Paper 2.

Also in Paper 3 semi-empirical relations were used to validate results predicted by Ansys 13. After obtaining satisfying results, the CFD simulations were used to find the most favorable geometrical design for a small shell-and-tube water-to-air heat exchanger. The results of the validation work in Paper 3 were presented in Fig. 3a-3b and 4-4b.

2.4 Analytical calculations

As mentioned in the beginning of section 2, analytical calculations were also used in this work. By analytical calculations are here meant semi-empirical and pure mathematical models used for estimation of:

- convective and radiative heat transfer,
- thermal power and pressure losses,
- change of thermal properties of working media and

Different types of analytical calculations were applied in all articles, and the results in these studies were partly or entirely based on this type of calculations. The applied calculation models were used in their average form.

In Papers 1 and 3, analytical calculations were used to determine space heat losses from a room. The losses were calculated by a global heat balance and with models suggested by prevailing norms. As previously detailed, the analytical calculations were also used for validation of CFD predictions in Papers 2 and 3. In these two papers this type of calculations was applied for estimation of air pressure loss as well as for radiative and convective heat transfer. The results obtained in Paper 4 were entirely based on analytical calculations. In this article the standard method of least-squares was applied to approximate the solution. In Paper 5 both CFD and analytical calculations were used while Paper 6 analytical calculations were used only.

3 Results and discussion

In this section a short summary of the most important results in Papers 1-6 is given. The results from the papers were reported in detail in each paper thus only a brief outline is given here. In addition, some part of the results that were not presented in the papers will be given and discussed here.

Paper 1
The aim of study in Paper 1 was to map thermal performance of low-height radiators (baseboard radiators) used for room heating. The performance was tested for different medium and low-temperature water supplies. The study particularly focused on analyzing at which supply temperature this hydronic system could suppress cold draught, created by glazed surfaces and low outdoor temperature.

The CFD simulations in Paper 1 showed that baseboard radiators, supplied with 55, 45 and 40 °C water flow and installed along two, three and four walls, respectively, were able to cover transmission heat losses of the investigated room space. Although the heaters were placed at the bottom of the walls, the heat distribution inside the room was even. The most symmetrical distribution was obtained with baseboards installed along three walls at 45 °C water supply. At supplies of 45 and 40 °C the predicted draught discomfort at ankle level was around or slightly above 15 %, which is currently the upper permissible limit according to European norm EN ISO 7730 [43]. The draught discomfort at 55 °C water supply was lower than 15 %.

Paper 2

The main focus in Paper 2 was to analyze thermal performance of a conventional baseboard radiator with integrated supply air in a room. The primary goal was to investigate the effects of forced cold airflow through a hot baseboard radiator. The goal was also to investigate whether this combined system was able to:

- cover transmission losses of a modern office space,
- preheat supply air of moderate temperature to room temperature, and
- create a draught-free indoor climate at low-temperature water supply.

The investigation revealed that this integrated system was fully able to both cover transmission heat losses and pre-heat an outdoor airflow of 14 l/s from -6 °C to room temperature using water supply of 45 °C. At this supply temperature the integrated system also efficiently countered cold draught from glazed areas. It was also found that this system gave about 2.1 times more heat output than the conventional system at the same operating temperature. The heat distribution inside the analyzed room space was uniform for both the combined and the conventional baseboard system. The temperature variation across the room length and height was less than 1.5 °C in both cases.

Paper 3

Paper 3 was a further development of the findings from Paper 2 and partly from Paper 1. The main objective was to improve the thermal efficiency of an existing supply-air heater in order to efficiently preheat the incoming supply air of low temperature using low-temperature water supply. The goal was also to investigate the effects of combining this improved air-heater with existing radiator systems in a room. The remaining goals were the same as in Paper 2.

It was shown that the proposed air heater was capable to preheat an outdoor airflow of 10 l/s from -15 °C to 18.7 °C using 40 °C water supply. It was also shown that the supply temperature to radiator systems could be decreased from 49 to 40 °C by combining them with the proposed air-heater, without reducing the heat output. Accordingly, the heat pump efficiency in these combined systems was 8 to 18 % higher than in conventional radiator systems.

Paper 4

The main goal in Paper 4 was to design an easy-to-use equation for calculation of heat outputs from radiant baseboards. In the study the heat emission from baseboard radiators was also compared with emission from conventional panel radiators. The goal was to present current knowledge on advantages and limitations regarding radiant baseboards.

The proposed equation was in excellent agreement with experimental data for excess temperatures and heights commonly used for baseboard radiators in built environments. It was also demonstrated that the total heat transfer of baseboard radiators was about 50 % higher than that of conventional panel radiators. It was further found that 12 m long and 185 mm high baseboard radiators could replace a 1.2 m long and 0.6 m high conventional double-panel radiator with two convector plates, i.e. of type 22.

Papers 5 and 6
The key objective in conference Paper 5 was to inform about different heating systems with integrated air supply. The possibilities, operating conditions, energy performance and sustainability of the integrated (combined) systems were presented. The role of the ventilation rates on the occupants' productivity was also included. In conference Paper 6 the thermal potential of a low L-shaped aluminum room heater placed in the crossing between floor and walls was presented.

In Papers 5 and 6 a brief summary of research conducted between 2006 and 2010 at the Division of Fluid and Climate Technology was given. In Paper 5, a concise review of achieved results and findings by others on similar topics was given. In one of our previous studies it was shown that a ventilation radiator was able to operate at lower water temperature than a conventional radiator generating approximately equal thermal conditions inside the room. In another study it was confirmed that a combined baseboard heating-ventilation system was fully able to cover both ventilation and transmission heat losses of a modern room space at low-temperature water supply. In Paper 6 it was also shown that L-shaped (200 mm x 200 mm) room heaters placed along four room walls, were able to cover space heat losses at outdoor temperature of -16 °C with a supply temperature of 35 °C.

3.1 Potential of proposed systems

An essential contribution of this work is presented in Fig. 9a to 9d. The objective of the presented subplots is twofold. Firstly, to show the mutual dependence of governing parameters that influence energy use in a building. Secondly, to demonstrate the connection between thermal efficiency and sustainability of a building.

In Fig. 9a, the increase of space heat loss with decreasing outdoor temperature is shown. In Fig. 9b, the supply water temperatures for different room heating systems required to meet the heat loss from Fig. 9a are demonstrated. Accordingly, the graphs Fig. 9a and 9b are interconnected, and the figures share x-axis. The change of HSPF value with supply water temperature is illustrated in Fig. 9c, and the variation of annual CO_2 emissions with HSPF value for a single-family dwelling is shown in Fig. 9d. Thus also these two subplots are connected via the joint x-axis. As can be observed, all four subplots are interconnected.

By following the path shown by the red line in Fig. 9a and 9b it can be seen that ventilation and baseboard radiators are able to cover a space heat loss of 28 watts per square meter floor area (W/m^2) using a water supply temperature of 45 °C. If floor heating were to be used instead, the supply water temperature could be additionally decreased by approximately 10 °C. With conventional radiator the supply temperature of 50 °C would be required to meet the same heat loss. The plots also indicate that floor heating could cover a heat loss of about 49 W/m^2 with a water supply temperature of 45 °C. This means that floor heating would be able to operate within low-temperature mode at an outdoor temperature of -16 °C in an average Norwegian single-family house built up to 2000 (Fig. 6a). It seems that the only way to partly meet this ability with existing radiator systems is to combine them with efficient air heaters. The potential of such a system was investigated in Paper 3, and it was revealed that a space heat loss of 35.6 W/m^2 could be met by a supply water temperate of 40 °C. This implies that the proposed system could cover a space heat loss of 40 W/m^2 using a supply temperature of 45 °C. Accordingly, this system would be able to operate with the water supply at 45 °C at

an outdoor temperature of -9 °C (Fig. 9a). If, on the other hand, the proposed system were to be installed in a dwelling built according to the German Energy Saving Regulation (EnEv) from 2009 [44], it would be able to operate with a 45 °C water supply temperature at an outdoor temperature of approximately -20 °C. This statement was derived from data presented in Paper 3.

Data presented in Fig. 9a and 9b also show that supply temperatures to ventilation and baseboard radiators are to a great extent determined by the thermal properties of the building. Unlike floor heating, conventional, ventilation and baseboard radiators are most likely unable to operate with low-temperature supplies in buildings with space heat losses higher than 28 W/m^2. On the other hand, floor heating requires insulated glazing and high under-floor insulation to operate properly. These findings once again highlight the importance of good thermal insulation and air-tightness of buildings, regardless the system used for space heating.

Data in Fig. 9 c show that seasonal heat pump efficiency (HSPF) increases by approximately 1.7 % per degree, for a supply temperature decrease from 55 to 35 °C. Correspondingly, the CO_2 emission decreases by about 1.6 % per degree for the same temperature range. This clearly shows that the thermal efficiency of a building is directly coupled to its energy sustainability, as stated in the beginning of this work. It should also be noted that heat pump efficiency is greatly affected by the production of domestic hot water (DHW). Therefore, by reducing the energy need for preparation of DHW, the system efficiency would further increase and thereby the CO_2 footprint would be further decreased. This especially applies for newly built houses where DHW usually accounts for about 40 % of the total energy use [45]. In Fig 9c, unlike in Table 1, the energy need for production of DHW was not included. The presented HSPF values were exclusively based on the space heating demand, i.e. on 20 MWh/year.

According to Swedish norm SBN 1980 [24], the supply water temperature in current radiator systems should not exceed 55 °C at any design outdoor temperature. In Paper 3 it was shown that space heat losses of a room built according to EnEv 2009, could be covered with a water supply at 40 °C at an outdoor temperature of -15 °C. Combining this result with the findings presented in Fig. 9c, it can be concluded that the heat pump efficiency in a 40/30-system would be 25.5 % higher than in a 55/45-system. Results also suggest that the CO_2 footprint would be lowered by 24 % when switching from a 55/45 to a 40/30-system (Fig. 9d). This means that a large part of the European targets, regarding increase of energy efficiency and reduction of greenhouse gas emissions, both with 20 %, by 2020 could be accomplished. It should also be remembered that the availability of free and sustainable energy supply increases considerably as the level of supply temperature in heating systems decreases. Thus it can be expected that the sustainability of buildings with low-temperature heating systems would be even higher if they were supported by renewable energy production systems.

As mentioned earlier, the cleanness of electricity is essential for the sustainability of buildings when using heat pumps for space heating. In 2008, about 360 kg of CO_2 emission was required to produce 1 MWh of electric energy in the European Union [46]. The corresponding emission rates for Sweden and the Nordic countries were in average around 20 kg and 100 kg, respectively, for the same period [47]. This implies that electricity production in Sweden and in the Nordic countries was 18 and 3.6 times cleaner, respectively, compared to the European Union at that time. Thus the use of renewables for primary energy supply is vital for the total sustainability in our society.

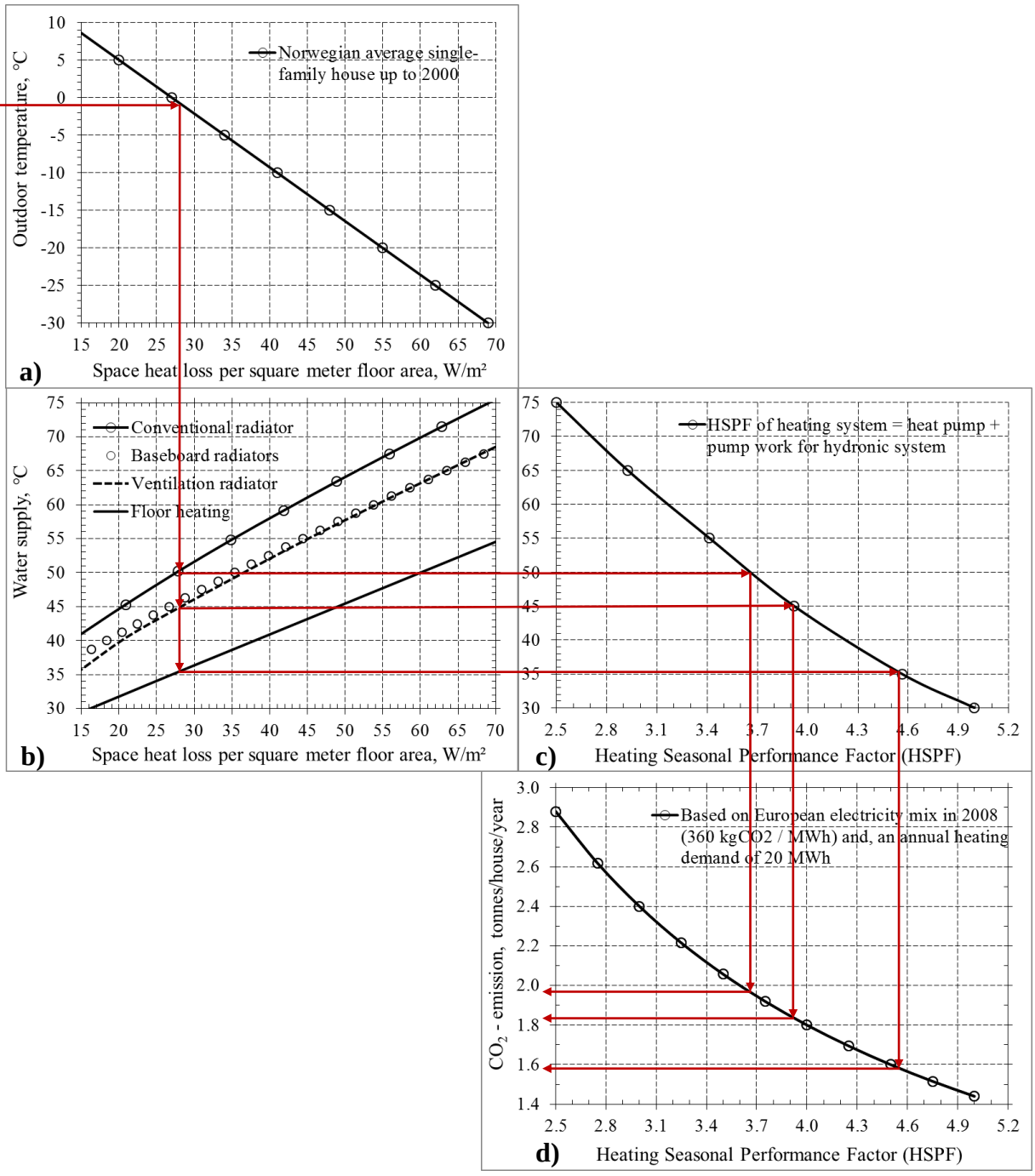

Figs. 9a-9d. **a)** Space heat loss versus outdoor temperature is shown [48]. **b)** Supply water temperatures for four heating systems versus space heat loss are shown. The conventional and ventilation radiator was 1.2 m long and 0.5 m high, and of type 21. Radiant baseboards were 12 m long and 0.15 m high. Center-to-center pipe distance for floor heating was 0.3 m, and thermal resistance of parquet flooring was 0.15 $m^2 \cdot °C/W$. The heat outputs for radiator and floor heating systems were estimated at temperature drops of 10 and 5 °C, respectively, according to [49-51]. The output for the ventilation radiator was also estimated at an airflow rate of 7 l/s. Obtained heat outputs from radiator systems were then divided by room floor area of 20 m^2 [52]. **c)** Supply water temperature versus Heating Seasonal Performance Factor (HSPF) for a ground source heat pump, at an annual heating demand of 20 MWh [20]. **d)** Annual CO_2 emission as a function of HSPF for the same building type as in c), according to data from [46, 53].

It should also be recalled that outdoor temperatures in range of -9 to -15 °C are often short-lived during the winter season in most parts of Europe, and thus should be regarded as extreme outdoor conditions. This can also be seen in Fig. 10. In this figure the variation of daily outdoor temperature during an entire year in Stockholm is shown [54]. The values on the y-axis represent the temperature variation, and the values on the x-axis show the time scale in hours during an entire year. By using the graph in Fig. 10 it can be easily determined for how many hours during a year the outdoor temperature is above or below a certain temperature limit.

The temperature limit when active heat supply is need is not constant, and varies among different building types. However, previous experience has shown that the limit for an "average" building in Sweden starts at an outdoor temperature of 11 °C [55, 56]. This means that the need for active heating in Stockholm is around 5950 h/year or 8.15 months/year. By combining data from Fig. 9a-9b and 10 it can be seen that ventilation and baseboard radiators would be able to operate with supply temperatures below 45 °C during a period of 4080 h/year or 5.6 months/year. Fig. 10 also shows that an outdoor temperature of -9 °C would occur during approximately 360 h/year (0.5 months/year). As detailed earlier, space heat loss generated by this outdoor temperature could be covered by the system proposed in Paper 3 using a water supply of 45 °C. Accordingly, this means that the proposed heating-ventilation systems in Papers 2-4 would be able to operate within low-temperature mode during 94 % of the heating season in the Stockholm region, in most building types. This is, however, not totally true - since the plot in Fig. 10 shows the variation of the daily mean outdoor temperature. The local outdoor temperature during a day between December and January can be much lower than -9 °C in Stockholm. Nevertheless, the plot clearly demonstrates the potential of the proposed systems, and shows that these systems are fully able to operate with low-temperature supplies during most of the heating season in the Stockholm region. Finally, an additional example of the advantage of local air preheating is shown in Fig. 11a-11b. As can be observed, an efficient air preheating would allowed a reduction of the supply water temperature by 8-9 °C with maintained heat output.

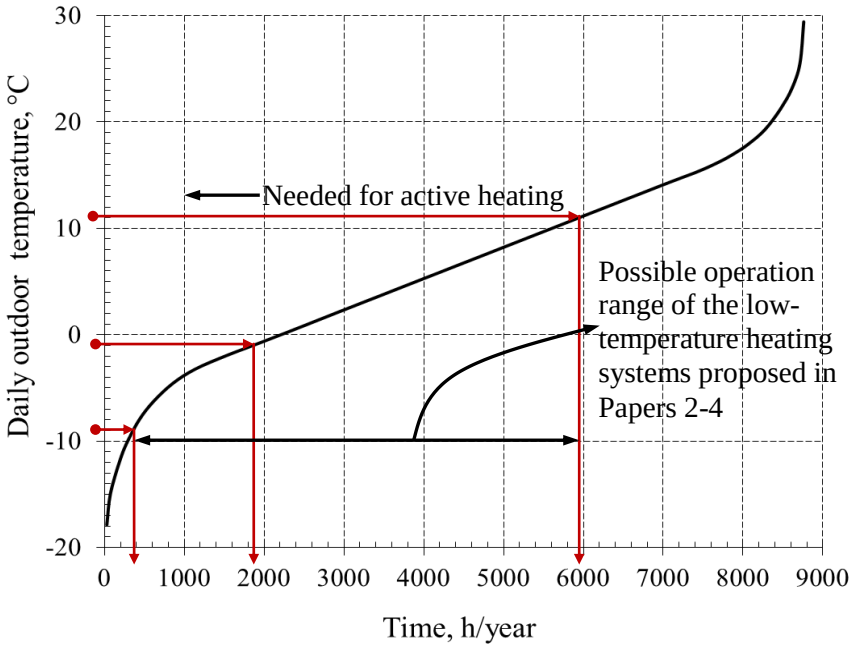

Figs. 10. Change of the mean daily outdoor air temperature during a year in Stockholm [54].

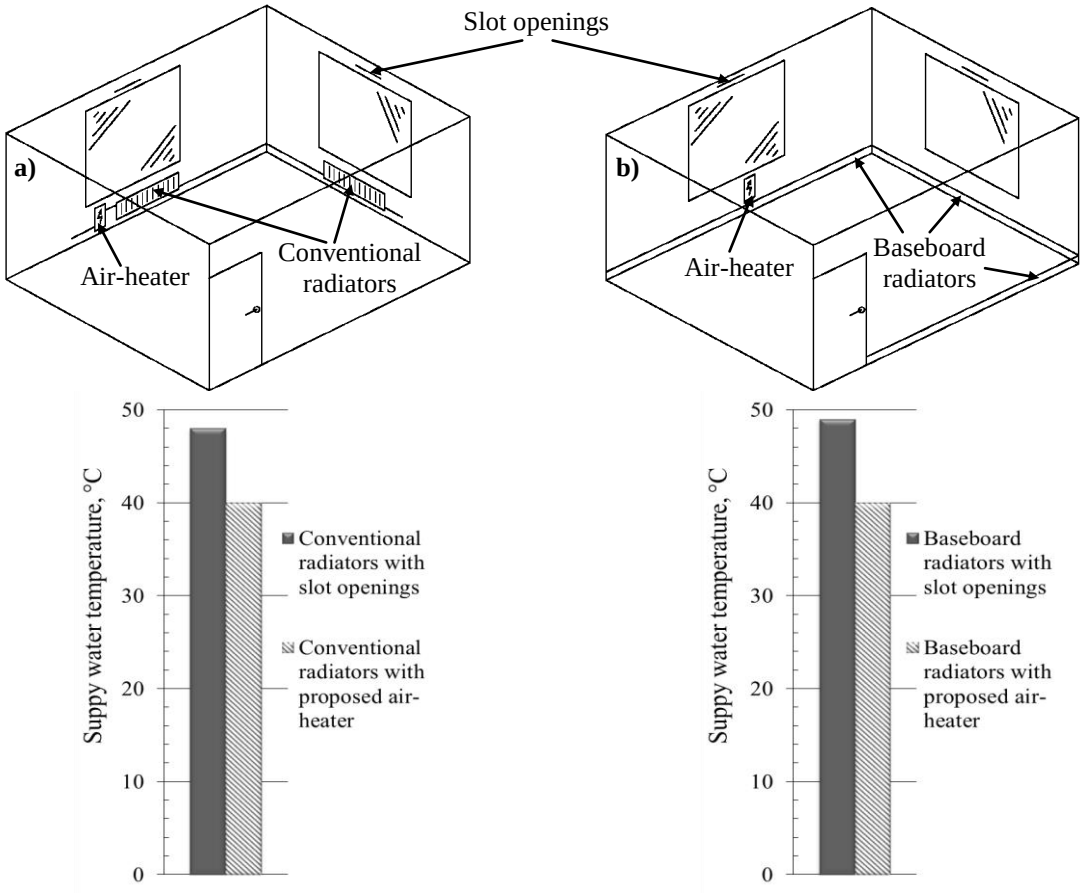

Figs. 11a-11b. Supply water temperatures needed to cover a space heat loss of 35.6 W per square meter floor area. **a)** Case I: conventional panel radiators with slot openings. Case II: conventional panel radiators with proposed air heater in Paper 3. **b)** Case I: baseboard radiators with slot openings. Case II: baseboard radiators with proposed air heater in Paper 3. The incoming supply air was 10 l/s in all four cases. In cases with slot openings, the supply air was not preheated. In cases with proposed air-heater, the supply-air was preheated as described in Paper 3.

4 Conclusions

Based on results presented in this work the following conclusions can be drawn.

Baseboard radiators are generally able to create a stable and comfortable indoor climate at low-temperature supplies. However, problems with draught discomfort could occur at supply temperatures $\leq$ 45 °C. To avoid this, thermal transmittance and the height of the glazed surfaces should be less than 1.2 W/m^2·°C and 2.0 m, respectively at an outdoor temperature of -12 °C. The total heat emission form conventional baseboard radiators was approximately equally divided between convection and thermal radiation.

Studies have also shown that it is favorable to combine a conventional baseboard radiator with outdoor supply air. This combined system is able to both preheat the incoming outdoor air and cover transmission heat losses using 45 °C water supply. With this supply temperature, the system also provids a draught-free indoor climate. Unlike the case with

conventional baseboard radiators, the heat emission from the combined system occures mainly by convection.

The vertical air temperature stratification between floor and ceiling in a room served by both systems did not differ more than 1.5 °C. The radiant asymmetry inside the room was around 4 °C, despite a large proportion of cold glazed areas and hot enclosing baseboard plates. It can therefore be concluded that baseboard radiators both with and without supply air are able to create comfortable indoor climate. It has also been found that by directing the preheated airflow towards cold glazed areas the draught discomfort could be greatly reduced. Therefore it seems reasonable to use this technique in spaces served by low-temperature radiators in order to achieve a draught-free climate.

By combining the proposed air heater with existing radiator systems, the supply temperature could be reduced from 49 to 40 °C without reducing the heat output from the system. Accordingly, the heat pump efficiency in radiator systems with the proposed air-heater would be 8 to 18 % higher than in systems without air heater. It was also shown that this combined system is able to cover a space heat loss of 35.6 watts per floor area using a water supply temperature of 40 °C. According to data presented in Fig. 9a, this rate of heat loss would occur at an outdoor temperature of -6 °C in an average Norwegian building built until 2000. This means that the proposed system is able to operate with low-temperature supplies during most of the heating season in the great majority of buildings in the Stockholm region.

Results also suggest that for additional reduction of supply temperatures in current radiator systems, the effects of forced convection and high-temperature gradients inside as well as alongside radiator surfaces should be utilized. In addition, supplementing existing radiators with efficient air heaters and radiant baseboards would also allow a considerable reduction of supply water temperature in the systems. According to data in Fig. 2, an elimination of ventilation and envelope heat losses would decrease annual energy consumption by about 55 % in an average Swedish family dwelling built during the period 1940-1989. All this clearly shows the energy saving potential of thermal insulation and efficient heating-ventilation systems. Several suggestions for improvements of the second option have been presented in detail in this work.

Since the low-temperature heating systems operate at water temperatures $\leq$ 45 °C, they are suitable for combination with renewable energy sources such as solar energy using heat pumps. Also, different types of waste heat from buildings can be more efficiently utilized by these systems. Besides, a wider use of low-temperature heating systems in our society would also reduce the distribution heat losses from district heating networks and lower CO_2 emissions.

5 Future work

A natural step in next phase would be implementation of the proposed systems. Long-term energy monitoring in buildings served by the proposed systems would reveal the real potential of systems. Currently there are only two studies dealing with energy utilization in buildings served by ventilation radiators [45, 57]. Thus further investigations of energy use in buildings served by the heating-ventilation systems proposed in this work also seems a natural step in the near future. The potential of combining add-on fans with conventional and ventilation radiators should also be further explored for use in single-family dwellings.

Besides, it would also be interesting to simulate the energy performance of a multi-family unit equipped with fan radiators and local ventilation preheaters. At the moment there is no such study. Further, more precise knowledge about maximum allowable temperature drop across low-temperature radiators is also needed. By an additional temperature decrease between supply and return flows, additional heat enhancement would be achieved. Of course, this heat power gain must be matched with hydraulic power loss. It therefore seems reasonable to work on mapping favorable operating water flows of the proposed systems in the next phase.

As the relative proportion of energy needed for domestic hot water in new single-family dwellings is constantly increasing, it also seems sound to work on finding new methods for efficient heat recovery from used tap water. Finally, as recently highlighted by Myhren [57], more attention should be put on advisory services. The construction companies, district heating companies, building owners and heat pump manufacturers must be informed about the potential of heating-ventilation systems investigated in this work.

6 References

[1] Nilsson PE (Editor). Achieving the Desired Indoor Climate. ISBN 91-44-03235-8; 2003, Introduction and Chapter 3. pp. 1, 145-146.
[2] International Energy Agency. World Energy Outlook 2004. Chapter – Energy-related CO_2 emissions, Table 2.3, p. 2. http://www.iea.org/textbase/nppdf/free/2004/weo2004.pdf [accessed 23.08.2010]
[3] PBL Netherlands Environmental Assessment Agency, http://www.pbl.nl/en/dossiers/Climatechange/TrendGHGemissions1990-2004 [accessed 30.07.2013]
[4] Bauermann K, Weber C. Heating Systems When Little Heating Is Needed. Energy, Sustainability and the Environment 2011. ISBN 978-0-12-385136-9. Chapter 14. pp. 417-442.
[5] European Commission. Directorate-General for Energy. Market Observatory for Energy. Key Figures. 2011. p. 25.
[6] Bertoldi P, Hirl B, Labanca N. Energy Efficiency Status Report 2012, Electricity Consumption and Efficiency Trends in the EU-27. 2012. p. 9.
[7] International Energy Agency (IEA). CO_2 emissions from fuel combustion. Highlights. 2012. p. 9.
[8] Bredenberg A. The Damage Done in Transportation - Which Energy Source Will Lead to the Greenest Highways? Available from: http://news.thomasnet.com/green_clean/2012/04/30/the-damage-done-in-transportation-which-energy-source-will-lead-to-the-greenest-highways/ [accessed 01.08.2013]
[9] Janson U, Berggren B, Sundqvist H. Improving the Energy Efficiency of Residential Buildings by Retrofitting, Report Number EBD-R-08/22, ISBN-978-91-85147-32-8, Date: 26-11-2008. (in Swedish)
[10] Gustafsson S-I. Optimisation of insulation measures on existing buildings, Energy and Buildings 33 (2000) 49-55.
[11] Al-Sanea SA, Zedan MF. Improving thermal performance of building walls by optimizing insulation layer distribution and thickness for same thermal mass, Applied Energy 88 (2011) 3113-3124.
[12] Leibundgut H, Baldini L, Sanchez J A. Energy Systems Analysis - Energy in Buildings. A lecture on building systems in 6 modules - Part 2. Institute of Technology in Architecture / Faculty of Architecture / ETH Zürich. 19-26 March 2012.
[13] Swedish Energy Agency. Energy statistics for one-and two-dwelling buildings in 2011. ISSN 1654-7543. ES 2012:04. pp. 12 and 16. Published in October 2012. (in Swedish)
[14] Swedish Energy Agency. Measurement of domestic cold and hot water consumption in 44 households. Improved energy statistics in buildings and industry. ISSN 1403-1892. ER 2009:26. Figure 19, p. 38. Published in July 2009. (in Swedish)
[15] Eriksson B. Energy Saving Potential in the housing stock. Heat Balance Model. ELIB report no. 8. Swedish Institute for Building Research. ISBN 91-7111-82-8. Gävle, December 1993. p. 32. (in Swedish)
[16] Swedish Energy Agency. Additional insulation in dwellings - facts, benefits and pitfalls. Article Number: 2127. ID number: ET2009:19. 2009. p 9. (in Swedish)
[17] European Geothermal Energy Council. Geothermal Heat pumps - Ground source Heat pumps. Brochure 2009. p. 3.
[18] SP Technical Research Institute of Sweden, Heat Pump Centre. Heat pumps can cut global CO_2 emissions by nearly 8%. Available from: http://www-v2.sp.se/hpc/publ/HPCOrder/viewdocument.aspx?RapportId=451 [accessed 23.08.2010]
[19] Swedish National Board of Housing, Building and Planning. Alternative forms of heating in existing permanently populated houses. ISBN: 978-91-85751-95-2. July 2008. pp. 32-38. (In Swedish)

[20] Vitocalc 2005, version 1.0. Viessman Värmeteknik AB. (In Swedish)
[21] Banjac M, Vasiljević B, Gojak M. Low Temperature Hydronic Heating System with Radiators and Geothermal Ground Source Heat Pump. Faculty of Mechanical Engineering, Belgrade. FME Transactions (2007) 35, pp. 129-134.
[22] Peterson F. Heating system, conventional and low temperature. Third Edition. Compendium I:4. Heating and Ventilation Technology, KTH Royal Institute of Technology, Stockholm. p. 20. (in Swedish)
[23] TÜV Rheinland. DIN CERTCO, Certification Scheme DIN-Geprüft, Radiators and Convectors according to DIN EN 442. Edition: August 2008, pp. 1-27.
[24] Swedish Constriction Norm SBN 1980. PFS 1980:1. ISBN 91-38-07565-2.1983. p. 307. (in Swedish)
[25] Fahlén P. Heat pumps in hydronic heating systems - effective solutions for heating and domestic hot water for conversion of electrically heated single-family dwellings. A final report from eff-Sys. Installation Engineering, Chalmers University of Technology, Gothenburg 2003. pp.17-18. (in Swedish)
[26] Boerstra A, Veld PO, Eijdems H. The Health, Safety and Comfort Advantages of Low Temperature Heating Systems: A Literature Review. Proceedings of the 6th International Conference on Healthy Buildings. 2000.
[27] Swedish Ventilation. Energy Efficient Installations, a new opportunity for Sweden. Technical Brochure. 1 Profu 2009. p. 4.
[28] SP Technical Research Institute of Sweden. Measurement of annual performance of five ground source heat pumps in Sjuhärad. 2005. pp. 8 and 24. Available from: http://www.sp.se/sv/index/services/heatpump/fieldmeasurements_hp/Sidor/default.aspx [accessed 26.08.2013] (in Swedish)
[29] Kjellsson E. Solar Collectors Combined with Ground Source Heat Pumps in Dwellings - Analyses of System Performance. Doctoral Thesis. ISBN 978-91-88722-40-9. Report TVBH-1018. Building Physics, Lund Technical University 2009. pp. 65 and 101. (in Swedish)
[30] Swedish Energy Agency. Sweden – the leader in heat pumps. Heat pumps, successful intervention in energy research ET 2009:23, (2009). (in Swedish)
[31] Ekonomifakta. Greenhouse gas emissions by sector. Available from: http://www.ekonomifakta.se/sv/Fakta/Miljo/Utslapp-i-Sverige/Vaxthusgaser/ [accessed 27.08.2013] (in Swedish)
[32] Donjerković P. Fundamentals and Control of Heating, Ventilation and Air-Conditioning. Part II. ISBN 953-168-069-8. 1996. Chapter 2. p. 53. (in Croatian)
[33] Bejan A. Convection Heat Transfer, second edition. ISBN 0-471-57972-6. 1995. Chapter 6. p. 269.
[34] Churchill SW, Chu SHS. Correlation Equations for Laminar and Turbulent Free Convection from a Vertical Plate. International Journal of Heat and Mass Transfer 1975 (18) 1323-1329.
[35] Çengel YA, Ghajar AJ. Heat and Mass Transfer – Fundamentals and Applications. ISBN 978-0-07-339812-9. 2010. Chapters 7 and 9. pp. 424 and 549.
[36] Myhren JA, Holmberg S. Design considerations with ventilation-radiators: comparisons to traditional two-panel radiators, Energy and Buildings 41 (2009) 92-100.
[37] Myhren JA, Holmberg S. Improving the thermal performance of ventilation radiators – the role of internal convection fins, International Journal of Thermal Sciences 50 (2011) 115-123.
[38] Johansson PO, Wollerstrand J. Improved Temperature Performance of Radiator Heating System Connected to District Heating By Using Add-On-Fan Blowers. Proceedings of 12th International Symposium on District Heating and Cooling. September 5th - 7th. 2010. Talinn, Estonia.
[39] Tu J, Yeoh GH, Liu C. Computational Fluid Dynamics, A Practical Approach. ISBN 978-0-7506-8563-4. First Edition 2008.

[40] Chen Q, Srebrić J. How to Verify, Validate and Report Indoor Environment Modelling CFD Analyses. ASHRAE RP-133. June 29, 2001.
[41] Omori T, Tanabe S, Akimoto T. Evaluation of thermal comfort and energy consumption in a room with different heating systems. Proceedings of 6th international conference in indoor air quality, ventilation and energy conservation in buildings, IAQVEC 2007.
[42] Omori T, Tanabe S. Coupled simulation of convection–radiation–thermoregulation for predicting human thermal sensation. Proceedings of 10th international conference on air distribution in rooms, Roomvent 2007.
[43] European Norm EN ISO 7730. Moderate thermal environments. Determination of the PMV and PPD indices and specifications of the conditions for thermal comfort (ISO Standard 1997) 1997.
[44] Radson. The guide to radiators for low temperature heating systems. Technical note. DM023030150602 - 02/2012. (2012). pp. 25-33.
[45] Hesaraki A, Holmberg S. Energy performance of low temperature heating systems in five new-built Swedish dwellings: A case study using simulations and on-site measurements. Building and Environment 64 (2013) 85-93.
[46] European Environment Agency. CO_2 Emissions per kWh of Electricity and Heat Output. Available from: http://www.eea.europa.eu/data-and-maps/figures/co2-emissions-per-kwh-of [accessed: 20.09.2013]
[47] Svenskt Näringsliv. Klimatkompassen. Calculation Methodology and Basic Assumptions. Available from: http://www.klimatkompassen.se/index.php?id=348257 [accessed: 20.09.2013] (in Swedish)
[48] Rekstad J, Meir M, Kristoffersen AR. Control and energy metering in low temperature heating systems. Energy and Buildings 35 (2003) 281-291.
[49] Ploskić A, Holmberg S. Performance evaluation of radiant baseboards (skirtings) for room heating - An analytical and experimental approach. Applied Thermal Engineering 62 (2014) 382-389.
[50] Radiator heat output calculator. Manufacturer's data. In accordance with EN 442. Available from: http://www.purmo.com/se/ladda-hem-filer/effektsimulering.htm [accessed 26.01.2012]. (in Swedish)
[51] Floor heating heat output calculator, Manufacturer's data. In accordance with EN 1246. Available from: http://www.purmo.com/de/produkte/flaechenheizung/planung-und-montage-planungsgrundlagen-waermeleistungen.htm [accessed 12.09.2013] (in German)
[52] Dol K, Haffner M. Housing Statistics in the European Union. OTB Research Institute for the Built Environment, Delft University of Technology. September 2010. pp 51-52.
[53] Sustainable Energy Ireland. Energy Policy Statistical Support Unit. Energy in the Residential Sector. 2008. p. 17.
[54] FläktWoods. Technical handbook - Air handling technology. Chapter 7. p. 42. Available from: http://www.flaktwoods.se/0/0/2/4293030b-bd15-4dad-9904-d9a0217086fa [accessed 10.10.2013] (in Swedish)
[55] Jensen L. Impact of outdoor temperature on annual energy demand - theory part. Report number TVIT--08/7023. Faculty of Engineering at Lund Technical University, Department of Building and Environmental Technology. 2008. pp. 6-7. (in Swedish)
[56] Warfvinge C. Compendium in HVAC technique for civil engineers. The Faculty of Engineering at Lund Technical University. 2000. Chapter 6. p. 6:41 [in Swedish].
[57] Myhren JA. Potential of Ventilation Radiators, Performance Assessment by Numerical, Analytical and Experimental Investigations. Doctoral Thesis. ISBN 978-91-7415-940-0. KTH Royal Institute of Technology. Civil and Architectural Engineering. Stockholm, Sweden 2011.

Building and Environment 45 (2010) 1123–1133

Contents lists available at ScienceDirect

Building and Environment

journal homepage: www.elsevier.com/locate/buildenv

Heat emission from thermal skirting boards

Adnan Ploskić*, Sture Holmberg

Royal Institute of Technology, School of Architecture and Built Environment, Fluid and Climate Technology, Marinens väg 30, SE-13640 Handen, Stockholm, Sweden

ARTICLE INFO

Article history:
Received 26 August 2009
Received in revised form
22 October 2009
Accepted 25 October 2009

Keywords:
CFD simulations
Draught (draft) sensation
Low-temperature heating
Skirting (baseboard) heating
Thermal comfort

ABSTRACT

The performance of three hydronic skirting heating systems was investigated. The main focus of the study was to ascertain whether thermal skirting boards served by low-temperature supply flow were able to suppress strong downdraught. The evaluation was made for a two-person office room with mechanical ventilation. Computational Fluid Dynamics (CFD) simulations and three different draught rating models were employed to predict the level of thermal discomfort inside the room. CFD results were validated against several analytical calculations and four sets of experimental data presented in previous studies. Numerical simulations showed that all three skirting heating arrangements were able to cover transmission and ventilation thermal losses of the office room. Horizontal and vertical heat distribution inside the room was uniform for all heating systems. CFD simulations also showed that thermal skirting boards served by 40 and 45 °C supply flow had difficulty in reducing the velocity of the downdraught at ankle level. Consequently the draught rating in this region was around or slightly above 15% for these cases. In contrast, heat-emitting skirting boards supplied by 55 °C hot water showed a better ability to suppress downdraught, and the proportion of people sensing draught at 0.1 m above the floor was low. The conclusion of this study was that thermal performance of hydronic skirting heaters with low-temperature water supply must be improved in order to counter strong downdraughts, in particular where such systems may be combined with heat pumps of other low-valued sustainable energy sources.

1. Introduction

The aim of this study was to investigate thermal performance of three water-based skirting heating systems in a modern office room during Swedish winter conditions. The study focused on whether thermal skirting panels served by low-temperature supply flow, were powerful enough to counteract cold airflow created by large glazing surfaces and a cold outdoor environment. Water-based thermal skirting boards are low-profile heat emitters placed along the inner periphery of the room instead of traditional wooden skirtings. Usually this heat-emitting unit consists of one long U-tube (supply and return pipe), panel joints and a thin rectangular casing plate. Thermal energy, carried by hot water circulating inside the U-tube, is transmitted to the thin metal casting plate and further to the ambient air. In view of the fact that nowadays modern office spaces often require not only energy efficiency but also cost efficient and well-designed heating systems, skirting heating can be appropriate. These long, low-profile thermal emitters give designers more flexibility to create an elegant and space-saving heating system. Skirting heating may also be installed in rooms where fast thermal response is needed. Figs. 1 and 2 illustrate placement of the skirting heaters inside a typical office room.

In the past, occupied spaces with large areas of glazing and high ventilation rates were likely to have problems with cold air downflow (downdraught) and thermal discomfort during cold periods of the year. Commonly problems with cold air downdraught have been solved by placing thermal sources underneath the coldest elements in the room, i.e. the windows and the outer walls. Nowadays buildings are more tightly sealed and better thermally insulated than before. This means that problems with cold air downdraught have considerably decreased. It also means that powerful radiators or convectors underneath cold surfaces may not always be needed. Heat emitters served by low-temperature supply flow can now gradually replace conventional high-temperature heating devices.

There are various techniques to increase thermal output from a heat emitter at constant surface temperature. The most common ways are to enlarge the emitter's heat-transferring surface, or to force airflow along it. The latter is preferred especially where the temperature difference between ambient air and heating unit is large. By these means, supply flow temperature to the heater can correspondingly be decreased, leading to energy savings. Such heat transferring mechanisms are used for creating low-temperature heating systems.

* Corresponding author. Tel.: +46 8 771 63 62; fax: +46 8 790 48 00.
E-mail address: adnan.ploskic@sth.kth.se (A. Ploskić).

0360-1323/$ – see front matter © 2009 Elsevier Ltd. All rights reserved.
doi:10.1016/j.buildenv.2009.10.016

Nomenclature

Latin letters

A_{skr}	surface area of skirting board [m^2]
A_{trans}	surface area of transmitting surface [m^2]
G	incident thermal radiation [W/m^2]
$H_{gl,\ surf}$	characteristic glazing height [m]
$h_{gl,\ sur}$	total heat-transfer coefficient at inner glazing surface [$W/(m^2\,°C)$]
L_{skr}	length of skirting board [m]
P_{skr}	total heat flux from skirting boards [W/m^2]
Q_{trans}	transmission losses [W]
Q_{vent}	ventilation losses [W]
T_{rad}	thermal radiation temperature [K]
U_{trans}	thermal transmittance (U-factor) [$W/(m^2\,°C)$]
$v_{in,\ air}$	indoor air velocity [m/s]
$v_{gl,\ ai}$	air velocity next to inner glazing surface [m/s]
x, y, z	Cartesian coordinates [m]

Greek letters

α_{tot}	total heat-transfer coefficient at skirting surface [$W/(m\,°C)$]
ε	emissivity of inner surfaces, 0.9 used in study [−]
$\Delta\theta_m$	mean temperature difference between heated skirting surface and indoor air [°C]
$\theta_{comfort}$	comfort temperature [°C]
$\theta_{gl,\ surf}$	surface temperature of the inner glazing [°C]
$\theta_{in,\ air}$	mean indoor air temperature [°C]
θ_{opr}	mean operative temperature [°C]
$\theta_{out,\ air}$	mean outdoor air temperature [°C]
θ_{return}	mean temperature of the return flow [°C]
$\theta_{skr,\ surf}$	mean surface temperature of the skirting board [°C]
θ_{supply}	mean temperature of the supply flow [°C]
$\overline{\theta}_{surf}$	mean surface temperature of the enclosing elements [°C]
σ	Stefan–Boltzmann constant [$W/(m^2\,K^4)$]
Φ_{skr}	heat output per skirting length metre [W/m]

1.1. Low-temperature heating systems

Different studies have indicated that occupants living in buildings served by low-temperature heating systems are very satisfied with ambient indoor conditions. In particular, perceived thermal comfort levels are considered to be higher than in buildings served by high-temperature heating systems [1]. Low-temperature heating is also beneficial regarding distribution losses and efficiency of heat generation. Heat emitters with large emitting surface area commonly known as floor, wall and ceiling heating, are typical examples of traditional low-temperature heating systems. Ventilation-radiators [2] and wall-mounted supply air convectors [3] are other types of thermal emitters that combine incoming ventilation air and heating. Large temperature differences between cold ventilation inflow and the hot transferring surfaces increase convective heat transfer and enable these emitters to extract additional heat energy from the supply flow. Low-temperature heating systems are usually combined with low-valued thermal energy, which can be delivered by sustainable energy sources such as heat pumps, solar or geothermal collectors, industrial waste heat and condensing boilers [4]. It has been established, both theoretically and in practice, that a combination of low-temperature heating systems and low-valued energy sources gives a higher Coefficient of Performance (COP). This combination is an environmentally friendly alternative and also leads to lower energy costs for building owners.

However, sometimes there are reasons to use other types of low-temperature heating solutions than traditional ones. Skirting heaters, due to their large heat-emitting surface area and high convective heat flux enable the supply flow temperature to be lowered and therefore may also be used in a low-temperature heating system. This paper presents the results from an evaluation of such a system.

1.2. Previous studies

Few studies have been performed on low-profile heat emitters. Molin [5] has analytically investigated the performance of radiators in low-temperature systems. He concluded that convective heat

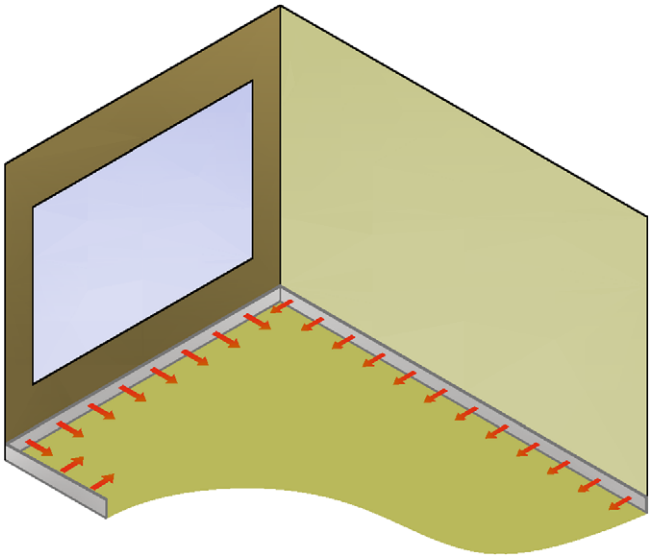

Fig. 1. Thermal skirting boards (heaters) placed along the inner perimeter of the room. Heat surrounds occupants in the room providing a "heat enclosure".

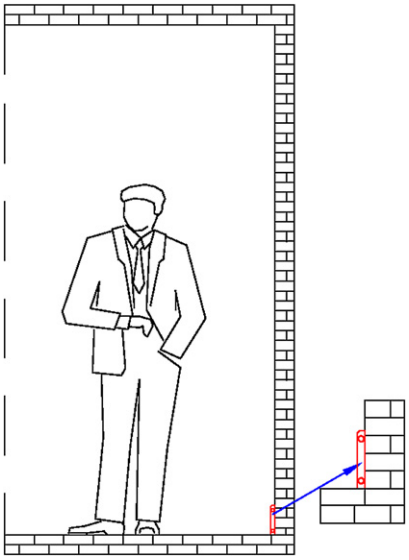

Fig. 2. Cross-section of a typical office room, showing the relation between room, occupant and skirting heater height.

transfer within natural convection is higher among low-profile radiators, especially when supply flow temperature was decreased from 55 to 35 °C. Stålberg [6] showed that it is possible to warm-up an office room during the Swedish winter season using L-shaped aluminium baseboards heated by 35 °C supply temperature. A comparison between three different heating systems was conducted by Chen [7]. He concluded that radiator heating creates the most uniform temperature distribution in the room. It was also emphasized that airflow caused by radiator heating was laminar in most parts of the room. Similar results regarding temperature distribution were obtained by Myhren and Holmberg [8]. Their investigation included comparison of four heating arrangements, of which two were radiator systems. They concluded that radiator heating systems caused only small vertical temperature changes in the room. Indoor air velocity induced by radiators was below the recommended limit in most of the occupied zone. Differences in heating performance between an air-conditioner and floor heating were analyzed by Omori et al. [9]. Results from this study showed that floor heating needed 70% of the total heat energy consumed by an air-conditioner in order to create a similar thermal climate in the chamber. The heat distribution inside the chamber was uniform in both cases but the temperature level for the case with an air-conditioner was slightly higher.

Another important factor that has a large impact on the thermal sensation of occupants and general indoor air movement is cold downdraught. The characteristic of cold downdraught and its behaviour inside the room is mainly dependent on the difference between outside and inside temperature, and the height of the cold inner surface. Ge and Fazio [11] analyzed cold downdraught caused by extremely low outdoor temperature and two different glazing types. Measurements showed that glazing units with poor transmittance resistance in combination with extremely low outdoor temperature can generate air velocity up to 1.0 m/s at the cold glazed surface. The benefits of using well-insulating glazing units instead of conventional ones, in order to reduce negative effects of cold downdraught and thermal discomfort, have been reported by several researchers [11–14]. A general conclusion was that well-insulating glazing panels created a better thermal climate for occupants. Apart from thermal properties of the glazing unit, the position and design of the window sill also plays an important role in velocity and momentum reduction of the downdraught [12]. Jurelionis and Isevicius [15] observed that a radiator installed below the window sill in combination with free falling downdraught may generate both warm and cold air jets that flow directly into the occupied zone. In order to prevent this phenomenon, the authors suggested use of window sills with openings or grills. The performance of such an arrangement was evaluated by Rueegg et al. [14]. Experimental investigation showed that only about 50% of the cold downdraught flowed through the openings in the window sill. The vertical velocity magnitudes measured 0.5 m from the glazed surface were strongly reduced in the case with openings, however.

Besides heating or cooling a room, ventilation also plays an essential role for well being of the occupants. Occupied places needed to be supplied with an adequate amount of fresh outdoor ventilation air in order to provide a healthy indoor environment and maintain productivity of employees. Mechanical ventilation is a primary mechanism used for creating and maintaining a desirable level of indoor climate and air quality in modern office spaces, and therefore this ventilation system was used in the present study. On the other hand, an oversupply of ventilation air can also lead to energy losses, so the ventilation rate used in this survey was chosen in line with current international norms.

Table 1
Dimensions of the office room and the position of glazed surfaces, skirting heaters, air intake and exhaust opening.

Item	Length	Width	Height	Location		
	Δx	Δz	Δy	x	y	z
Room	5.3	3.8	2.6	0.0	0.0	0.0
Glazing I	1.6	0.0	2.0	0.7	0.3	0.0
Glazing II	1.6	0.0	2.0	3.0	0.3	0.0
Diffuser	0.24	0.24	0.02	2.65	2.58	1.9
Exhaust	0.3	0.02	0.15	2.65	2.23	3.8
Skirting heater I	5.3	0.0	0.15	0.0	0.0	0.0
Skirting heater II	0.0	3.8	0.15	0.0	0.0	0.0
Skirting heater III	0.0	3.8	0.15	5.3	0.0	0.0
Skirting heater IV	5.3	0.0	0.15	0.0	0.0	3.8

2. Method

2.1. Description of the studied room

The comparisons between skirting heating arrangements were performed in a two-person office room. The modelled office space had one external wall that was exposed to the outdoor environment. This wall had two frameless glazed surfaces. The rest of the walls were assumed to adjoin other indoor spaces of the building and therefore were considered as non-conducting enclosing elements. Design outdoor temperature during the winter season in central Sweden is about −12 °C [18], so this temperature level was also used as a reference in the present study. Heat-emitting skirtings placed along the inner perimeter of the room were used for heating. The ventilation arrangement was modelled in agreement with Swedish construction regulation standard BFS 1998:38 and American Society of Heating, Refrigerating and Air-Conditioning Engineers (ASHRAE) guide lines [16,17]. The studied room was regarded as an empty office space without window sills, occupants or office-equipment. A detailed room description is given in Fig. 3 and Table 1.

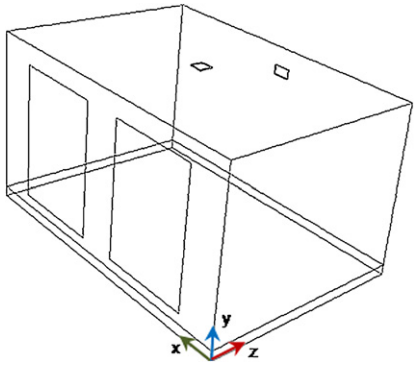

Fig. 3. The room model used in this study.

2.2. Quality control of CFD model

Computational Fluid Dynamics (CFD) is a powerful and widely used engineering tool for prediction of air velocity, turbulence intensity, temperature stratification and contaminant concentration in indoor environments. Over past decades, CFD software has showed considerable potential and advantages for evaluating properties of indoor climate. The accurate specification of boundary conditions plays a crucial role in CFD simulations, yet these often must be simplified. All turbulence models that are commonly used for prediction of indoor air movement contain uncertainties. Therefore CFD simulation results require experimental validation. Comparison between simulation results and measurements helps the user to localize and estimate eventual errors in the CFD model. However, it is also important to highlight that experimental data are

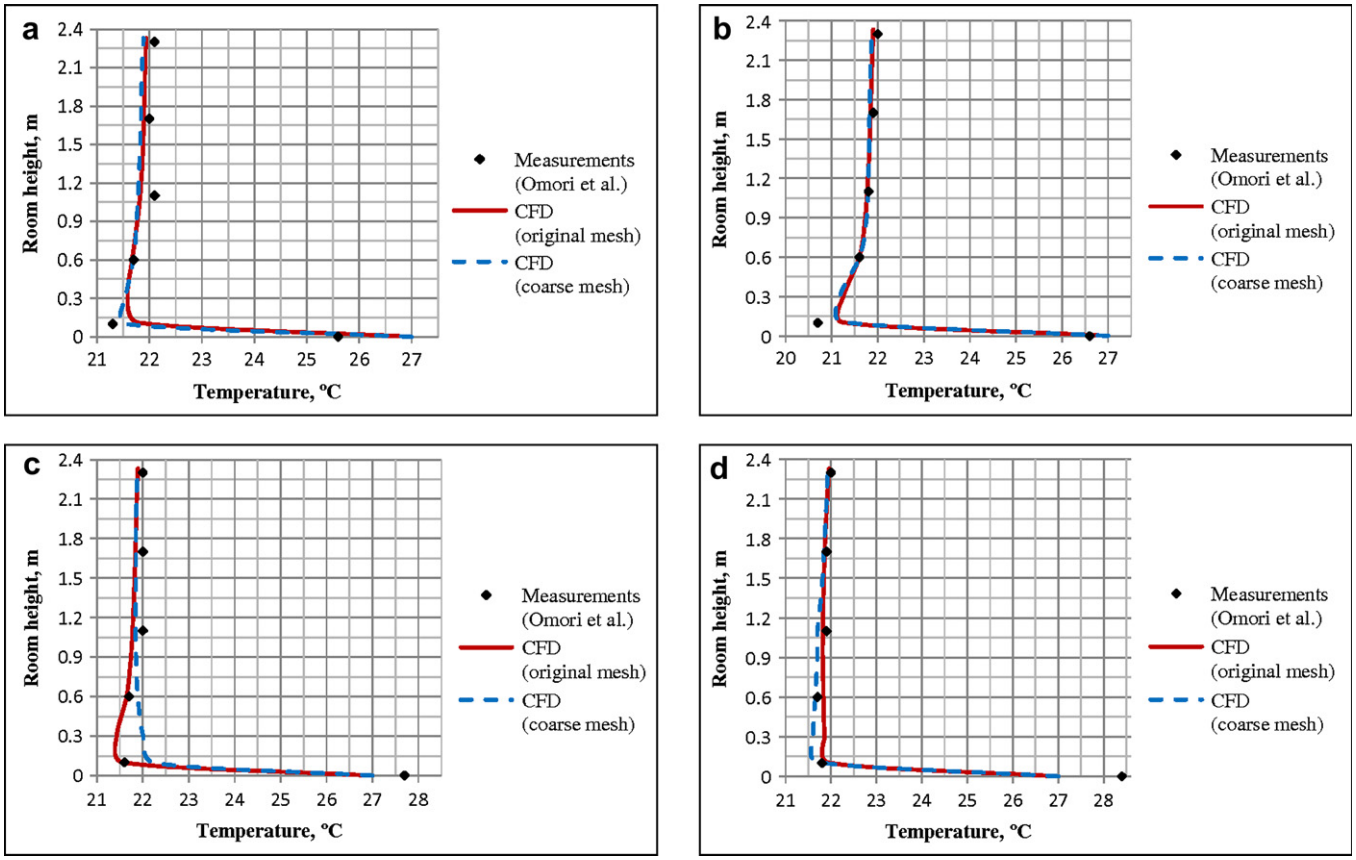

Fig. 4. (a) Comparison between measurements and CFD simulated temperature profiles. The measurement points were at $x = 2.0$ m, $\Delta y = 2.3$ m, $z = 0.4$ m, with x giving chamber length, y chamber height and z chamber width. (b) Comparison between measurements and CFD simulated temperature profiles. The measurement points were at $x = 4.0$ m, $\Delta y = 2.3$ m, $z = 1.1$ m, with x giving chamber length, y chamber height and z chamber width. (c) Comparison between measurements and CFD simulated temperature profiles. The measurement points were at $x = 4.0$ m, $\Delta y = 2.3$ m, $z = 2.4$ m, with x giving chamber length, y chamber height and z chamber width. (d) Comparison between measurements and CFD simulated temperature profiles. The measurement points were at $x = 2.0$ m, $\Delta y = 2.3$ m, $z = 3.15$ m, with x giving chamber length, y chamber height and z chamber width.

not always fully reliable and that high quality measurements of indoor climate are limited.

In the present study, a virtual model of an artificial climate chamber presented by Omori et al. [9,10] was reproduced by CFD. CFD codes, GAMBIT (pre-processor) and FLUENT (post-processor), were utilized in the investigation. This CFD model was validated against numerical and experimental findings reported by Omori and Tanabe [10]. Outdoor temperature level, air mass flow rate, size and position of the glazed surfaces, air intakes and exhaust opening, were the same as previously used by Omori et al. [9,10]. Inner surface temperatures of the enclosing elements and floor heaters, presented in these investigations, were also used as boundary conditions in this CFD model. The human model was created with same surface area using rectangular blocks of different sizes. The model released heat to the office room with a constant heat flux of 61 W/m^2. Originally, the modelled CFD room contained about 1.17 million tetrahedral cells. The grid distribution inside the room was not uniform. A refined grid was applied near important boundary zones, and an unrefined mesh was arranged towards the centre of the room. The grid independence was tested by decreasing the original grid by 25%. In the important regions, such as cylindrical and rectangular air intakes, around the occupant and windows where usually strong air diffusion occurs the face grid was maintained unchanged both with the original and the coarse grid. Instead the volume grid in the room was replaced. CFD simulations performed in this study showed that the ambient air temperature inside the chamber was uniformly distributed for both (original and coarse) grid arrangements and was around 21.8 °C. This temperature level was in close agreement with numerical findings presented in [10], where the predicted mean air temperature remained around 21–22 °C inside the room with insignificant vertical variations. Additionally, a good agreement between simulated vertical temperature variations and experimental data was also obtained, see Fig. 4a–d. The locations of metering points shown in Fig. 4a–d are valid only for the climate chamber presented by Omori et al. [9,10], and do not refer to the room dimensions presented in Table 1.

2.3. Boundary conditions and ancillary models

In this section a detailed overview of boundary conditions and ancillary models used in current investigation is given. The boundary conditions are divided into two main categories. The first includes conditions for supply and exhaust airflow, while the second presents settings for heat transfer from the heated objects. Additionally, reasons for choice of radiation and turbulence models are explained.

2.3.1. Ventilation system

The ventilation system was of a mixing type that is widely utilized in office buildings. The incoming ventilation air was supplied by a four-way radial diffuser placed at the centre of the ceiling. The diffuser supplied incoming air through four equal rectangular openings. Supply air was considered to be preheated and had a constant temperature. Ventilation flow rate was held constant and unchanged during the entire simulation process. Swedish construction regulation standards [16] and ASHRAE [17] recommend 7.0 l/s and 10 l/s per person respectively, as minimum fresh air supply for office spaces. Since the office space in the current

Table 2
Initial boundary conditions for the four-way radial diffuser and exhaust opening used in this study.

Properties	Unit	Diffuser	Exhaust
Air temperature	°C	18	Predicted by CFD
Air density	kg/m^3	1.2	Predicted by CFD
Air mass flow rate	kg/s	$2.4 \cdot 10^{-2}$	Pressure outlet
Air turbulence intensity	%	10	Predicted by CFD
Length scale (height)	m	$2.0 \cdot 10^{-2}$	$1.5 \cdot 10^{-1}$

investigation was regarded as a two-person room, a constant supply airflow of 20 l/s was used, giving about 1.4 hourly nominal changes of indoor air. Ambient air was evacuated via an exhaust opening located opposite to the external wall. Detailed boundary conditions for the square diffuser and the exhaust opening are given in Table 2.

2.3.2. Heating system

Thermal skirtings of 150 mm height placed along the inner periphery of the room were used for heating. Three different cases were investigated. In all cases there was a thermal skirting board underneath glazed areas.

(1) Case 1, skirting heaters placed along the external wall and three internal walls.
(2) Case 2, skirting heaters placed along the external wall and two internal walls.
(3) Case 3, skirting heaters placed along the external and one internal wall.

In each case thermal power of the skirting heaters was adjusted to cover transmission and ventilation losses and to maintain indoor air temperature around 22 °C. Thermal transmission losses through enclosing elements and heat release from the skirting heaters were calculated by Eqs. (1)–(3) and used as thermal boundary conditions in CFD. The simulations were made using a negative and constant heat flux on the glazed areas and external wall. The heat flux magnitude was the same for all three cases as presented in Table 3. Skirting heaters had a positive and fixed thermal flux, but intensity and surface area varied between cases as showed in Table 4. Overall heat-transfer coefficients α_{tot} at skirting surfaces were calculated by well-known analytical models for natural convection and thermal radiation for a heated vertical plate inside an enclosure. The set of equations used for estimation of α_{tot} was previously presented by Myhren and Holmberg [2]

$$Q_{trans} = U_{trans} \cdot (\theta_{out,air} - \theta_{in,air}) \quad (1)$$

$$P_{skr} = \alpha_{tot} \cdot \Delta\theta_m \quad (2)$$

$$\Delta\theta_m = \theta_{skr,surf} - \theta_{in,air} = \frac{\theta_{supply} - \theta_{return}}{\ln\left(\frac{\theta_{supply} - \theta_{in,air}}{\theta_{return} - \theta_{in,air}}\right)} \quad (3)$$

.

Table 3
The initial thermal boundary condition for the external wall and the glazed surfaces (Q_{trans}) used in this study.

Transmission losses						
Type of element	$\theta_{in,air}$	$\theta_{out,air}$	U_{trans}	A_{trans}	Q_{trans}	Case
	°C	°C	W/(m^2 °C)	m^2	W/m^2	
External wall	22	−12	0.25	6.6	−8.5	1, 2
Triple glazing, with argon gas between the panes and low emissive coating layer	22	−12	1.2	3.2	−40.8	and 3

2.3.3. Thermal radiation and turbulence model

Indoor airflow and thermal climate were analyzed employing the SIMPLE computational algorithm and second-order upwind scheme for all differential equations. Thermal radiation was predicted by the Discrete Ordinates (DO) radiation model. This model was available in FLUENT and can be used for heat-transferring problems ranging from surface-to-surface to participating radiation in combustion chambers. The DO radiation model is used when accurate prediction of the radiant temperature distribution inside an enclosure is of interest [19]. The Re-Normalization Group (RNG) turbulence model was employed to simulate indoor air movement. This turbulence model is similar in form to the standard k–ε model, but includes refinements that account for a low Reynolds number, which is preferable for indoor environment simulations. Chen [20] compared five different k–ε models and found that RNG showed better stability than others and recommended it for simulations of indoor airflow.

2.4. Comparison between CFD predictions and analytical calculations

The reliability of the CFD results was verified by comparison with several analytical models. CFD-predicted surface temperature of the glazing and the air velocity in the boundary layer next to it were matched up with analytical calculations. The mean air temperature at the centre of the inner glazed surface was calculated by Eq. (4). The downdraught velocity in the film layer at the centre of the glazing was estimated by Eq. (5) [18], where $H_{gl,\ surf}$ symbolized the characteristic glazing height above the centre-point. A more detailed and precise equation for calculation of downdraught air velocity next to a cold surface can be found in [21]. Calculation of the total heat-transfer coefficient ($h_{gl,\ surf}$) at the inner glazed surfaces is generally a complicated process that requires a climate laboratory, accurate measurements, and a rigorous mathematical approach. Thus, for this comparison, an average value of 7.6 W/(m^2 °C) was taken according to findings by others [13,15,22]. Additionally, predicted mean indoor air temperature was compared to that obtained by Eq. (6), where transmission and ventilation losses are expressed in watts. A good agreement between CFD-predicted and calculated values was found, as can be seen in Table 5. Obtained velocity magnitudes were also in line with experimental findings reported by Peng and Peterson [23], which were performed in a similar enclosure exposed to the same outdoor temperature as used in the current investigation.

$$\theta_{gl,surf} = \theta_{in,air} - \frac{U_{trans}}{h_{gl,surf}} \cdot (\theta_{in,air} - \theta_{out,air}) \quad (4)$$

$$v_{gl,air} = 0.1 \cdot \sqrt{\left(\theta_{in,air} - \theta_{gl,surf}\right) \cdot H_{gl,surf}} \quad (5)$$

$$\theta_{in,air} = \theta_{skr,surf} - \frac{\sum Q_{trans} + Q_{vent}}{\alpha_{tot} \cdot A_{skr}} \quad (6)$$

3. Results

3.1. Thermal comfort analysis

Draught is a common cause of complaints in ventilated spaces. It is defined as an unwanted local cooling of the body, and is a function of air temperature, mean air velocity and turbulence intensity. The percentage of occupants in an occupied space who may experience draught discomfort is assessed by a draught rating index that can be estimated by several different draught models. Three models were employed here to map draught risk. Vertical temperature and velocity profiles were also analyzed. Finally, radiant temperature

Table 4
Thermal properties of skirting boards and heat fluxes (P_{skr}) used as boundary conditions in this study.

Skirting heaters										
Thermal properties	$\theta_{in,\ air}$	$\theta_{out,\ air}$	θ_{supply}	θ_{return}	$\theta_{skr,\ surf}$	L_{skr}	A_{skr}	α_{tot}	Φ_{skr}	P_{skr}
	°C	°C	°C	°C	°C	m	m^2	$W/(m^2\,°C)$	W/m	W/m^2
Case 1	22	−12	40	34	37	18.2	2.73	10.13	22.7	152
Case 2	22	−12	45	40	42	12.9	1.94	10.63	32.1	214
Case 3	22	−12	55	44	49	9.1	1.37	11.23	45.6	304

variation was investigated in order to evaluate its impact on perceived thermal comfort.

3.1.1. Temperature and velocity variations

CFD simulations showed that skirting heaters, served by low-temperature supply water, were fully able to cover heat demand in the office room and to create an even heat distribution throughout the whole room. Indoor air temperature in all investigated cases remained between 21.5 and 22.1 °C in the entire occupied space with very small vertical variations. Vertical reference lines extending from the floor to ceiling at the centre ($x = 1.5$ m) of Glazing I, and at distance of 0.5, 1.0 and 2.0 m away (in z-direction) were used to show velocity and temperature profiles. Vertical temperature difference between head and ankle level was about 0.5 °C in all cases; see Figs. 5a, 6a and 7a. In Cases 1 and 2, upright heat distribution was the most uniform and very similar, while in Case 3 hot ambient air accumulated in the upper regions below the ceiling. This should not be surprising, since the surface temperature of the skirting heaters in Case 3 was higher than in the other two cases.

Numerical simulations also indicated that skirting heaters in Cases 1 and 2 were not powerful enough to fully overcome down-flow created by low outdoor temperature and large glazed surfaces. Thus air velocity at floor level in both cases was similar and ranged between 0.2 and 0.25 m/s. Only in Case 3 were the skirting heaters able to decrease velocity of the down-flow to the recommended level. For Case 2, air velocity at floor level remained almost constant regardless of the distance from glazed surfaces. For Cases 1 and 3, air velocity between 0.5 and 2.0 m from the glazing decreased by approximately 0.05 m/s, see Figs. 5b, 6b and 7b. The cooling effect due to high air velocity in Cases 1 and 2 was also observed in the vertical temperature profiles. The temperature difference between 0 and 0.3 m above the floor was about 0.2 °C. This may not be considered important, but the vertical temperature difference should be seen in relation to the total temperature variation between ankle and head level, which was around 0.5 °C. Temperature profiles also revealed the airflow pattern created by these two skirting heating systems. The highest temperature level 0.5 m away from the glazing was observed around 2.0 m above the floor. Later, at distances of 1.0 and 2.0 m away from the glazing, hot ambient air started to accumulate below the ceiling and began to cool and flow downwards. This airflow movement was observed for all skirting heating systems evaluated in the present study and is also commonly observed in rooms served by traditional radiator heating.

3.1.2. Draught risk

Commonly, draught discomfort in ventilated spaces is estimated by Eq. (7), where TI represents local turbulence intensity in percent. This Draught Rating (DR) model is included both in ASHRAE Standard 55 [24] and EN ISO 7730 [25]. Fanger and Christensen [26] presented Eq. (8) for prediction of Percentage Dissatisfied (PD) people due to draught. The equation refers to sedentary people occupying ventilated space with turbulence intensity ranging between 35 and 55%, having normal indoor clothing and exposed to indoor air velocity in the occupied zone. Berglund and Fobelets [27] put forward another mathematical model for predicting the Percentage Experiencing Draught (PED) for sedentary persons. Their study involved 50 normally clothed persons exposed to several simultaneous local thermal discomfort factors in an environment chamber. Turbulence intensity in their investigation was between 5.0 and 44%. All three draught models (DR, PD and PED) were defined as Custom Field Functions in FLUENT and employed to estimate rate of draught discomfort. According to EN ISO 7730, standard percentage dissatisfied due to draught should be less than 15% inside the occupied zone.

$$\mathrm{DR} = \left(3.143 + 0.3696 \cdot v_{\mathrm{in,air}} \cdot \mathrm{TI}\right) \cdot \left(34 - \theta_{\mathrm{in,air}}\right) \cdot \left(v_{\mathrm{in,air}} - 0.05\right)^{0.6223} \tag{7}$$

$$\mathrm{PD} = 13.8 \cdot 10^{3} \cdot \left[\left(\frac{v_{\mathrm{in,air}} - 0.04}{\theta_{\mathrm{in,air}} - 13.7} + 2.93 \cdot 10^{-2} \right)^{2} - 8.54 \cdot 10^{-4} \right] \tag{8}$$

$$\mathrm{PED} = 113 \cdot \left(v_{\mathrm{in,air}} - 0.05\right) - 2.15 \cdot \theta_{\mathrm{in,air}} + 46 \tag{9}$$

Horizontal lines, extending from the centrelines of glazed areas I and II, at the external wall to the opposite wall, at 0.1, 1.1 and 1.7 m above the floor, were used for construction of DR, PD and PED profiles. The comparison between three draught models for all three skirting heating systems is given in the diagrams presented in Figs. 8a, b, 9a, b and 10a, b. Although thermal skirting boards served by low-temperature supply showed difficulties in suppressing downdraught, the temperature of downdraught air was similar to that of ambient air. However, at 1.1 and 1.7 m above floor level, air velocity inside the occupied zone had markedly declined in all cases and did not significantly contribute to unpleasantness. The draught rate in these regions was less than 10%. Therefore DR, PD

Table 5
Comparison between CFD-predicted and analytically calculated magnitudes. The estimation point was at $x = 1.5$ m, $y = 1.3$ m, $z = 0.0$ m for the temperature, and $z = 0.05$ m for the velocity, with x giving room length, y giving room height and z giving room width.

	Indoor air temperature		Glazed surface temperature		Air velocity next to glazing	
	CFD	Analytical	CFD	Analytical	CFD	Analytical
	°C	°C	°C	°C	m/s	m/s
Case 1	21.8	21.9	16.0	16.5	0.26	0.23
Case 2	22.0	22.0	16.0	16.6	0.25	0.23
Case 3	22.1	22.1	16.0	16.7	0.15	0.23

and PED profiles at 1.1 and 1.7 m over the floor level were not shown in the diagrams below.

Eq. (8) gave higher percentage dissatisfied than Eqs. (7) and (9). The same phenomenon was also observed by Awbi [28] who concluded that the difference between PD and PED may be caused by a higher turbulence intensity used in the former. In contrast, the proportions of dissatisfied people predicted by DR and PED were very similar. Analyzing draught rating, temperature and velocity profiles for the whole office room, it was easily observed that highest draught risk occurred at ankle level. Cold outdoor environment, large and high glazed surfaces and relatively weak thermal power from the skirting heaters created high air velocity at ankle level that markedly contributed to higher thermal discomfort. In this part of the occupied zone the percentage dissatisfied due to draught ranged between 15 and 22% for Cases 1 and 2, depending on which draught model was used. CFD simulations also showed that the percentage of dissatisfied persons in front of Glazing II was about 5.0–8.0% higher than at Glazing I. A clear reason for this behaviour could not be established since vertical temperature and velocity variation in this part of the room was

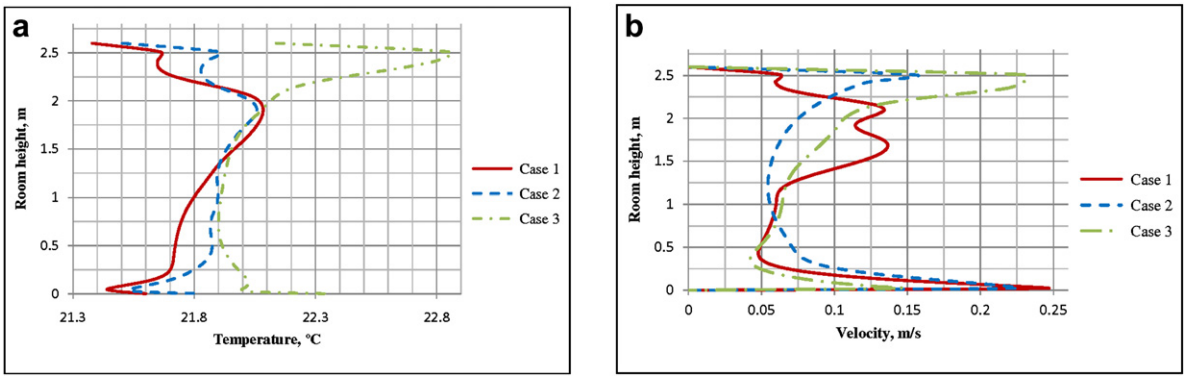

Fig. 5. (a and b) Vertical temperature and velocity profiles at $x = 1.5$ m, $\Delta y = 2.6$ m and $z = 0.5$ m (Glazing I).

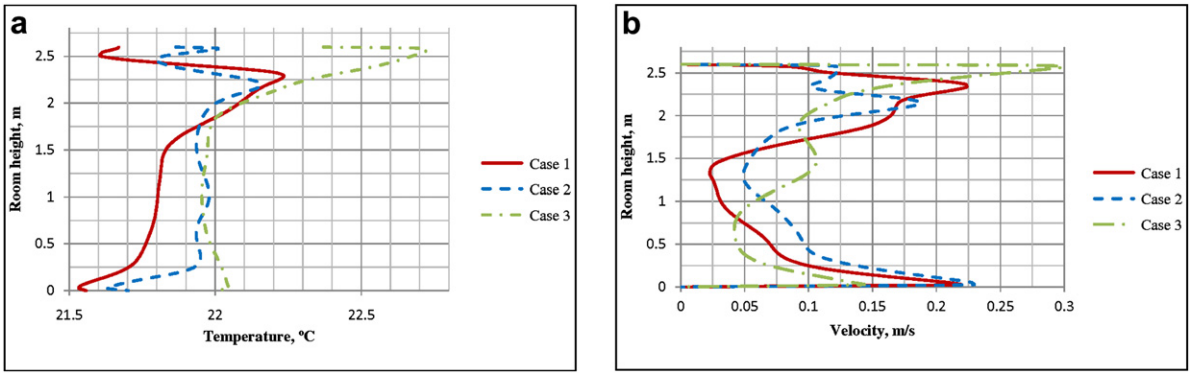

Fig. 6. (a and b) Vertical temperature and velocity profiles at $x = 1.5$ m, $\Delta y = 2.6$ m and $z = 1.0$ m (Glazing I).

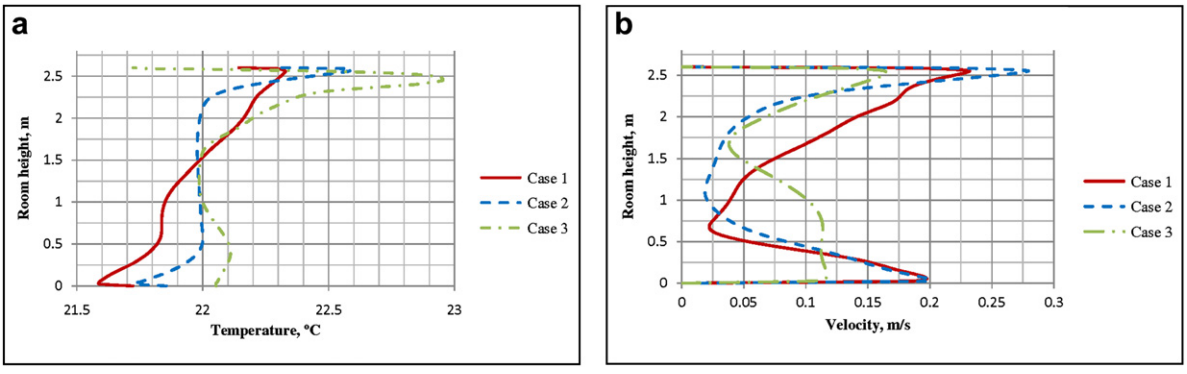

Fig. 7. (a and b) Vertical temperature and velocity profiles at $x = 1.5$ m, $\Delta y = 2.6$ m and $z = 2.0$ m (Glazing I).

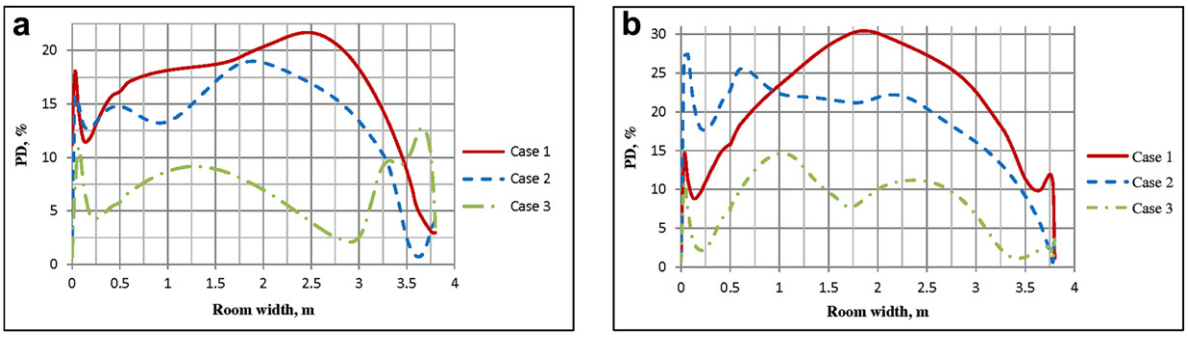

Fig. 8. (a) PD profile at $x = 1.5$ m, $y = 0.1$ m and $\Delta z = 3.8$ m (Glazing I). (b) PD profile at $x = 3.8$ m, $y = 0.1$ m and $\Delta z = 3.8$ m (Glazing II). Predictions were performed according at to Eq. (8).

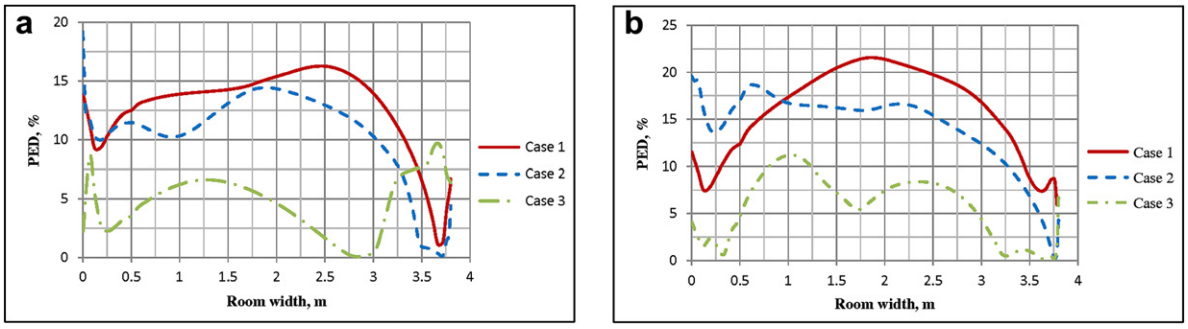

Fig. 9. (a) PED profile at $x = 1.5$ m, $y = 0.1$ m and $\Delta z = 3.8$ m (Glazing I). (b) PED profile at $x = 3.8$ m, $y = 0.1$ m and $\Delta z = 3.8$ m (Glazing II). Predictions were performed according to Eq. (9).

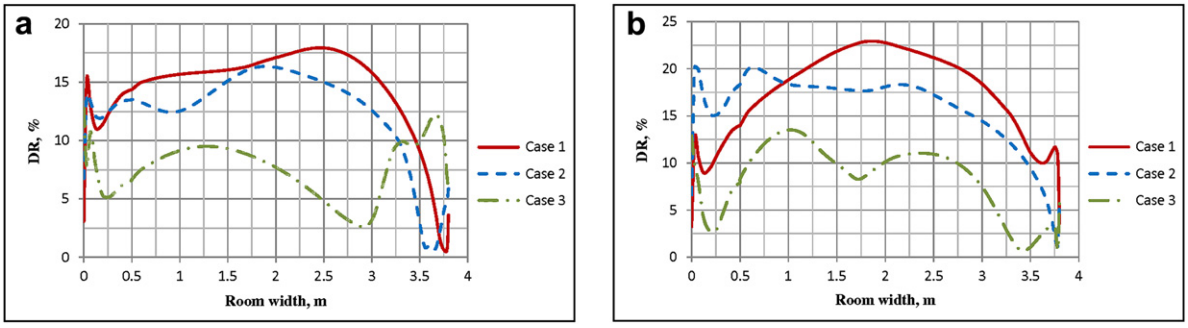

Fig. 10. (a) DR profile at $x = 1.5$ m, $y = 0.1$ m and $\Delta z = 3.8$ m (Glazing I). (b) DR profile at $x = 3.8$ m, $y = 0.1$ m and $\Delta z = 3.8$ m (Glazing II). Predictions were performed according to Eq. (7).

similar to those obtained near Glazing I. One possible explanation could be the complex interaction between indoor air temperature, velocity and turbulence intensity occurring in every point or region inside the room. Even if the heat and velocity distribution indoors was uniform, total symmetry can never be expected. It should be emphasized, however, that the shapes of the graphs for all three draught models were analogous. Outside the occupied space large thermal dissatisfaction was observed, probably caused by steep temperature gradients and high air velocity.

3.1.3. Thermal environment considerations

Usually, indoor thermal environment is described using operative temperature θ_{opr}. This analytical model is defined as mean temperature of the indoor air temperature and the mean surface temperature of surrounding walls $\overline{\theta}_{surf}$. Numerical simulations showed that the temperature of surrounding walls and ambient air was similar in all cases. Only at floor surfaces was a temperature variation of 1.0 °C between different skirting heating systems observed. Mean operative temperature and the temperature of the enclosing elements were also close and differed no more than 0.5 °C between the three cases. A detailed overview of CFD-predicted temperature levels inside the room is given in Table 6.

An additional factor influencing thermal sensation for occupants is radiant asymmetry. Variation of thermal radiant temperature in the present survey was demonstrated in a vertical section at the centre of Glazing II using Eq. (11). Contours obtained in this section are presented in Fig. 11a–c. The employed radiation model T_{rad} was available in FLUENT and defined as the temperature a body would have attained by absorbing the incident radiation assuming the body was black ($\varepsilon = 1.0$) [29]. Since in this work all enclosing elements of the room, including equipment inside it, were considered as gray bodies the emissivity factor ε was changed to 0.9. Thermal radiant temperature variation between the glazed surface and the back wall was around 4.0 °C for all skirting heating systems, and therefore did not additionally contribute to thermal discomfort. A more precise way to describe perceived indoor thermal comfort than using

Table 6
Mean inner surface temperatures of enclosing elements of the room, together with mean operative temperatures of the room.

	Mean inner surface temperature						Mean operative temperature
	Floor	Ceiling	External wall	Back wall	Left wall	Right wall	Room
	°C	°C	°C	°C	°C	°C	°C
Case 1	21.9	21.9	21.4	22.5	22.3	22.1	22.0
Case 2	22.9	22.0	21.3	22.1	22.2	22.2	22.1
Case 3	23.1	22.0	21.3	22.0	22.7	22.0	22.3

operative temperature can be obtained by Eq. (12). In contrast to operative temperature, comfort temperature considers the influence of indoor air velocity and the radiant temperature induced by heating or cooling equipment. A detailed comparison between operative and comfort temperature focusing on relative limitations and advantages in predicting the perceived thermal climate was made by Myhren and Holmberg [30]. In the current study, comfort temperature was used to illustrate thermal climate in a horizontal section placed 1.1 m above floor level, see Fig. 12a–c. Results confirmed that temperature distribution across both room width and length was uniform and ranged between 20–23 and 21.5–23 °C, respectively.

$$\theta_{opr} = \frac{\theta_{in,air} + \overline{\theta}_{surf}}{2} \tag{10}$$

$$T_{rad} = \left(\frac{G}{4\cdot\sigma}\right)^{1/4} \tag{11}$$

$$\theta_{comfort} = \frac{(T_{rad} - 273.15) + \theta_{in,air}\cdot\sqrt{10\cdot v_{in,air}}}{1 + \sqrt{10\cdot v_{in,air}}} \tag{12}$$

4. Discussion

Recently reported studies have indicated that various heating systems operating within the range of natural convection may sometimes have difficulty in overcoming strong downdraughts. In particular, heating systems with large heat-emitting surfaces (floor and wall heating) and low-temperature supply showed a weaker counteraction of downdraught compared to medium and high-temperature radiators [8,15]. Numerical and experimental investigations showed that air velocity at floor level in rooms served by large surface heaters ranges between 0.22 and 0.3 m/s. [8,23]. As a result, draught rating at floor level was considerably higher than in the rest of the room. This of course should be avoided since occupants are sensitive to cooling of feet and ankles. Usually, draught discomfort increases when the ambient air temperature decreases and the mean indoor air velocity and turbulence intensity increase, which is commonly the case in regions exposed to downdraught.

Comparable patterns were also observed in the current investigation. Thermal skirting boards, with large heat-transferring surface areas (Cases 1 and 2) served by low-temperature supply flow behaved in general like floor heating and also showed difficulties in suppressing strong downdraught. On the other hand, thermal skirtings installed along two adjoining walls and supplied by higher water temperature, performed similarly to medium-temperature radiators and managed to create a comfortable thermal climate at ankle level. CFD simulations also showed that skirting heating had similarities with both floor and radiator heating. Vertical temperature variation created by thermal skirting boards was comparable to that usually obtained by floor heating while airflow movement was like that commonly observed in rooms served by radiator heating. The ratio between convective and radiative parts (*C*:*R* ratio) of the total heat flux released from skirting heaters to the office room was roughly 45:55 in all cases. This was additional evidence that thermal skirting panels distribute heat in a similar way to floor or other typical low-temperature heating systems.

It should be emphasized that many possibly important and highly variable factors have been omitted from this study. The effect of global solar radiation on the indoor thermal conditions was disregarded. Also, air leakage (infiltration) and heat transfer (conduction) between tubes and skirting casting plates were omitted from consideration here. Further, the study was performed in an empty office room. In reality obstacles such as window sills, furniture, occupants and office-equipment have a major effect on the air and heat distribution inside a room. The influence of above-mentioned factors on indoor air movement and thermal transfer should be further investigated. Moreover, the temperature of supply and return flow varies along the skirting heater which has an impact on its overall heat output. Since the water flow inside the skirting tubes was not reproduced, a constant Logarithmic Mean Temperature Difference (LMTD) $\Delta\theta_m$ was applied to calculate thermal boundary conditions. The LMTD method is widely used in the design of heat exchangers because it gives an accurate representation of exponential temperature rise over the exchanger. It should also be noted that the outdoor temperature used in the current survey does not

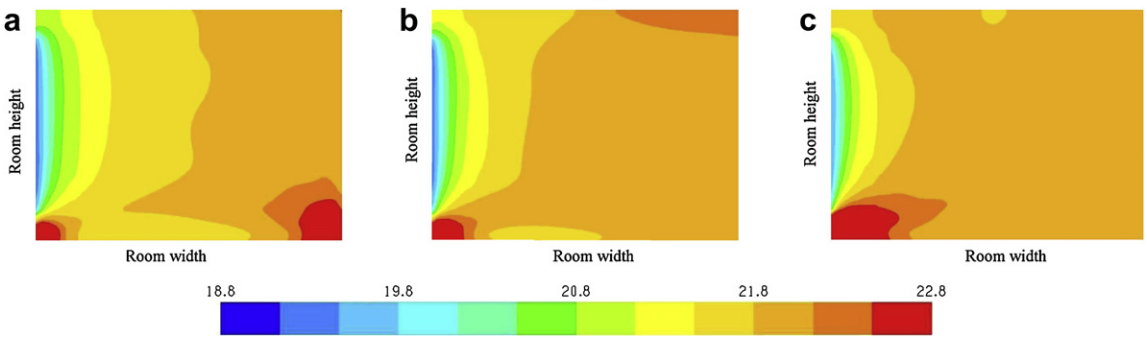

Fig. 11. (a) (Case 1), (b) (Case 2), and (c) (Case 3). Radiant temperature variation in a vertical section at the centre of Glazing II ($x = 3.8$ m).

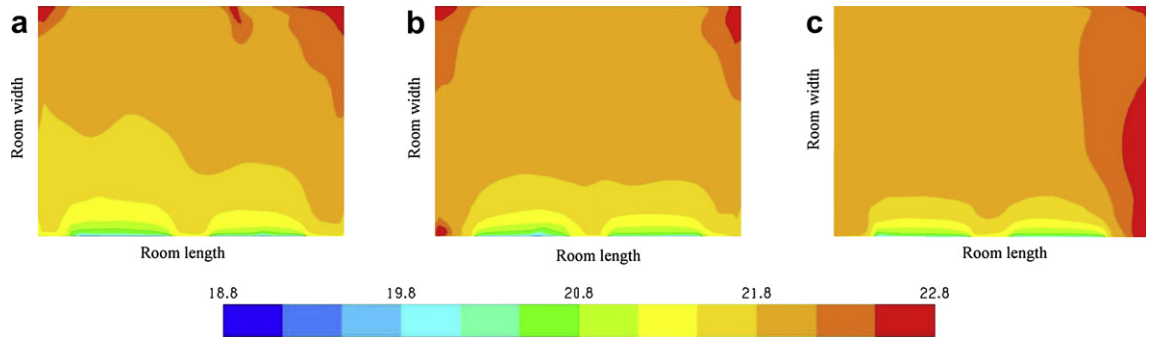

Fig. 12. (a) (Case 1), (b) (Case 2), and (c) (Case 3). Distribution of comfort temperature in a horizontal section 1.1 m above floor level ($y = 1.1$ m).

occur every day during the winter season in central Sweden, and should be considered as an extreme condition. However, the main goal of this investigation was to evaluate whether skirting heaters served by low-temperature supply could suppress strong downdraught and provide an acceptable level of thermal comfort in a modern office room. Therefore the design variables such as outdoor temperature, thermal properties of the enclosing elements, glazing size and heating configuration were prioritized here.

5. Conclusions

Based on the results obtained in the present work the following conclusions can be drawn:

1. Numerical simulations showed that thermal skirting boards, whether used along two, three or four walls, were able to cover transmission and ventilation heat losses in the office model. Vertical and horizontal temperature distribution inside the office was uniform in all cases. The temperature of the inner walls was also consistent and did not differ significantly from the temperature of the ambient air. Radiant temperature variation between glazed surfaces and their opposite walls was about 4.0 °C for all three skirting heating systems and did not contribute to thermal dissatisfaction. The most symmetrical heat distribution inside the room was observed in the case where thermal skirting boards were installed along three walls.
2. CFD results also showed that thermal skirting boards served by 40 and 45 °C supply flow could not markedly reduce air velocity at floor level induced by low outdoor temperature (−12 °C) and 2.0 m high glazed surfaces. Consequently the draught discomfort in the region inside the occupied zone was around or above 15% for these two cases. In contrast, heat-emitting skirtings supplied by 55 °C hot water showed better ability to suppress downdraught and the proportion of people sensing draught at 0.1 m above floor was low.
3. Thermal skirting boards supplied by low-temperature water flow should not be used in environments where outdoor temperature during the heating season is often lower than −10 °C. The thermal transmittance (U-factor) and the height of the glazing should be less than 1.2 W/(m^2 °C) and 2.0 m respectively, in spaces served by low-temperature skirting heating if extreme outdoor conditions during the winter period are expected.
4. Predicted percentage of dissatisfied people due to draught according to Eq. (8) (PD) was about 5.0% higher than that obtained by Eq. (7) (DR) and Eq. (9) (PED). The difference was probably the result of a higher rate of turbulence intensity used in the PD-model. The percentage of dissatisfied persons according to DR and PED models was almost the same. Since the PED model is considerably simpler than DR, it can be applied in situations where a prompt evaluation of draught risk inside a room is needed.
5. Thermal performance of heat-emitting skirtings with large transmitting surface areas and served by low-temperature supply flow needs to be improved in order to suppress strong downdraughts, particularly if the heating system is to be combined with heat pumps or other low-valued sustainable energy sources.

Acknowledgements

Financial support from the Swedish Energy Agency and the building industry group is gratefully acknowledged. The authors wish to thank Stephan Pitsch and Sven Alenius for help with CFD-modelling, and Heather Robertson for language correction.

References

[1] Juusela MA, editor. Heating and cooling with focus on increased energy efficiency and improved comfort. Guidebook to IEA ECBCS; 2004. ISBN 951-38-64-88-8 [annex 37].
[2] Myhren JA, Holmberg S. Design considerations with ventilation-radiators: comparisons to traditional two-panel radiators. Journal of Energy and Buildings 2008;41:92–100.
[3] Elmualim AA, Awbi HB, Fullford D, Wetterstad L. Performance evaluation of a wall mounted convector for pre-heating naturally ventilated spaces. Journal of Ventilation 2003;3(2):213–22.
[4] Babiak J, Olesen BW, Petras D. Low temperature heating and high temperature cooling. REHVA guidebook;, ISBN 2-9600468-6-2; 2007. p. 64–70 [chapter 6].
[5] Molin F, Holmberg S (supervisor). Radiators in low-temperature heating systems. Bachelor degree project, Royal Institute of Technology, School of Technology and Health in Stockholm; 2004 [in Swedish].
[6] Stålberg A, Holmberg S (supervisor). Ledges for building heating. Bachelor degree project, Royal Institute of Technology, School of Technology and Health in Stockholm; 2007 [in Swedish].
[7] Chen Q. Comfort and energy consumption analysis in buildings with radiant panels. Journal of Energy and Buildings 1989;14:287–97.
[8] Myhren JA, Holmberg S. Flow patterns and thermal comfort in a room with panel, floor and wall heating. Journal of Energy and Buildings 2008; 40:524–36.
[9] Omori T, Tanabe S, Akimoto T. Evaluation of thermal comfort and energy consumption in a room with different heating systems. In: Proceedings of 6th international conference in indoor air quality, ventilation and energy conservation in buildings, IAQVEC 2007; 2007.
[10] Omori T, Tanabe S. Coupled simulation of convection–radiation–thermoregulation for predicting human thermal sensation. In: Proceedings of 10th international conference on air distribution in rooms, Roomvent 2007; 2007.
[11] Ge H, Fazio P. Experimental investigation of cold draft induced by two different types of glazing panels in metal curtain walls. Journal of Building and Environment 2004;39:115–25.
[12] Moshfeg B, Larsson U. Experimental investigation of downdraught from well-insulated windows. Journal of Building and Environment 2002;37: 1073–82.
[13] Moshfeg B, Larsson U, Sandberg M. Thermal analysis of super insulated windows (numerical and experimental investigations). Journal of Energy and Buildings 1999;29:121–8.
[14] Rueegg T, Dorer V, Steinemann U. Must cold down draughts be compensated when using high insulating windows. Journal of Energy and Buildings 2001;33:489–93.

[15] Jurelionis A, Isevicius E. CFD predictions of indoor air movement induced by cold window surfaces. Journal of Civil Engineering and Management 2008;14:29–38.
[16] Ekberg L. Guidelines for specification of indoor climate requirements. BFS 1998:38;, ISBN 91-976271-0-0; 2006. p. 57 [in Swedish].
[17] McQuiston CF, Parker DJ, Spitler D. Heating, ventilating and air conditioning. 6th ed. American Society of Heating, Refrigerating and Air-Conditioning Engineers, ISBN 978-0-471-47015-1; 2004. p. 104 [chapter 4].
[18] Warfvinge C. HVAC technique for civil engineers. The Faculty of Engineering at Lund University; 2000. p. 1:5 [in Swedish].
[19] Braun S, Cremer I. Radiating warmth at a Raclette party, Fluent Germany, www.fluent.com/about/news/newsletters/04v13i2/a21.htm; 2004 [accessed 02.05.09].
[20] Chen Q. Comparison of different *k–e* models for indoor airflow computations. Journal of Numerical Heat Transfer 1995;28:353–69.
[21] Zukowski M. A new formula for determining a minimum recommended value of inlet air velocity from UFAD system to prevent occupants from draught risk. Journal of Building and Environment 2007;42:171–9.
[22] Griffin BT, Turler D, Arasteh D. Surface temperatures of insulated glazing units: infrared thermography laboratory measurements. ASHRAE Transactions 1996;102:2.
[23] Peng S, Peterson F. Convection from a cold window with simulated floor heating by means of a transiently heated flat unit. Journal of Energy and Buildings 1995;23:95–103.
[24] ASHRAE Standard 55-1992. Thermal environmental conditions for human occupancy. American Society of Heating, Refrigerating, and Air Conditioning Engineers; 1992.
[25] Olsen BW, Parsons KC. Introduction to thermal comfort standards and the proposed new version of ISO EN 7730. Journal of Energy and Buildings 2002;34:537–48.
[26] Fanger PO, Christensen NK. Perception of draught in ventilated spaces. Journal of Ergonomics 1986;29:215–35.
[27] Berglund L, Fobelets A. Subjective human response to low-level air currents and asymmetric radiation. ASHRAE Transactions 1987;93(1): 497–523.
[28] Awbi H. Ventilation of buildings. 2nd ed.;, ISBN 0-415-27055-3; 2003. p. 29 [chapter 1.5].
[29] Fluent 6.3 user's guide. Alphabetical listing of field variables and their definitions; 2009.
[30] Myhren JA, Holmberg S. Comfort temperatures and operative temperatures in an office with different heating methods. In: Proceedings of 8th International Conference on Healthy Buildings 2006, 2; 2006. p. 47–52.

Building and Environment 46 (2011) 176–186

Contents lists available at ScienceDirect

Building and Environment

journal homepage: www.elsevier.com/locate/buildenv

Low-temperature baseboard heaters with integrated air supply – An analytical and numerical investigation

Adnan Ploskić*, Sture Holmberg

Fluid and Climate Technology, School of Architecture and Built Environment, KTH, Marinens väg 30, SE-13640 Handen, Stockholm, Sweden

ARTICLE INFO

Article history:
Received 7 May 2010
Received in revised form
12 July 2010
Accepted 14 July 2010

Keywords:
Baseboard (skirting) heating
Low-temperature hydronic heating
Forced convective heat transfer
Channel airflow
Thermal comfort
CFD

ABSTRACT

The functioning of a hydronic baseboard heating system with integrated air supply was analyzed. The aim was to investigate thermal performance of the system when cold outdoor (ventilation) airflow was forced through the baseboard heater. The performance of the system was evaluated for different ventilation rates at typical outdoor temperatures during the Swedish winter season. Three different analytical models and Computational Fluid Dynamics (CFD) were used to predict the temperature rise of the airflow inside the baseboard heater. Good agreement between numerical (CFD) and analytical calculations was obtained. Calculations showed that it was fully possible to pre-heat the incoming airflow to the indoor temperature and to cover transmission losses, using 45 °C supply water flow. The analytical calculations also showed that the airflow per supply opening in the baseboard heater needed to be limited to 7.0 l/s due to pressure losses inside the channel. At this ventilation rate, the integrated system with one air supply gave about 2.1 more heat output than a conventional baseboard heating system. CFD simulations also showed that the integrated system was capable of countering downdraught created by 2.0 m high glazed areas and a cold outdoor environment. Draught discomfort in the case with the conventional system was slightly above the recommended upper limit, but heat distribution across whole analyzed office space was uniform for both heating systems. It was concluded that low-temperature baseboard heating systems with integrated air supply can meet both international comfort requirements, and lead to energy savings in cold climates.

1. Introduction

Water-based (hydronic) thermal devices are predominantly used for internal heat emission within the residential sector and office buildings in Europe. Although the design of the thermal units is similar the variation of the supply water temperature is high among the European countries, ranging from 55 to 90 °C for radiator/convector heating [1] and from 35 to 45 °C for floor heating [2]. Generally hydronic heating systems are classified by their supply water temperature. Heaters supplied by 75–90 °C water flow are normally considered as high-temperature systems while 55 and 45 °C supply flows are used in medium and low-temperature heating systems, respectively. Thermal energy for the heating systems can be produced by several different methods. The most energy efficient and sustainable technical solution may be to combine a heating system with a low-valued energy device such as a heat pump. To make this integration efficient the supply water temperature to the heating units should be lower than 50 °C. Recent studies have shown that different kinds of heating arrangements supplied with 45 °C water flow were fully able to cover transmission and ventilation heat losses of modern buildings [3,4]. Low-temperature heat emitters showed many advantages, such as energy savings and ability to generally create a good indoor thermal climate, but also a weakness in countering cold air downflow (downdraught) [3,4]. Usually, the thermal energy supplied by the conventional low-temperature heating systems is mainly emitted by the thermal radiation. Natural convection is also present but its influence on air movement is much weaker than in traditional high-temperature heating systems where natural convection accounts for the main part of total heat emission. Weak convective power among low-temperature heating systems is probably the main reason for problems with cold downdraught. Cold air downflow, normally caused by low outdoor temperature and large areas of glazing, could be blocked by directing the warm ventilation airflow towards the glazed surfaces. This technical arrangement might also be a solution to the elimination of cold draughts in spaces served by low-temperature heating systems.

* Corresponding author. Tel.: +46 8 790 48 84; fax: +46 8 790 48 00.
E-mail address: adnan.ploskic@byv.kth.se (A. Ploskić).

0360-1323/$ – see front matter © 2010 Elsevier Ltd. All rights reserved.
doi:10.1016/j.buildenv.2010.07.011

Nomenclature

Latin letters

A_c	Cross-sectional area of baseboard channel [m^2]
A_s	Inner surface area of baseboard channel [m^2]
$c_{P_{air}}$	Specific heat capacity of air, 1005 used in study [J/(kg °C)]
$c_{P_{water}}$	Specific heat capacity of water, 4180 used in study [J/(kg °C)]
D_h	Hydraulic diameter of baseboard channel [m^2]
f	Friction factor between air and inner channel surfaces [−]
g	Gravitational acceleration, 9.81 used in study [m/s^2]
Gr	Grashof number [−]
L	Baseboard channel or plate length [m]
$\dot{m}_{air}$	Air mass flow [kg/s]
$\dot{m}_{water}$	Water mass flow [kg/s]
Nu	Nusselt number [−]
P	Inner perimeter of baseboard channel [m]
p_{air}	Atmospheric pressure, 101 325 used in study [Pa]
$P_{ext.wall}$	Transmission loss through external wall [W]
$P_{glazing}$	Transmission loss through glazed areas [W]
Pr	Prandtl number [−]
P_{vent}	Ventilation heat demand [W]
Q_{vent}	Ventilation flow rate per person [l/s/prs]
Re	Reynolds number [−]
R_{air}	Specific gas constant for dry air, 287 used in study [J/(kg °C)]
T_{mbt}	Absolute mean air bulk temperature [K]
T_s	Absolute mean surface (baseboard) temperature [K]
v_{air}	Mean air velocity inside baseboard channel [m/s]
$v_{air,in}$	Indoor air velocity [m/s]
U-value	Total thermal transmittance [W/(m^2 °C)]
x, y, z	Cartesian coordinates [m]

Greek letters

α_{air}	Mean air-side convective heat transfer coefficient [W/(m^2 °C)]
α_{water}	Mean water-side convective heat transfer coefficient [W/(m^2 °C)]
β_{air}	Mean air thermal expansion [1/°C]
$\theta_{air,in}$	Mean indoor air temperature [°C]
$\theta_{air,out}$	Mean outdoor air temperature [°C]
$\theta_{comfort}$	Comfort temperature [°C]
$\Delta\theta_{lmtd}$	Logarithmic mean temperature difference [°C]
Δp	Pressure loss [Pa]
θ_{mbt}	Mean air bulk temperature [°C]
θ_s	Mean surface (baseboard) temperature [°C]
$\theta_{water,in}$	Mean supply water flow temperature [°C]
$\theta_{water,out}$	Mean return water flow temperature [°C]
θ_{rad}	Radiation temperature [°C]
λ_{air}	Air thermal conductivity [W/m °C]
μ_{air}	Air dynamic (absolute) viscosity [kg/m s]
ρ_{air}	Mean air density [kg/m^3]

Pre-heating of the ventilation air can be arranged in several ways. One method is to force it along or through a heating unit. This heating–ventilation arrangement may not only pre-heat the ventilating air but also enhance the total heat transfer from the heating unit. The higher the air velocity inside the unit, the higher the heat output will be. Furthermore, the greater the temperature difference between the cold incoming air and the heating unit, the higher the heat flow to the air will be. Consequently, the supply water temperature to the heater can be lowered without affecting over-all thermal performance, which will most likely result in energy savings. This technical design can be achieved by forcing cold outdoor (ventilation) airflow throughout a baseboard (skirting) heater. The idea is to lead the cold outdoor airflow via one or more openings in the building structure to the baseboard radiator. The incoming air is then pre-heated in the narrow horizontal baseboard channel before it exits throughout the slot opening at the top. The warm airflow is then directed towards glazed areas to meet air down-flow crated by cold glazed surfaces. By these means the negative effects of downdraught might also be reduced in spaces served by low-temperature heating systems. The general principle of baseboard heating–ventilation system is illustrated in Fig. 1(a) and (b). In general, conventional baseboard radiators are

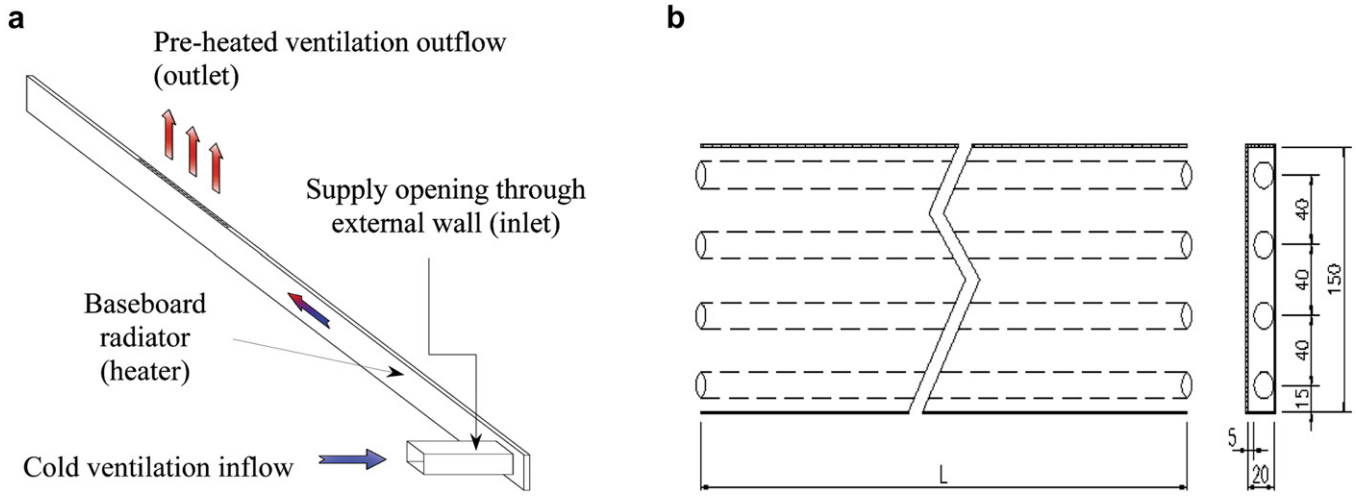

Fig. 1. (a) General illustration of integrated baseboard heating system with one air supply. (b) Elevation (left) and section (right) of the four-pipe baseboard radiator system. The channel consists of two feed and two return water heated pipes enclosed by thin metal plates. Dimensions are given in millimetres.

long and low-profile heat-emitting panels installed at the bottom of walls along all or most of the inner periphery of a room. More detailed information about such heating systems was given by Ploskić and Holmberg [3].

The aim of this study was to estimate whether the suggested baseboard heating–ventilation system was powerful enough to:

- cover transmission losses of an office room,
- pre-heat outside ventilation air to the room temperature,
- create a draught-free indoor climate

at supply water temperatures lower than 50 °C during Swedish winter conditions. The investigation also included a comparison in thermal performance between conventional and proposed baseboard heating systems.

1.1. Previous studies

A similar heating–ventilation system was analyzed by Myhren and Holmberg [5]. The main goal of their investigation was to map the interaction between a conventional two-panel radiator and ventilation air supply. The thermal performance of such a system was evaluated at air velocities of 0.35 and 0.7 m/s between the panels. It was found that the ventilation–radiator supplied with low-temperature water flow had roughly the same heat output as the conventional high-temperature radiator. Computational Fluid Dynamics (CFD) was also employed to analyze the heat distribution inside the room. Simulations showed that the ventilation–radiator created a uniform heat distribution throughout whole room without downdraught. Elmualim et al. [6] studied the performance of a wall-mounted air supply convector installed underneath the window in a naturally ventilated test laboratory during winter conditions. The incoming outdoor airflow at a constant rate was pre-heated by various temperature levels of water circulating inside the convector coil. They concluded that this heating–ventilation system installed at a low level could increase the ventilation efficiency of the room and eliminate the problems with cold draught. The reported average indoor air temperature was lower than recommended by international standards but in line with design temperatures. Jurelionis and Isevicius [7] investigated the behaviour of cold downdraught caused by different types of glazing in various winter conditions. According to their CFD results, problems with cold draught may also appear in rooms with 2.0 m high super-insulating (U-value = 1.0 W/m^2 °C) glazing at outdoor temperature of −6.0 °C if no heating equipment underneath the glazing is installed. CFD predictions also showed that a conventional low-profile heating convector was insufficient to suppress cold draught induced by 5.0 m high glazing and −20 °C external temperature. Despite the low U-value glazing and a powerful heating device used in this case, the air speed at ankle level inside the occupied zone was twice as high as recommended by current international norms. They concluded that the best way to suppress strong downdraught was to counter it with a warm air jet of 1.0 m/s. Zukowski [8] put forward an analytical model for predicting a minimum required air jet velocity to block downdraught. According to his model, an air velocity of 0.5 m/s was needed to suppress cold downdraught created by 2.0 m high glazing and −20 °C outside temperature. The U-factor of the glazing was 1.0 W/m^2 °C in this case. The analytical findings were also tested using CFD simulations. These showed that draught discomfort inside the occupied zone was below the allowed upper limit according to international standards. The temperature of air jets used in CFD models was 7.0–8.0 °C higher than the room temperature. Gan and Awbi [9] used CFD to study air movement and heat distribution inside a room with one 1.5 m high single-pane glazing exposed to outdoor temperature of 10 °C. In order to create a draught-free climate they used an air jet of 1.1 m/s to meet cold air down-flow. The temperature of the jet was 5.5 °C higher than the indoor temperature. Jägbeck et al. [10] reported results based on field indoor climate measurements and extensive interviews with occupants in spaces with different heating arrangements. Their general conclusion was that forced air-heating systems provided a draught-free indoor climate. The supply air temperatures in their investigation were around 23–24 °C, while the air velocity ranged between 0.8 and 1.1 m/s. Based on the above findings two different conclusions can be drawn. First, the combined heating–ventilation system significantly improved thermal power from the heating unit. Second, the most efficient way to neutralize the cold downward airflow was to mix it with warm air jet. Therefore, the proposed integration of baseboard radiator and ventilation air supply seemed to be well-founded.

2. Method

The main focus of the first part of the study was to analyze the heat transfer inside the baseboard channel. Detailed explanation of all governing parameters and the theoretical background to the analytical models used for analysis is presented. Both analytical models and numerical (CFD) simulations were employed to predict the temperature rise of airflow inside the baseboard channel. Ventilation rates were modeled in accordance with national and international recommendations of minimum fresh air requirement for office users, of 7.0–10 l/s per person [11,12]. The performance of the system was evaluated for the Swedish winter climate. According to the Swedish Meteorological and Hydrological Institute (SMHI), the mean outside temperature during the coldest months of the year (December, January and February) for the entire country is around −6.0 °C [13]. The design external temperature, representing extreme outdoor condition in central Sweden is about −12 °C [14]. Both temperature levels as inflow boundary conditions were used here. In the second part of the study, CFD simulations were used to analyze thermal climate inside the room for both the proposed and the conventional baseboard heating systems.

2.1. Heat exchange between baseboard channel and air supply

Thermal exchange between heated parts of the baseboard channel and cold air supply, as illustrated by Fig. 1(a) and (b), was estimated by the energy balance as shown in Equation (1).

$$\underbrace{\dot{m}_{\mathrm{air}}\cdot c_{\mathrm{P_{air}}}\cdot\left(\theta_{\mathrm{air,out}}-\theta_{\mathrm{air,in}}\right)}_{\text{Ventilation heat demand}}=\underbrace{\dot{m}_{\mathrm{water}}\cdot c_{\mathrm{P_{water}}}\cdot\left(\theta_{\mathrm{water,in}}-\theta_{\mathrm{water,out}}\right)}_{\text{Water heat supply}}$$
$$\approx\underbrace{\left(\frac{1}{\alpha_{\mathrm{water}}}+\frac{1}{\alpha_{\mathrm{air}}}\right)^{-1}\cdot A_{\mathrm{s}}\cdot\Delta\theta_{\mathrm{lmtd}}}_{\text{Water–air heat exchange}} \quad (1)$$

The first part of Equation (1) represents the heat energy required to bring airflow from outside up to indoor temperature. The middle part represents the thermal energy produced by circulating water inside the baseboard pipes, while the last (third) part refers to heat flow from hot water to the cold airflow. The four parameters in the last part of Equation (1) represent respectively, the rate of convective thermal transfer from water to walls α_{water} and between walls and the cold air supply α_{air}, the heat transmitting surface area A_{s} and the Logarithmic Mean Temperature Difference (LMTD)

$\Delta\theta_{lmtd}$. The average LMTD is usually used when designing heat exchangers because it gives an accurate representation of exponential temperature rise over the exchanger. Since both hot water flow and cold airflow move in the same direction inside the baseboard channel, LMTD for the parallel heat exchanger was used as shown in Equation (2).

$$\Delta\theta_{lmtd} = \frac{(\theta_{water,out} - \theta_{air,out}) - (\theta_{water,in} - \theta_{air,in})}{\ln\left(\frac{\theta_{water,out} - \theta_{air,out}}{\theta_{water,in} - \theta_{air,in}}\right)} = \frac{(\theta_{air,in} - \theta_{air,out})}{\ln\left(\frac{\theta_s - \theta_{air,out}}{\theta_s - \theta_{air,in}}\right)} \quad (2)$$

Different dimensionless numbers such as Reynolds number Re, Prandtl number Pr, Grashof number Gr, and Nusselt number were employed to calculate the magnitude of the total convective heat transfer coefficient. A practical implication of Equation (1), for the investigated application where $\alpha_{water} \gg \alpha_{air}$ and thermal resistance of the heated walls is negligible, is that total heat transfer is controlled by α_{air}. To illustrate this [15], a doubling of the water-side heat transfer coefficient (α_{water}) increases the over-all heat transfer coefficient only by approximately 2%. On the other hand a doubling of the air-side heat transfer coefficient (α_{air}) increases the over-all heat transfer coefficient by 93%. Therefore, the predicted over-all heat transfer coefficient values in this study were exclusively based on the air-side heat transfer coefficient.

In view of the fact that all four dimensionless numbers used here are temperature dependent, all calculations were approximated at mean air bulk temperature $\theta_{mbt} = (\theta_{air,in} + \theta_{air,out})/2$. The Reynolds number was also estimated at average air velocity (v_{air}) inside the channel as shown in Equation (3).

$$Re = \frac{v_{air} \cdot D_h \cdot \rho_{air}}{\mu_{air}} \quad (3)$$

Where $D_h = 4 \cdot A_c/P$, $\rho_{air} = p_{air}/R_{air} \cdot T_{mbt}$ and

$$\mu_{air} = 1.458 \cdot 10^{-6} \cdot \sqrt{T_{mbt}}/1 + 110.4/T_{mbt}$$

D_h represents the hydraulic diameter, A_c the area and P the perimeter of the channel cross-section. The air density ρ_{air} and dynamic viscosity μ_{air} were evaluated at absolute mean air bulk temperature T_{mbt} while the atmospheric pressure p_{air} and specific gas constant R_{air} were considered as constants. The above empirical relationships can be found in Ref. [16]. The Prandtl number was calculated using Equation (4) where the air thermal conductivity was estimated by the following expression $\lambda_{air} = 0.0241 \cdot (1 + 0.003 \cdot \theta_{mbt})$ [17].

$$Pr = \frac{c_{P_{air}} \cdot \mu_{air}}{\lambda_{air}} \quad (4)$$

In order to determine which Nusselt (heat transfer) correlations were most suitable to use for correct prediction of convective heat flow rate, the convection characteristics inside the channel required definition. Normally, this would be determined by evaluating the ratio between Reynolds and Grashof number. Generally, it is accepted that when $Gr/Re^2 \ll 1$, $Gr/Re^2 \approx 1$ and $Gr/Re^2 \gg 1$, convection is forced, mixed and natural (free), respectively. The magnitude of the Grashof number was calculated by Equation (5) where the rate of air thermal expansion was estimated using following relation $\beta_{air} = 1/T_{mbt}$.

$$Gr = g \cdot \beta_{air} \cdot (\theta_s - \theta_{mbt}) \cdot D_h^3 \cdot \left(\frac{\mu_{air}}{\rho_{air}}\right)^{-2} \quad (5)$$

The analytical calculations showed that the Prandtl number was 0.715 and that the Reynolds number varied from about 5060 to 8870, while the Gr/Re^2 ratio is ranged from 0.002 to 0.005 in all investigated airflows. It was clear that flow inside the baseboard channel was transitional-to-turbulent and that convection was forced. Therefore three well-known Nusselt relations appropriate for this convection and flow regime were employed to predict the temperature increase of the airflow inside the channel, and for comparison with CFD simulations.

$$Nu = 0.116 \cdot \left(Re^{2/3} - 125\right) \cdot Pr^{1/3} \cdot \left[1 + \left(\frac{D_h}{L}\right)^{2/3}\right] \cdot \left(\frac{T_{mbt}}{T_s}\right)^{3/8} \quad (6)$$

The Nusselt relation expressed by Equation (6) was developed by Hausen and is applicable for forced convective transitional flow regimes with constant heat flux. The equation is valid for $2300 < Re < 10^6$ and $0.6 < Pr < 500$ according to Ref. [17] while in Ref. [18] another range is suggested $2200 < Re < 10^4$ and $Pr > 0.6$.

Another widely used Nusselt relation (Equation (7)) for approximation of transitional and turbulent forced convective flows, that can be applied both for thermal situations with uniform wall temperature and constant wall heat flux [19] was put forwarded by Gnielinski [20]. This correlation is valid for $3000 < Re < 5 \cdot 10^6$ and $0.5 < Pr < 2000$ where flow friction inside the channel is evaluated by the following expression $f = (1.82 \cdot \log(Re) - 1.64)^{-2}$. The friction factor is applicable for prediction of turbulent flow losses inside smooth ducts for same Reynolds number range as the Nusselt relation.

$$Nu = \frac{(f/8) \cdot (Re - 1000) \cdot Pr}{1 + 12.7 \cdot \sqrt{(f/8)} \cdot \left(Pr^{2/3} - 1\right)} \cdot \left[1 + \left(\frac{D_h}{L}\right)^{2/3}\right] \cdot \left(\frac{T_{mbt}}{T_s}\right)^{3/8} \quad (7)$$

The last semi-empirical expression used here to estimate the level of the dimensionless heat transfer coefficient was the so-called Dittus–Boelter correlation [21], Equation (8). Originally this equation was developed for high turbulent forced convection flows based on experimental data covering $10^4 < Re < 1.2 \cdot 10^5$ and $0.7 < Pr < 120$, but it has been found that for fluids with relatively low viscosity ($\mu_{fluid} < 2 \cdot \mu_{water}$), as in this study, it can also be applied for flow regimes with Reynolds numbers down to 2300–3000 [22].

$$Nu = 0.023 \cdot Re^{4/5} \cdot Pr^{2/5} \cdot \left[1 + \left(\frac{D_h}{L}\right)^{2/3}\right] \cdot \left(\frac{T_{mbt}}{T_s}\right)^{3/8} \quad (8)$$

After the Nusselt number was computed, the total convective heat transfer coefficient between transmitting surfaces and the heat absorbing airflow could easily be approximated by the next relation $\alpha_{air} = Nu \cdot \lambda_{air}/D_h$. As it can be noticed, all three Nusselt relations used here consisted of three different elements. The first (main) part was developed to predict the heat transfer rate for long ducts where the internal flow is both fully thermodynamically and hydraulically developed, typically the expression applied for ducts with a length-to-hydraulic diameter ratio larger than 60. In view of the fact that the turbulent flow in short ducts, as was the case here, is often hydraulically developed but thermodynamically undeveloped, use of entrance correction factor $[1 + (D_h/L)^{2/3}]$ is recommended. The third (last) multiplier on the right side of the Nusselt equations was used to correct the variation of fluid properties between hot duct surfaces T_s and the mean airflow temperature at the channel centre T_{mbt}. In the literature various suggestions to the exponent n in $(T_{mbt}/T_s)^n$ ratio for $(T_s/T_{mbt}) > 1$ can be found. The usual recommendations for n for air heating are 0.25 [23], 0.36 [24]

and 0.45 [20]. However, for the investigated configuration in this study it was found that $n = 3/8$ gave best agreement with Equation (9) for a wide range of temperature variations. A more detailed explanation of this equation and both correction factors can be found in Ref. [25].

$$\left(\frac{T_s}{T_{mbt}}\right)^{-[0.3\,\log\left(\frac{T_s}{T_{mbt}}\right)+0.36]} = \left(\frac{T_{mbt}}{T_s}\right)^{n} \quad \text{where} \qquad n = 3/8 \quad \text{when } \frac{T_s}{T_{mbt}} > 1 \tag{9}$$

The aim of this study was to investigate whether a balance between transmission and ventilation heat losses and heat supply could be achieved at acceptable pressure loss. Therefore the upper limit for pressure loss inside the baseboard pipes was set between 80 and 100 Pa/m, which is also the usual practice in piping design. The total pressure loss was estimated by combination of Equations (1) and (10) where friction factor was evaluated using a previously presented expression in Equation (7). Equation (10) was also used for the estimation of airflow friction (pressure) losses inside the baseboard channel.

$$\Delta p = \left[f\frac{L}{D}\cdot\frac{\rho v^2}{2}\right]_{\text{pipes/channel}} \tag{10}$$

In order to make all presented equations and CFD modeling easier to handle, the following approximation was made. Since the total surface area of the vertical baseboard plate and its four attached pipes, (Fig. 1(b)), is the same as that of the inner channel shell area, the pipes were omitted from further consideration. So instead of a complex cross-section, a single rectangular channel 150 mm high and 20 mm wide was analyzed. A detailed overview of all calculated governing parameters also used in the CFD simulations is given in Table 1.

2.2. CFD model of baseboard channel

The CFD code Gambit (pre-processor) was used to create channel geometry and for computational grid (mesh) construction, while the Fluent 6.3 was utilized to post-process simulation results. A straight rectangular duct with one inlet and one outlet at the opposite side was analyzed. In order to create hydraulically fully developed flow before it entered the heated part of the channel, a 350 mm long ($10 \cdot D_h$) isothermal entrance length was modelled. Different airflow rates with corresponding uniform heat flux magnitudes P_{heat}, as illustrated in Table 1, were studied. The temperature of the cold air inflow was set to be the same for all cases while the temperature distribution inside the channel was predicted by CFD. The prediction was performed using second-order discretization scheme for all differential equations. The coupling between the pressure and velocity was handled by the Simple algorithm. The standard wall function was also applied for simulation of heat transfer and turbulence generation near the channel walls. Different non-uniform structured (hexahedral) mesh arrangements and turbulence models were tested and compared with analytical models. The computational grid inside the channel was not uniformly distributed. A refined grid was applied near all solid walls while an unrefined grid was arranged towards the centre of the channel. The transition from refined to unrefined grid was made gradually in a smooth way. The grid independence was checked by changing the grid density near solid walls as well as around the channel centre. Convergent solutions with consistent results were obtained in all cases regardless of which grid arrangement was applied. Nevertheless, it was found that a 5.0 mm wide wall cell, which was the first grid cell adjoined to solid walls, in combination with all available k–ε turbulence models in Flunet 6.3 gave best agreement with analytical calculations. The mean air temperature variation inside the baseboard channel calculated by different analytical equations and CFD simulations using the Re-Normalization Group (RNG) turbulence model is shown in Fig. 2(a)–(d).

2.3. The room model

The indoor thermal climate inside a two-person empty office space, served by the convectional baseboard heating system and the heating–ventilation system proposed here was investigated. The room model geometries are described in Fig. 3 and Table 2 where the dimensions are given in metres. The same room was previously used and validated against experimental data and analytical calculations, and a good agreement was found between CFD predicted, measured and calculated values for this room configuration [3].

The office room was considered as having one external wall with two frameless glazing areas. It was assumed that the whole wall surface area was exposed to an outdoor temperature of −12 °C. The mean U-values of the external wall and glazing areas were set to 0.25 and 1.2 W/m^2 °C, respectively. The other walls were regarded as thermally non-conducting (adiabatic) enclosing elements. In the simulations, the heat loss through glazed surfaces was set to 39.6 W/m^2, and 8.25 W/m^2 for the external wall. The transmission losses were estimated applying the calculation procedure reported in Ref. [3]. The ventilation air supply was modelled in two different ways. In the case with conventional baseboard heating, a square four-way radial diffuser positioned at the centre of the ceiling was used for air supply. The temperature of the supply air was held constant at 18 °C which was approximately 3.0 °C lower than the assumed room temperature. In the case of the proposed heating–ventilation system, supply air temperature was calculated separately. The temperature profile of supply air was separately approximated by analytical models and CFD simulations, to be then used as a boundary condition in the room model. In this case, ventilation flow at two different rates was supplied via two slot openings placed underneath glazed areas I and II at the top of the baseboard heater I. The air jets from these two slot openings were directed towards glazed surfaces while the used indoor air was evacuated through an opening positioned in the upper corner at the opposite side of the external wall. The transmission losses of the

Table 1
The presented heat fluxes (P_{heat}) were used as thermal boundary conditions for CFD simulations. In all cases the heat flux magnitudes were adjusted to raise the temperature of the airflow from −6.0 to 21 °C using 45 °C supply and 40 °C return water flow.

	Q_{vent}, l/s/prs	v_{air}, m/s	D_h, mm	L, m	A_s, m^2	Pr, –	Re, –	Gr/Re^2, –	P_{heat}, W/m^2
Case 1	6.0	2.0	35.3	2.0	0.68	0.715	5066	0.005	401.6
Case 2	7.5	2.5	35.3	2.0	0.68	0.715	6332	0.003	501.9
Case 3	9.0	3.0	35.3	2.0	0.68	0.715	7598	0.002	602.4
Case 4	10.5	3.5	35.3	2.0	0.68	0.715	8865	0.002	702.8

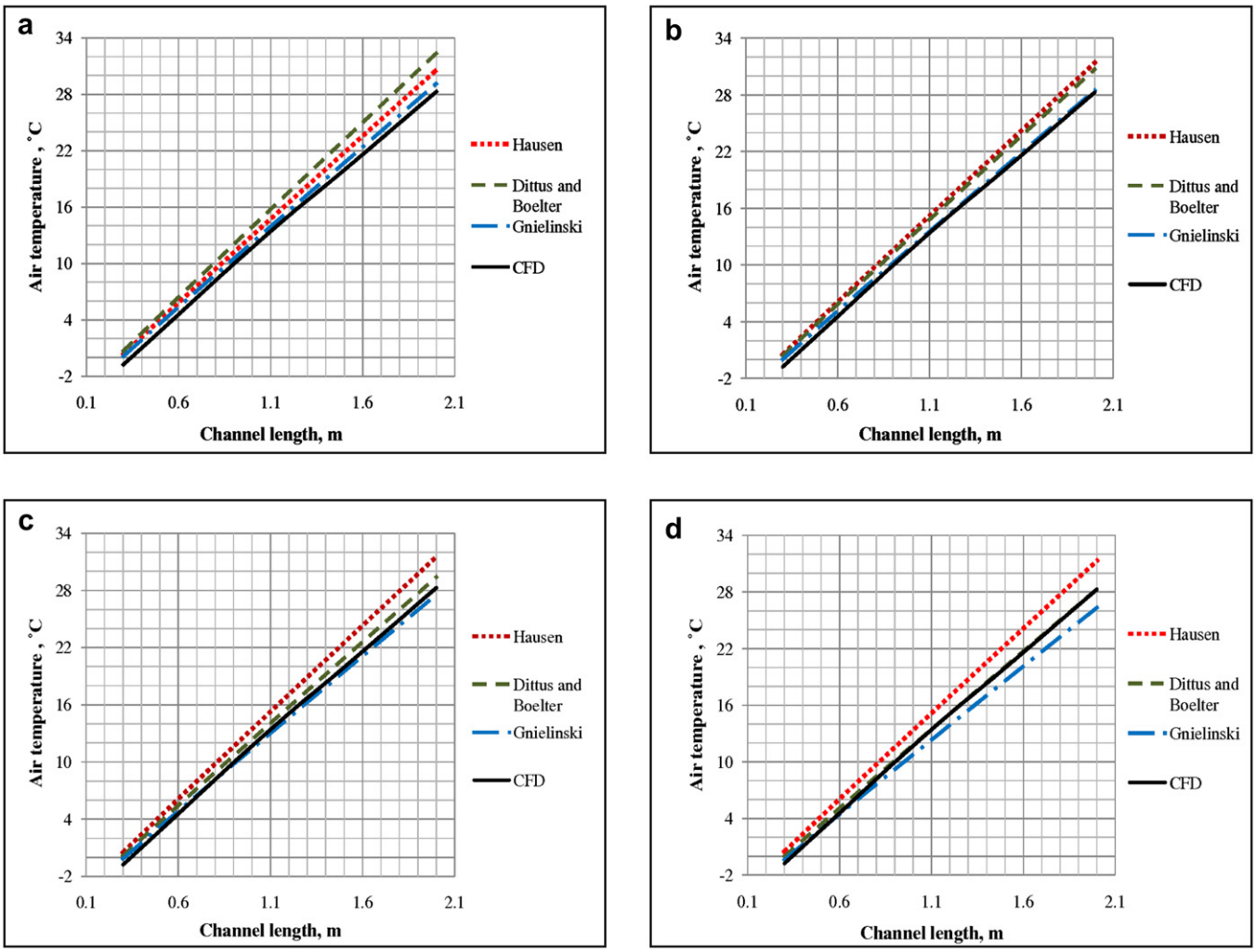

Fig. 2. (a) Mean air temperature variation inside the channel at 2.0 m/s. (b) Mean air temperature variation inside the channel at 2.5 m/s. (c) Mean air temperature variation inside the channel at 3.0 m/s. (d) Mean air temperature variation inside the channel at 3.5 m/s.

room were covered by the heat emission from baseboard heaters II and IV. The first computational grid point is set at 5.0 mm distance from all heat-emitting walls. This rate of near-wall grid refinement has been recommended for spaces with natural convection when standard wall functions are applied in order to obtain an accurate heat transfer prediction [26]. All other CFD settings previously presented in Section 2.2 were also employed here to analyze the thermal climate conditions. In addition, radiative heat exchange between transmitting surfaces of the room was simulated using a Discrete Ordinates (DO) radiation model. All room surfaces were assumed to be gray and have an emissivity factor ε of 0.9. All the investigated cases were simulated using the same CFD settings but different boundary conditions.

3. Results

Both analytical calculations and CFD simulations, as illustrated in Fig. 2(a)–(d), showed that it was fully possible to achieve a balance between ventilation thermal demand and heat supply with the proposed heating–ventilation system using 45 °C water

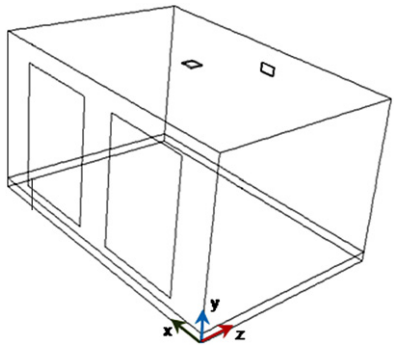

Fig. 3. The schematic view of the investigated office model.

Table 2
Dimensions of the office model and position of glazed surfaces, baseboard heaters, air intake and exhaust opening.

Item	Length	Width	Height	Location		
	Δx	Δz	Δy	x	y	z
Room	5.3	3.8	2.6	0.0	0.0	0.0
Glazing I	1.8	0.0	2.0	0.7	0.3	0.0
Glazing II	1.8	0.0	2.0	3.0	0.3	0.0
4-Way radial diffuser	0.24	0.24	0.02	2.65	2.58	1.9
Exhaust	0.3	0.02	0.15	2.65	2.23	3.8
Baseboard heater I	5.3	0.0	0.15	0.0	0.0	0.0
Baseboard heater II	0.0	3.8	0.15	0.0	0.0	0.0
Baseboard heater III	0.0	3.8	0.15	5.3	0.0	0.0
Baseboard heater IV	5.3	0.0	0.15	0.0	0.0	3.8

flow. In order to achieve this, the length-to-hydraulic diameter ratio should be around 44. In practice this means that the length of the baseboard channel should be approximately 1.55 m per air supply inlet. Fig. 2(a)–(d) also shows that the analytical model based on the Nusselt relation proposed by Gnielinski gave the best agreement with CFD. The other two models based on equations developed by Hausen and Dittus–Boelter showed generally a higher mean airflow temperature inside the baseboard channel compared to CFD. In this context it should also be mentioned that predicted air temperature rise based on Dittus–Boelter correlation agreed better with CFD for high Reynolds numbers, while the temperature increase calculated by the Hausen relation was roughly constant regardless of the air velocity level inside the channel. Since the analytical model established on the Nusselt expression proposed by Gnielinski showed the best agreement with CFD for the wide range of Reynolds number used here, it was utilized to demonstrate the variation of the Nusselt number as a function of the ratio between channel length and its hydraulic diameter (L/D_h) as shown in Fig. 4(a). The same model was also applied (Fig. 4(b)) to show the channel surface temperature required to pre-heat different airflow rates at various inlet conditions to the room temperature. The nonlinear lines in Fig. 4(a) illustrate the change of the Nusselt number while the straight diagonal lines represent the pressure loss increase along the baseboard duct. The total pressure loss including the duct in the building structure, channel changeover and baseboard channel, as illustrated in Fig. 1(a), was estimated by an extended version of the Equation (10), where the minor and the friction losses were calculated at the prevailing dynamic pressure inside the baseboard duct. The minor contraction loss coefficient was taken to be 0.43 [27]. Fig. 4(a) also shows that the heat transfer rate was highest for $L/D_h \leq 20$, after which the thermal exchange was nearly constant regardless of channel length. On the other hand the pressure loss grew rapidly across the channel with increased air velocity.

Airflow rates of 7.0 and 10 l/s at inlet temperatures of 0.0, −6.0 and −12 °C were used to test the performance of the proposed heating–ventilation system. Fig. 4(b) shows that the baseboard channel length in the case with air inflow of -12 °C needed to be about 29% longer compared to the inflow of 0.0 °C, to be able to raise its temperature to 21 °C. On the other hand, the channel length needed to be approximately 14% greater when air was brought in at -6.0 °C compared to 0.0 °C. Furthermore, in order to pre-heat the outdoor airflow of 10 l/s to room temperature, the channel length needed to be around 5.8% longer compared to the case with a ventilation rate of 7.0 l/s.

Table 3 presents the balance between ventilation heat demands, transmission losses and the heat supply for the different case scenarios. Results indicated that in some cases it was fully possible to cover both transmission and ventilation heat losses using low-temperature water supply. In the case with an airflow rate of 7.0 l/s at inlet temperature of −6.0 °C, the ventilation and transmission losses could be covered by a water supply at 45 °C. On the other hand, in the case with the same airflow at −12 °C, a water supply at 50 °C was required to cover both heat demands. The data presented in Table 3 was based on the assumption that air inflow entered via two intakes placed along the centre baseboard heater I. One intake was placed on the right hand side of glazing I while the other was placed at the left of the glazing II. Water flow temperatures and baseboard channel lengths required to cover ventilation heat losses were estimated by the model based on Gnielinski's heat transfer expression. Baseboard lengths (baseboard heaters II and IV) with corresponding water supply and return flow temperatures required to cover transmission losses were calculated using the expressions a for heat-emitting vertical plate. The set of equations for estimation of the total heat transfer from a vertical flat plate can be found in Ref. [5].

Heat output from baseboard heaters with one and two air supplies was also compared to the thermal power produced by the conventional baseboard radiator system (without air supplies). Dimensions of baseboard heater I were taken as reference. The calculation procedure was as follows. The total heat output for the integrated system was calculated in two steps. First, the magnitude of forced convection for the channel lengths (2×1.55 m) where the airflow is pre-heated was estimated. The contribution of natural convection and thermal radiation for this channel part facing the room was also included. Second, the remaining 2.2 m of baseboard length was treated as a vertical flat plate and the levels of natural convection and thermal radiation for this part were calculated. These were then added to heat output of channel parts with forced convection. In the case with a conventional system, the whole baseboard length (5.3 m) was seen as vertical flat plate, and the magnitudes of the natural convection and the thermal radiation for this arrangement were estimated in line with this assumption. The baseboard height of 0.15 m was kept constant both for integrated and the conventional systems during all calculations. The findings in Table 4 show that thermal emission from the integrated system

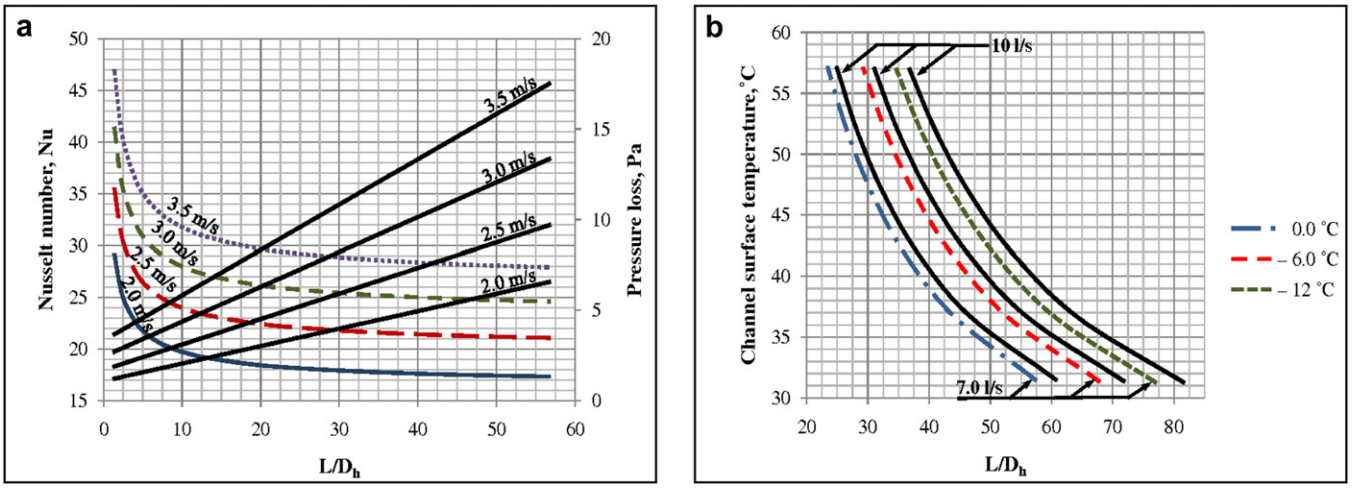

Fig. 4. (a) Variation of the Nusselt number and pressure loss as function of L/D_h ratio at different velocity levels. (b) The required baseboard channel surface temperature to pre-heat the outdoor air of 0.0, −6.0 and −12 °C to 21 °C at different ventilation rates.

Table 3
Ventilation and transmission heat losses for the two-person room configuration shown in Table 2. The supply and return water flow temperatures required to cover both heat demands are also given.

Item	Ventilation						Transmission			
	Heat demand			Heat supply			Heat demand		Heat supply	
	Q_{vent}, l/s/prs	Person	$\theta_{air,in}/\theta_{air,out}$, °C	P_{vent}, W	$\theta_{water,in}/\theta_{water,out}$, °C	L, m	$P_{glazing}$, W	$P_{ext.\ wall}$, W	$\theta_{water,in}/\theta_{water,out}$, °C	L, m
I	7.0	2	21/−6.0	478	45/40	2 × 1.55	233	45	45/36	9.1
II	10	2	21/−6.0	683	50/40	2 × 1.55	233	45	50/33	9.1
III	7.0	2	21/−12	590	50/45	2 × 1.55	285	54	50/39	9.1
IV	10	2	21/−12	843	55/45	2 × 1.55	285	54	55/36	9.1

with two air supplies (2 × 7.0 l/s) at total airflow rate of 14 l/s was about 3.3 times higher compared to the conventional system and around 4.0 times higher in the case with airflow of 20 l/s (10 l/s per supply intake). The amount of radiative and convective heat outputs per metre length for the conventional and integrated system with one air supply inlet is illustrated in Fig. 5. As it can be seen, the total heat output from the integrated system with single air supply at airflow of 7.0 l/s with inlet temperature of −6.0 °C was about 2.1 times higher compared to the conventional system. Forced and natural convection stood for nearly 80% of total heat emission in this case, while thermal radiation contributed with about 20%. In case with conventional system the proportion was quite different. Natural convection stood for about 46% of the overall heat release while thermal radiation contributed by approximately 54%. On the other hand, the system with two air supplies gave around 1.5 times more thermal power compared to the arrangement with one air supply under the same conditions.

3.1. Thermal comfort inside the office

Draught sensitivity of occupants in ventilated spaces is commonly estimated by Equation (11), where TI represents local turbulence intensity in percent. This Draught Rating (DR) expression is a result of empirical studies by Fanger et al. [28] and is included in ASHRAE Standard 55 [29] and EN ISO 7730 thermal comfort standard [30]. The model predicts the percentage of persons dissatisfied due to draught. This draught model was also used here to predict the rate of draught discomfort at 0.1 m above the floor level. According to EN ISO 7730 standard, the percentage of dissatisfied people due to draught should be less than 15% inside the occupied zone. The occupied zone is usually defined as the space where the occupants normally dwell and is commonly set 1.0 m away from the glazed areas, 0.6 m from the internal walls and between 0.1 and 1.8 m above floor level.

$$DR = (3.143 + 0.3696 \cdot v_{air,in} \cdot TI) \cdot (34 - \theta_{air,in}) \cdot (v_{air,in} - 0.05)^{0.6223} \quad (11)$$

As detailed in Section 2.3, three different ventilation case scenarios were simulated and compared. A conventional baseboard heating system where airflow of 20 l/s was supplied by a four-way radial square ceiling diffuser was compared to baseboard heaters with integrated air supplies. The performance of the integrated baseboard system at airflows of 20 and 14 l/s was analyzed. Two 0.5 m long and 20 mm wide slot openings positioned at the top of the baseboard I at the centre of glazings I and II were used for supply of pre-heated airflow to the room. The indoor flow patterns induced by air jets, of 1.0 m/s in the case with airflow of 20 l/s and of 0.7 m/s in the case with 14 l/s were investigated. The air jets in both cases were directed towards cold glazed areas of the room. The main goal of the comparison was to estimate the ability of each system to block cold downdraught and to create an acceptable thermal climate. Two straight horizontal lines positioned at 0.1 m above floor level and 0.5 m away from glazed areas I and II, and extending to the opposite wall were used for construction of DR profiles.

The draught rating profiles presented in Fig. 6(a) and (b) indicate that baseboard heaters with integrated air supplies were able to eliminate draught problems at the ankle level inside the occupied zone. The percentage of predicted draught discomfort at this level was less than 15% inside the occuped space. In the case with conventional baseboard radiators a slightly higher proportion of draught discomfort was observed. The draught rating for the region located between 1.0 and 2.8 m distant from the glazing II ranged from 18 to 15%. Also in front of glazing I the draught rating for the conventional system was slightly over the recommended limit. Apart from the draught rating index, the distribution of comfort

Table 4
The heat outputs produced by conventional and integrated baseboard heating system with two air supplies. Ventilation heat demands and temperature of the water flows (heat supply) are as previously shown in Table 3.

Baseboard heater I									
Design parameters				Conventional			With air supply		
				Natural convection and thermal radiation			Forced and natural convection + thermal radiation		
Item	$\theta_{water,in}/\theta_{water,out}$	L	H	Heat output			Heat output		
	°C	m	m	W/m	W/m^2	W	W/m	W/m^2	W
I	45/40	5.3	0.15	34.4	229	182	114	762	606
II	50/40	5.3	0.15	38.6	257	205	156	1041	828
III	50/45	5.3	0.15	44.1	294	234	147	982	781
IV	55/45	5.3	0.15	48.7	324	258	197	1311	1043

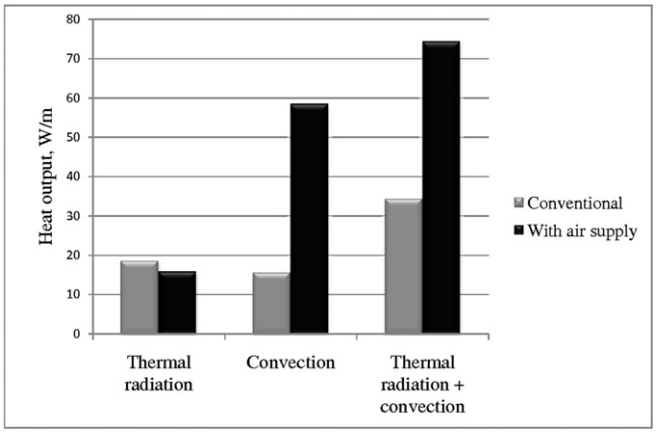

Fig. 5. Comparison of thermal radiation and convection heat outputs, for the conventional system and the integrated baseboard heating arrangement with one air supply inlet. An airflow of 7.0 l/s at −6.0 °C was used.

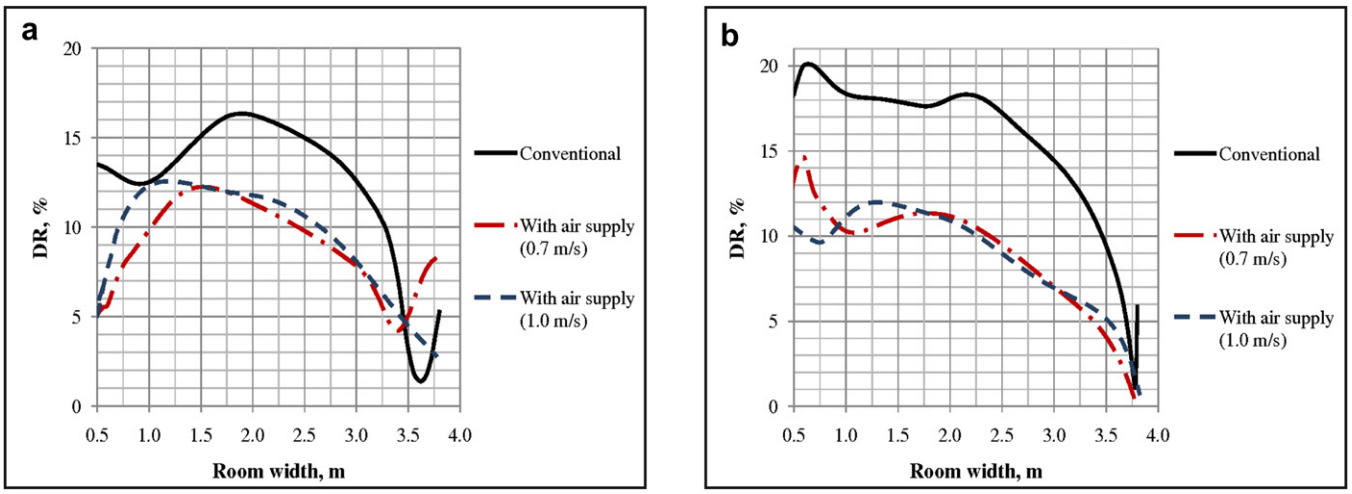

Fig. 6. (a) DR profiles at $x = 1.5$ m, $y = 0.1$ m and $\Delta z = 0.5–3.8$ m (glazing I). (b) DR profile at $x = 3.8$ m, $y = 0.1$ m and $\Delta z = 0.5–3.8$ m (glazing II).

temperature was also used to investigate thermal climate inside the studied room. Myhren and Holmberg [31] compared comfort temperature (Equation (12)) with operative temperature and concluded that this model gave a more comprehensive picture of perceived thermal climate. The mathematical expression used for calculation of radiant temperature in Equation (12) can be found in Ref. [3]. CFD simulations showed that the mean indoor air temperature ranged from 20.4 to 20.9 °C and the temperature stratification between the floor and ceiling was about 1.5 °C in all three cases.

$$\theta_{comfort} = \frac{\theta_{rad} + \theta_{air,in} \cdot \sqrt{10 \cdot v_{air,in}}}{1 + \sqrt{10 \cdot v_{air,in}}} \quad (12)$$

Simulations also confirmed that heat inside the whole office room was evenly distributed both with the conventional and proposed systems.

Fig. 7(a) and (b) shows heat distribution inside the office with an integrated baseboard system with airflow of 14 l/s (7.0 l/s per supply inlet). The red colour in the figures illustrates the placement of the heat-emitting baseboard panels. Two vertical sections intersecting glazed areas I and II, and two horizontal sections positioned 0.1 and 1.1 m above the floor, were used to demonstrate the variation of comfort temperature (heat distribution). Simulation results showed that temperature variation across the room length ranged from 20.2 to 21.3 °C, while the difference along the room height varied between 20 and 21 °C inside the occupied space for this case. The temperature scale in Fig. 7(a) and (b) was adjusted to give a readily apparent colour contrast for heat distribution inside the room, and a precise representation of glazing and baseboard surface temperatures was not prioritized. It should be mentioned that the temperature along width and length of glazed areas was uniformly distributed with an average variation of 0.5 °C. The mean surface temperature of glazings I and II was about 15.7 °C and 15.5 °C, respectively.

4. Discussion

Analytical and numerical (CFD) calculations estimated for an average Swedish outdoor winter temperature, showed that the baseboard heating system with integrated air supply was fully able to cover both transmission and ventilation heat losses using low-

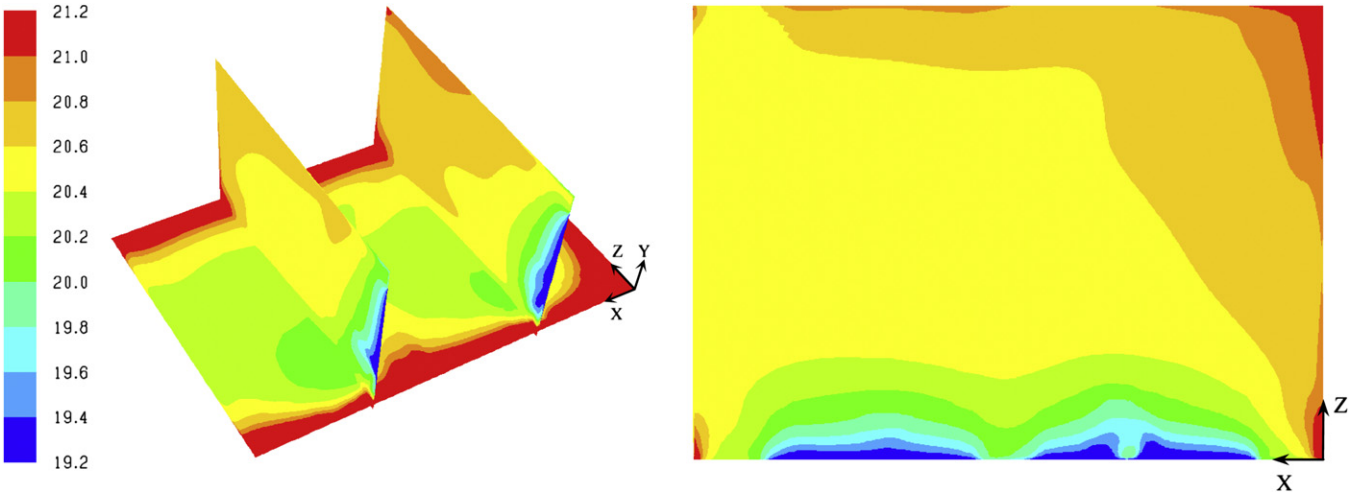

Fig. 7. (a) Comfort temperature distribution in vertical sections placed at $x = 1.5$ m (first from right) and at $x = 3.8$ m. Horizontal distribution is demonstrated in a plane positioned 0.1 m above the floor level. (b) The comfort temperature variation in a horizontal section placed at $x = 1.1$ m above floor level.

temperature water supply. The arrangement was also able to cover both these heat demands at design outdoor temperature in central Sweden, but in this case a water flow of 50 °C was required. This water temperature level is usually taken as an upper limit when designing heat pump systems. Thus, when the heat pump is forced to heat up the supply water to higher levels it starts to function approximately as an electrical boiler. Therefore a low supply temperature is essential for the heat pump's efficiency. For example, when the supply flow temperature in a hydronic heating system is lowered from 50 to 45 °C the heat pump energy efficiency increases by approximately 8.8% [5]. Although the proposed heating–ventilation baseboard system needed to operate at 50 °C water supply to pre-heat the outdoor airflow at design temperature, this condition should be regarded as an extreme external situation which would probably only occur for a few days during the heating season in central Sweden. Normally, the average outdoor temperature during Swedish winter period is around −6.0 °C, which means that system would often operate at water supply lower than 50 °C.

By forcing cold outdoor air through the baseboard heater two different effects were simultaneously achieved. The thermal efficiency of the heating unit was automatically increased and the outdoor ventilation air was directly heated inside the unit. Calculations showed that thermal power from the heater increased rapidly with change of convection characteristics. Turbulent forced convection inside the baseboard channel boosted the total heat output to more than twice that of the conventional system. Although heat transfer inside the heating unit increased rapidly with higher air velocity rates, so did pressure losses. Therefore excessive air speed levels should be avoided due to large increases in pressure loss. This would be particularly important in exhaust-ventilated buildings where the pressure difference between indoor and outdoor is the driving force for ventilation flow, and is normally around 10–15 Pa.

Calculations have also shown that total heat emission from the conventional system was fairly well balanced between convection and thermal radiation while in the integrated system heat was mainly transmitted by convection. Moreover, the integrated system might also contribute to healthier indoor environments since outdoor ventilation air entered via a short duct where potential of contamination was limited. This contrasts with the conventional approach where ventilation air is handled in a separate unit and distributed to the final users via long and complex ducts, which require professional maintenance. In this arrangement, heating is exclusively used to cover transmission losses and suppress cold draughts. The proposed integrated system both heats and ventilates at the same time.

Furthermore, in rooms served by heating systems where the energy is mostly transmitted by natural convection and thermal radiation, problems with cold feet (downdraught) are not unusual [3,4,7]. One way of solving this is to direct warm ventilation air towards the cold glazed areas of the room, as tested here using heating–ventilation baseboards. The predicted percentage of occupants experiencing draught discomfort at ankle level was under the upper limit recommended by international comfort standards [26,27]. All these findings confirmed that baseboards with air supply are not only energy efficient, but also a solution for creating a draught-free indoor environment.

5. Conclusions

Results presented in this work indicated that the proposed heating–ventilation baseboard system was able to cover both ventilation heat demand and transmission losses of a modern office room using low-temperature water flow. Apart from this, the proposed system efficiently countered cold downdraught. Moreover, the low energy requirement of the system made possible the utilization of low-valued sustainable energy sources such as heat-pumps. Some detailed conclusions are given below.

Both analytical and numerical (CFD) calculations showed that a baseboard heating system with integrated air supply served by 45 °C water flow was powerful enough to pre-heat the ventilation airflow of 7.0 l/s from -6.0 to 21 °C, with a baseboard channel length of approximately 1.55 m. Results also indicated that it was fully possible to pre-heat supply airflow of 10 l/s at −6.0 and −12 °C to room temperature using the same channel length, but that a supply water temperatures of 50 and 55 °C respectively, would then be required.

The airflow rate per supply inlet in the baseboard heater should not exceed 8.5 l/s and should preferably be limited to 7.0 l/s. Consequently, the internal channel air velocity should be around 2.3–2.8 m/s. At these air speed levels the baseboard heating–ventilation arrangement, with the cross-sectional geometry used here, was fully capable to pre-heat the outdoor airflow of 7.0–8.5 l/s at moderate channel pressure loss (5.0–7.1 Pa).

The baseboard heater with two air inlets gave about 1.5 times more heat power than the heater with one inlet, which gave approximately 2.1 times more thermal output than a conventional system (without air supplies) under the same conditions. By additional improvement of thermal transfer inside the heating unit both transmission and ventilation losses could be covered using two baseboard panels installed along the external wall and one internal wall. This might not only facilitate installation work, but also reduce the interface between the panels and furniture and save on material costs.

Of the total heat generated by the conventional system, around 54% was transmitted by thermal radiation and 46% by natural convection. On the other hand, about 80% of total heat energy produced by the integrated system with one air supply was transmitted by forced and natural convection but only around 20% by thermal radiation.

The conventional baseboard heating system served by 45 °C supply water showed weakness in suppressing cold downdraught. The predicted draught discomfort at ankle level inside the occupied zone was above 15%. In contrast, baseboard heating system with integrated air supplies showed better ability to block downdraught. The percentage of dissatisfied people due to draught at ankle height ranged from 5.0 to 13% in this case. Heat distribution inside the office room was uniform for both systems and the temperature variation across both room length and height was less than 1.5 °C.

Acknowledgements

Financial support from the Swedish Energy Agency and the building industry group is gratefully acknowledged. The authors also wish to thank Heather Robertson for language correction.

References

[1] Nilsson PE, editor. Achieving the desired indoor climate. ISBN 91-44-03235-8; 2003. pp. 468–484 [chapter 9].
[2] SP Technical Research Institute of Sweden, IEA Heat Pump Centre. Available from: http://www.heatpumpcentre.org/About_heat_pumps/HP_buildings.asp; 2010 [accessed 26.01.10].
[3] Ploskic A, Holmberg S. Heat emission from thermal skirting boards. Journal of Building and Environment 2010;45:1123–33.
[4] Myhren JA, Holmberg S. Flow patterns and thermal comfort in a room with panel, floor and wall heating. Journal of Energy and Buildings 2008;40:524–36.
[5] Myhren JA, Holmberg S. Design considerations with ventilation-radiators: comparisons to traditional two-panel radiators. Journal of Energy and Buildings 2008;41:92–100.
[6] Elmualim AA, Awbi HB, Fullford D, Wetterstad L. Performance evaluation of a wall mounted convector for pre-heating naturally ventilated spaces. Journal of Ventilation 2003;3(2):213–22.
[7] Jurelionis A, Isevicius E. CFD predictions of indoor air movement induced by cold window surfaces. Journal of Civil Engineering and Management 2008;14:29–38.

[8] Zukowski M. A new formula for determining a minimum recommended value of inlet air velocity from UFAD system to prevent occupants from draught risk. Journal of Building and Environment 2007;42:171–9.
[9] Gan G, Awbi HB. Numerical simulation of the indoor environment. Journal of Building and Environment 1994;29:449–59.
[10] Jägbeck PO, Werner G, Engwall K. Air heating systems in airtight multifamily residential builsings. Proceedings of 9th international conference on air infiltration and ventilation centre. AIVC 1988; 1988.
[11] Ekberg L. Guide lines for specification of indoor climate requirements. BFS 1998:38, ISBN 91-976271-0-0; 2006, pp. 57 (in Swedish).
[12] McQuiston CF, Parker Dj, Spitler JD. Heating, ventilating and air conditioning. ISBN 978-0-471-47015-1. 6th ed. American Society of Heating, Refrigerating and Air-Conditioning Engineers; 2004. pp. 104 [chapter 4].
[13] Swedish Meteorological and Hydrological Institute, Faktablad (Data sheet) no. 22, December 2004. Available from: http://www.smhi.se/sgn0102/n0205/faktablad_variationer_och_trender.pdf [accessed 05.02.10, in Swedish].
[14] Warfvinge C. HVAC technique for civil engineers. The Faculty of Engineering at Lund University; 2000. pp. 1–5 [in Swedish].
[15] Long CA. Essential heat transfer. ISBN 0-582-29279-4; 1999. pp. 272–275 [chapter 9].
[16] Çengel YA, Cimbala JM. Fluid mechanics fundamentals and applications. ISBN-13: 978-007-125764-0; 2006. pp. 49, 322–353 [chapters 2 and 8].
[17] Alvarez H. Energiteknik (Energy technology). ISBN 91-44-02894-6; 2003. pp. 360–374 [chapter 5.3, in Swedish].
[18] Young PL, Kandlikar SG. Surface roughness effects on heat transfer in micro-scale single phase flow: a critical review. Proceedings of 6th international conference ASME on Nanochannels. Microchannels and Minichannels ICNMM 2008; 2008.
[19] Sunden B. Värmeöverföring (Heat transfer). ISBN 91-44-00087-1; 2006. pp. 182–183 [chapter 9, in Swedish].
[20] Gnielinski V. New equations for heat and mass transfer in turbulent pipe and channel flow. Journal of International Chemical Engineering 1976;16:359–68.
[21] Dittus FW, Boelter LMK. Heat transfer in automobile radiators of the tubular type, vol. 2. University of California at Berkley. Publications on Engineering; 1930. pp. 443–461.
[22] Granryd E. Heat transfer – collection of formulas and tables of thermal properties. Department of Applied Thermodynamics and Refrigeration, The Royal Institute of Technology; 2005. pp. 14.
[23] Thome JR. Engineering databook III. LTCM-BOOK-2005-003; 2004. pp. 5–4 [chapter 5].
[24] Spang B. Correlations for convective heat transfer. The Chemical Engineers' Resource Page. Available from: http://www.cheresources.com/convection.shtml [accessed 13.10.09, chapters 1-3 and 1-4].
[25] Kakaç S, Hongtan L. Heat exchangers – selection, rating and thermal design. ISBN 0-8493-0902-6; 2002. pp. 89, 99–112 [chapters 3.2.3 and 3.5].
[26] Awbi HB. Calculation of convective heat transfer coefficient of room surfaces for natural convection. Journal of Energy and Buildings 1998;28:219–27.
[27] Pal R, Hwang CJ. Flow of two-phase oil/water mixture through sudden expansions and contractions. Journal of Chemical Engineering 1997;68:157–63.
[28] Fanger PO, Melikov AK, Hanzawa H, Ring J. Air turbulence and sensation of draught. Journal of Energy and Buildings 1988;12:21–39.
[29] ASHRAE Standard 55-1992. Thermal environmental conditions for human occupancy. American Society of Heating, Refrigerating, and Air Conditioning Engineers; 1992.
[30] ISO 7730. Moderate thermal environments. Determination of the PMV and PPD indices and specifications of the conditions for thermal comfort (ISO Standard 1997); 1997.
[31] Myhren JA, Holmberg S. Comfort temperatures and operative temperatures in an office with different heating methods. Proceedings of 8th International Conference on Healthy Buildings 2006;2:47–52.

Energy and Buildings 65 (2013) 248–259

Contents lists available at ScienceDirect

Energy and Buildings

journal homepage: www.elsevier.com/locate/enbuild

Low-temperature ventilation pre-heater in combination with conventional room heaters

Adnan Ploskić*, Sture Holmberg

KTH Royal Institute of Technology School of Architecture and Built Environment, Department of Civil and Architectural Engineering, Division of Fluid and Climate Technology, Brinellvägen 23, 10044 Stockholm, Sweden

ARTICLE INFO

Article history:
Received 18 October 2012
Received in revised form 4 February 2013
Accepted 28 April 2013

Keywords:
Low-temperature heating
Forced convective heat transfer
Transitional flow regime
Energy efficiency
Heat exchangers
Radiator heating
Ventilation
CFD

ABSTRACT

The main focus of the present study was to find design requirements for an air-heater that would be able to operate at low pressure loss and low-temperature water supply. The idea was to combine this low-temperature air-heater with existing radiator systems so that they can operate at similar low-temperature supply as used in floor heating systems. Results indicated that the proposed air-heater was able to lift the temperature of supply air at 10 l/s from −15 °C to 18.7 °C using 40 °C water supply. In addition, a thermal performance analysis showed that radiator systems equipped with the proposed air-heater could meet a space heat loss of 35.6 W per square meter floor area, using supply water of 40 °C. It was also shown that the heat pump efficiency in the hydronic system with proposed air-heater was 8–18% higher than in system without air-heater. All results in the present study were obtained by analytical (semi-empirical) and numerical (Computational Fluid Dynamics – CFD) calculations.

1. Introduction

1.1. Background

In 2009 Sweden stood for about half of the European heat pump market [1]. At that time approximately 20% of Swedish family homes were served by different kinds of heat pumps, while around 90% of newly built homes were heated by exhaust-air heat pumps [1]. The useful heat produced by the heat pumps or other systems was usually distributed by different types of hydronic room heaters in Swedish residential buildings [2]. In general, the efficiency of heat pumps is measured by their Coefficient of Performance (COP), which is the ratio between the consumed electrical power and the produced useful heat by the heat pump. The COP is mainly influenced by the temperature of the heat source and the temperature level of the supply water to the room heaters. The higher the heat source temperature and the lower the supply water temperature the higher the COP of the heat pump [3]. Temperature level of the heat sources such as brine, ground and exhaust-air is relatively stable during the heating season. On the other hand, the temperature level of the supply water to the room heaters depends on the heating demand of the building and the thermal efficiency of the heaters. Heat losses of modern buildings have constantly decreased over past decades due to better thermal insulation, which has greatly reduced their heating demand [4,5]. At the same time, as a result of continuous and goal-oriented research and development in heat pump technology, the COP of heat pumps has increased by approximately 2% per year since 1995 [1]. On the contrary, very little has been done on adapting the conventional convector and radiator systems for use with heat pumps. Conventional radiators and convectors are optimized to operate at high-temperature (75–90 °C) [6] water supply. This supply temperature range is not suitable for heat pumps because it decreases their COP-value significantly. In order to increase the COP of the heat pumps, the room heaters must operate with low-temperature (35–45 °C) [6] water supply. At the moment, these operating temperatures are normally used for room heaters with large transmitting surfaces such as floor heating. In order to use similar operating temperatures for conventional radiator/convector systems, their thermal efficiency must be improved. In addition, the low-temperature heating systems can also be combined with other arrangements that extract the heat from low-valued thermal sources besides the heat pumps [7]. Furthermore, the low-temperature heating systems could also contribute to reduction of heat losses in the distribution network of district heating due to reduced thermal gradients [8].

Taking all the above-mentioned into account it can be concluded that low-temperature heating systems have an energy saving potential. However, some other studies also indicate that

* Corresponding author. Tel.: +46 8 790 48 86; fax: +46 8 790 48 00.
E-mail address: adnan.ploskic@byv.kth.se (A. Ploskić).

0378-7788/$ – see front matter © 2013 Elsevier B.V. All rights reserved.
http://dx.doi.org/10.1016/j.enbuild.2013.04.011

Nomenclature

Latin letters

A	area (m^2)
c_P	specific heat capacity of: air (1006), water (4175) (J/(kg °C))
D	diameter (m)
d	outer diameter of pipe-loop of air-heater (m)
H	height (m)
f	flow friction factor between air and air-heater
L	length (m)
$\dot{m}$	mass flow (kg/s)
N	number of tube rows (piece)
Nu_D	$\equiv \alpha_{air} D/\lambda_{air}$ Nusselt number based on diameter D
Nu_d	$\equiv \alpha_{air} d/\lambda_{air}$ Nusselt number based on diameter d
P	total wetted perimeter of flow cross-section(s) (m)
Pr	Prandtl number at mean bulk temperature
Q	heat (thermal) loss/output/power/rate (W)
R	centreline radius (m)
Re_D	$\equiv D v_{air}/\upsilon_{air}$ Reynolds number based on diameter D and velocity v_{air}
$Re_{d,max}$	$\equiv d v_{max}/\upsilon_{air}$ Reynolds number based on diameter d and velocity v_{max}
S	distance between two consecutive tubes (m)
T	absolute (thermodynamic) temperature (K)
U-value	total thermal transmittance (W/(m^2 °C))
$\dot{V}$	volume flow (l/s)
v_{air}	mean air velocity (m/s)
v_{app}	mean approach air velocity outside tube bank (m/s)
v_{max}	$\equiv S_x v_{app}/(S_x - d)$ maximum air velocity in minimum flow area inside tube bank (m/s)

Greek letters

α	mean convective heat-transfer coefficient (W/(m^2 °C))
θ	mean temperature (°C)
$\Delta\theta$	temperature difference (°C)
Δp	pressure difference or pressure loss (Pa)
λ	thermal conductivity (at mean bulk temperature) (W/m °C)
υ	kinematic viscosity at mean bulk temperature (m^2/s)
ρ	density at mean bulk temperature (kg/m^3)
χ	correction factor for tube bank

Subscripts

air	air/air-side
ann	inside annular passage
bend	bending or bend
c	cross-sectional (flow area) of wall channel
c,i	inner coil
c,o	outer coil
cs	coil spring or inside coil spring
filter	filter
h	hydraulic
i	inner
in	inlet
lm	logarithmic mean
loss	loss
m	mass-weighted mean
mbt	mean bulk temperature
o	outer
out	outlet
pipe	inside pipe passage
tb	tube bank
tot	total
tube	tube
vertical	vertical tube rows inside tube bank
w	wall/wall opening
water	water/water-side
x	in x-direction, coordinate
y	in y-direction, coordinate
z	in z-direction, coordinate

radiant heaters may have problems in counteracting cold draught which may cause thermal discomfort, especially around the foot level [9,10]. Therefore, finding methods of increasing the heat output from different types of low-temperature hydronic radiators without compromising the perceived thermal comfort has in recent years been the main goal of research at the division of Fluid and Climate Technology at KTH Royal Institute of Technology in Stockholm.

1.1.1. Potential of local air supply heaters

In the past, many studies have been performed to find methods of increasing thermal efficiency of different room heaters and ways of reducing transmission heat losses from the buildings [4,7,11–15]. In contrast, very few studies have focused on exploring the possibility of pre-heating cold incoming supply air, using heating systems that are already in operation. One way to preheat the cold incoming air is to force it directly through an existing room heater. By this arrangement three different benefits can be simultaneously achieved. The temperature of the incoming airflow would be automatically raised, the heat output from the heater instantly improved and the potential for air contamination considerably reduced due to short ducting [16]. By forcing the entering supply air to pass through a room heater the convection character inside the heater would also change. The forced convection would dominate over the weaker natural convection which would considerably increase the internal convection heat transfer. In addition, large temperature difference between the heat-emitting surfaces of the room heater and the cold passing airflow would additionally increase the convective heat flow from the heater to the streaming air. As a result of this enhanced heat exchange, the supply water temperature to the heater can correspondingly be decreased without lowering its heat output. Consequently, the efficiency of the heat pumps connected to these combined heating-ventilation systems would be significantly increased.

The performance of such a combined system was analyzed by Myhren and Holmberg [17]. They investigated the effects of forced cold airflow through a hot double-panel radiator installed in an exhaust-ventilated room. The investigation was followed by another study where the major focus was on finding the methods for additional improvement of internal convective heat transfer by rearrangement of the inner fin design inside the radiator [18]. The performance of the radiators in both studies was evaluated at water supply temperatures of 35–40 °C and airflows of 7–10 l/s at −5 and 0 °C. The general conclusion from the studies was that internal forced airflow roughly doubled the radiator heat output. A similar study was performed by Ploskic and Holmberg [19] who analyzed the effects of forced airflow through a baseboard radiator. The investigation showed that incoming airflow of 10 l/s at −6 °C could be heated to 21 °C by water supply of 45 °C. Elmualim et al. [20] investigated the performance of a wall-mounted vent-convector (air-heater) placed under the window in a naturally ventilated test laboratory. The cold outdoor air was forced through vent-convector by artificially produced wind. The airflow

at a constant rate and inlet temperatures varying from 2 to 10 °C was heated by hot water of 67, 51 and 38 °C circulating inside the convector coil. The airflow rates in their investigation were about 15 times higher than in studies by Myhren and Holmberg [17,18] and Ploskic and Holmberg [19]. Mundt et al. [21] reported results based on field measurements from two different exhaust-ventilated school rooms, each served by three vent-convectors similar to those analyzed by Elmualim et al. [20]. The thermal performance of the vent-convectors was evaluated at outdoor airflows ranging from 30 to 279 l/s at inlet temperatures of 4 and 10 °C. Measurements indicated that vent-convectors operating at 54 °C water supply could not raise the temperature of airflow rates higher than 82 l/s to an acceptable level. A separate hot-water circuit for vent-convectors was suggested to overcome this problem.

Summarizing the results from earlier studies the following can be concluded. First, the thermal performance from existing room heaters can considerably be increased through a proper combination with supply air. Second, conventional vent-convectors may under certain conditions have problems in lifting the temperature of the cold supply air to an acceptable level. Third, the inlet (outdoor) temperatures of the supply air used in most of earlier studies corresponded approximately to the mean Swedish winter temperatures [22] rather than to design temperatures in central Sweden.

1.2. Objectives

The main goal of the present study was therefore to investigate whether it was possible to pre-heat supply air at winter design conditions in central Sweden using an improved version of vent-convector, here called the proposed air-heater. The second goal was to analyze the effects of combining the proposed air-heater with two different radiator systems in a room.

1.3. Description of the proposed air-heater

The general principle of the analyzed system and proposed air-heater is illustrated in Fig. 1a–d. The pre-heating of supply air was thought to occur in two steps. In the first step, the cold supply air was forced through the hot compact coil spring and in the second step through the hot finless tube bank, before it entered the room. The coil spring and the tube bank were assumed to be connected by a mutual closed-loop piping system. The airflow through the air-heater was driven by the negative pressure in the room caused by an exhaust fan. This exhaust-ventilation system is common in the Swedish residential sector and normally the pressure difference between outdoor and indoor ranges between 10 and 15 Pa. To control ventilation flow rate in case of high outdoor wind loads the proposed air-heater was assumed to be equipped with a pressure controlled wind damper.

1.3.1. Impact of the pipe-loop design on controlling parameters

The rate of the internal heat transfer and pressure loss over the air-heater was mostly influenced by the pipe-loop design of the coil spring and the tube bank. The inner and outer coil diameters had a direct impact on the internal heat transfer and pressure losses inside the wall channel. Moreover, the heat transferring surface area of the coil spring was also directly dependent on the coil diameters. The design of the pipe-loop inside the tube bank had the same influence on these three governing parameters as for the coil spring. Consequently, the upper limit for airflow and thereby the heat transfer through the entire air-heater was controlled by pressure loss over the air-heater. Therefore in the present study much effort was made to find a pipe-loop design for both coil spring and tube bank to achieve efficient air heating at low pressure loss and low-temperature water supply.

2. Calculation methods

Both analytical and numerical calculations were applied to estimate the heat transfer and pressure loss inside the proposed air-heater. By analytical calculations are here meant models and estimations based on semi-empirical relations and by numerical calculations predictions by CFD (Computational Fluid Dynamics; Ansys Fluent 13). The calculations were made in two stages. In the first (Fig. 1c, section A-A) the temperature lift of the passing airflow through the wall channel was calculated using an analytical model suggested by VDI Heat Atlas (VDI-model) [23], while the internal pressure loss was estimated by available semi-empirical expressions. In the second part (Fig. 1d, section B-B), numerical calculations were applied to estimate internal heat transfer and pressure loss inside the analyzed tube banks since the investigated arrangements could not be addressed analytically.

2.1. Analytical model of the coil spring

2.1.1. General information

The airflow through the coil spring was treated as pipe flow, while the airflow in the gap between coil spring and wall channel as annular flow. These assumptions were the starting point for all analytical calculations inside the wall channel. Pipe flow calculations were based on the inner coil diameter $D_{c,i}$, and annular flow calculations on the hydraulic diameter $(D_w - D_{c,o})$ of the annular passage. The amount of airflow passing through the pipe and annular passage was determined by calculating the flow resistance (pressure loss) in each part.

In general, most of the presently available semi-empirical heat transfer equations (Nusselt-relations) were originally constructed for long circular ducts where entrance effects often can be neglected and where the internal flow is both thermally and hydrodynamically fully developed. The relations were also restricted for predominantly laminar or high-turbulent pipe and/or annular flows. In the present study neither of these was the case since the wall channel was short and the internal airflows were often in transition from laminar to turbulent flow regime. Because of this, the Nusselt-relations used here were supplemented with appropriate mathematical functions to include the effects of four factors: entrance (Eq. (4)), change of air properties due to temperature variation along the coil spring (Eq. (5)), undeveloped thermal and hydrodynamic flow conditions (Eq. (6)) and transitional flow regime. The functions are given in Table 1. The thermal air properties such as density, conductivity, dynamic viscosity, expansion coefficient and Prandtl number were calculated using expressions given in [19].

2.1.2. Verification of analytical models

In order to ensure the correctness of the constructed VDI-model the first step in creating the model was the reproduction of the calculation examples given by Volker Gnielinski in VDI Heat Atlas [23]. In examples, a detailed calculation procedure for estimation of internal convective heat transfer through annular and pipe passage was reported and followed here. After the results from the created VDI-model were found to be consistent with values given in the examples, the fluid properties in the model were changed to those of air for the appropriate range. To further verify the correctness of the VDI-model, the calculation results from this model were also compared to results obtained by the model presented in Table 1. The main difference between these two models lay in calculation of heat transfer in the transitional flow regime. In VDI-model an intermittency function was used to bridge the gap from

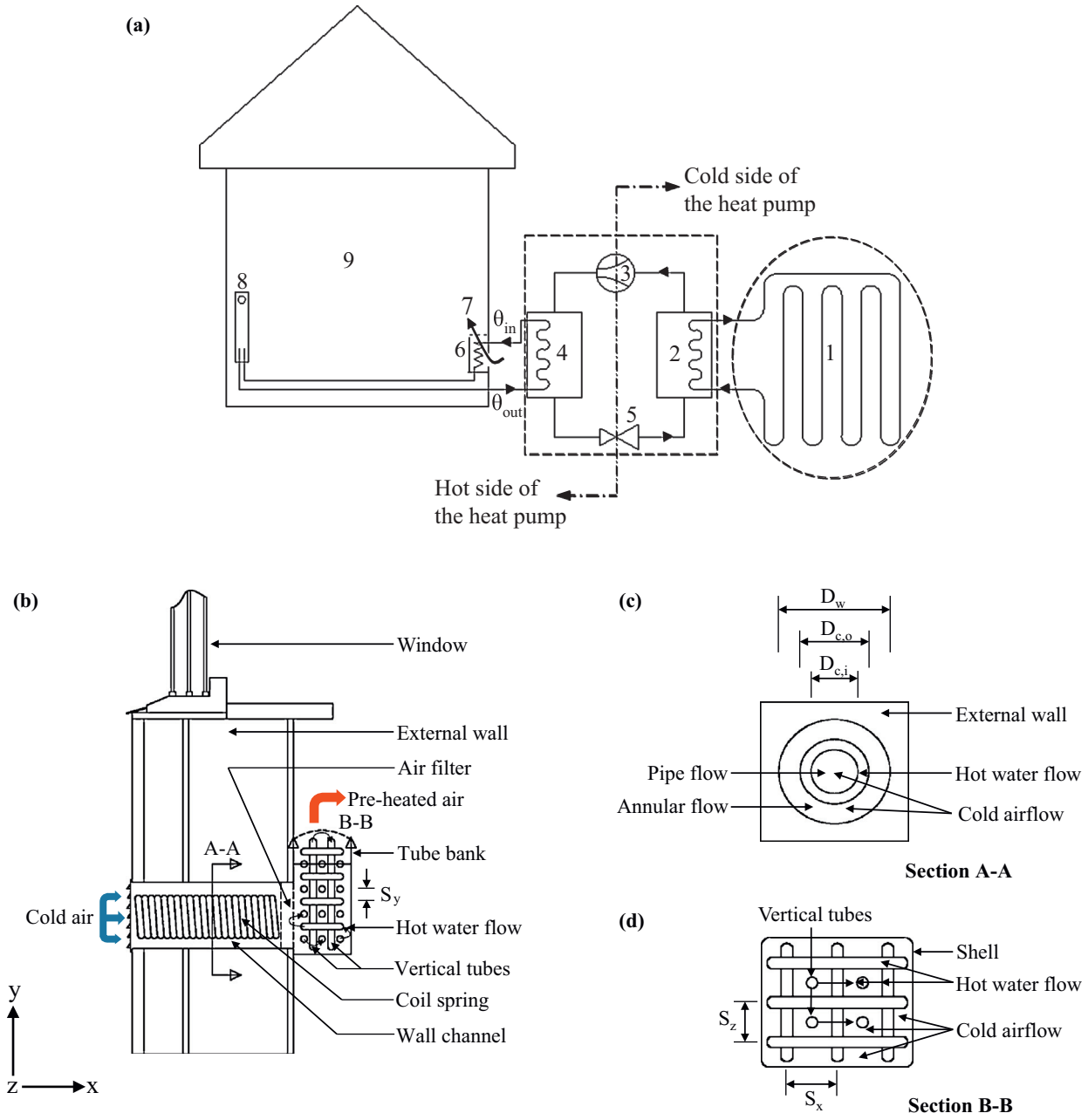

Fig. 1. (a) The schematics of the analyzed hydronic systems connected to a heat pump. Dashed lines illustrate the boundaries of the heat source and heat pump respectively. θ_{in} and θ_{out} represent, respectively, the supply and return water temperatures of the hydronic system. 1 = heat collector, 2 = evaporator, 3 = compressor, 4 = condenser, 5 = expansion valve, 6 = proposed air-heater, 7 = air supply, 8 = radiator and 9 = heated space. (b) General illustration of proposed air-heater and its components. Vertical section not to scale. (c and d) Illustration of the cold air and hot water flow through the coil spring (upper) and tube bank (lower). Vertical (upper) and horizontal (lower) sections not to scale.

laminar to turbulent flow, while in the model presented in Table 1 this was done using the well-known Gnielinski's Nusselt-relation [24] together with appropriate equations for flow friction factor [25,26].

The predictions of Nusselt-number by both models were in close agreement and did not deviate more than 5% for $2300 \leq Re_D \leq 10^4$, as can be seen in Fig. 2a. Moreover, calculations used for estimation of friction factors inside the wall channel were also compared to chart data given in [26,28], as illustrated by Fig. 2b. The over-all agreement between calculations and charts was good and differed less than ±5% for $2300 \leq Re_D \leq 10^4$. A larger disagreement of about 7% was detected for $Re_D \approx 3000$ only. The results presented in Fig. 2a and b confirm that created models for calculation of heat transfer and pressure loss inside the wall channel were reliable and constructed in correct way.

2.2. Validation of CFD model

Since it was important to ensure the correctness of the CFD predictions, the simulation results by CFD were first validated with data obtained by semi-empirical relations. This validation method was also used in previous studies [29–32]. As in the analyzed arrangements (Fig. 1d, section B-B) the airflow was mostly in-line (parallel) with the tubes, the semi-empirical relations for in-line

Table 1
The mathematical and semi-empirical equations used for approximation of heat transfer and pressure loss through the coil spring and four-row square in-line tube bank. Eqs. (1)–(7) were used for comparison to an analytical model based on VDI Heat Atlas, while Eqs. (8)–(10) were used for validation of CFD predictions.

Reference	Equation		Flow	Geometry	Correction/comment	Validity
Gnielinski [24]	$_{\mathrm{I}}\mathrm{Nu} = \frac{(f/8)\cdot(Re_D - 1000)\cdot Pr}{1 + 12.7\cdot\sqrt{(f/8)}\cdot(Pr^{2/3} - 1)}$	(1)	Transitional and fully developed turbulent	Circular		$3000 \le \mathrm{Re}_D \le 10^5$ $0.5 \le \mathrm{Pr} \le 2000$ $L/D \ge 10$
Abraham et al. [25]	$f = 3.03\times10^{-12}\cdot Re_D^3 - 3.67\times10^{-8}\cdot Re_D^2 + 1.46\times10^{-4}\cdot Re_D - 0.151$	(2)	Transitional and fully developed turbulent	Circular		$2300 \le \mathrm{Re}_D \le 4500$
(Petukhov), Çengel and Ghajar [26]	$f = [0.79\cdot\ln(Re_D) - 1.64]^{-2}$	(3)	Transitional and fully developed	Circular		$3000 \le \mathrm{Re}_D \le 10^5$
(Hausen), Kakaç and Hongtan [27]	$C_1 = 1 + \left(\frac{D}{L}\right)^{2/3}$	(4)	Transitional and turbulent	Circular	For entrance effects	$L/D \le 60$
Kakaç and Hongtan [27]	$C_2 = \left(\frac{T_s}{T_{\mathrm{mbt}}}\right)^{-[0.3\cdot\log(T_s/T_{\mathrm{mbt}})+0.36]}$	(5)	Transitional and turbulent	Circular	For property variation	Air
VDI Heat Atlas [23]	$_{\mathrm{II}}\mathrm{Nu} = \left(\frac{2}{1+22\cdot Pr}\right)^{1/6}\cdot\left(2300\cdot Pr\cdot\frac{D}{L}\right)^{1/2}$	(6)	Transitional and turbulent	Circular	For hydro-and-thermodynamically developing flow	$\mathrm{Re}_D \ge 2300$ $\mathrm{Pr} > 0.1$
VDI Heat Atlas [23]	$\mathrm{Nu}_D = [(_{\mathrm{I}}\mathrm{Nu}\cdot C_1)^3 + {}_{\mathrm{II}}\mathrm{Nu}^3]^{1/3}\cdot C_2$	(7)		Circular		
(Žukauskas), Çengel and Ghajar [26]	$\mathrm{Nu}_d = 0.52\cdot Re_{d,\max}^{1/2}\cdot Pr^{0.36}\cdot\left(\frac{Pr}{Pr_s}\right)^{1/4}$	(8)		Tube bank	In-line arrangement	$100 \le \mathrm{Re}_{d,\max} \le 10^3$ $0.7 \le \mathrm{Pr} \le 500$
(Žukauskas), Çengel and Ghajar [26]	$\mathrm{Nu}_d = F\cdot 0.27\cdot Re_{d,\max}^{0.63}\cdot Pr^{0.36}\cdot\left(\frac{Pr}{Pr_s}\right)^{1/4}$	(9)		Tube bank	In-line arrangement $F = 0.9$ for $N_x = 4$	$10^3 \le \mathrm{Re}_{d,\max} \le 2\times10^5$ $0.7 \le \mathrm{Pr} \le 500$ $N_x = 4$
(Žukauskas), Çengel and Ghajar [26]	$\Delta p_{\mathrm{tb}} = N_x\cdot\chi\cdot f_{tb}\cdot\left(\frac{\rho_{\mathrm{air}}\cdot v_{\max}}{2}\right)^2$	(10)	Entire	Tube bank	$\chi = 1$ for square in-line arrangement. $N_x = 4$.	$3 \le \mathrm{Re}_{d,\max} \le 10^6$

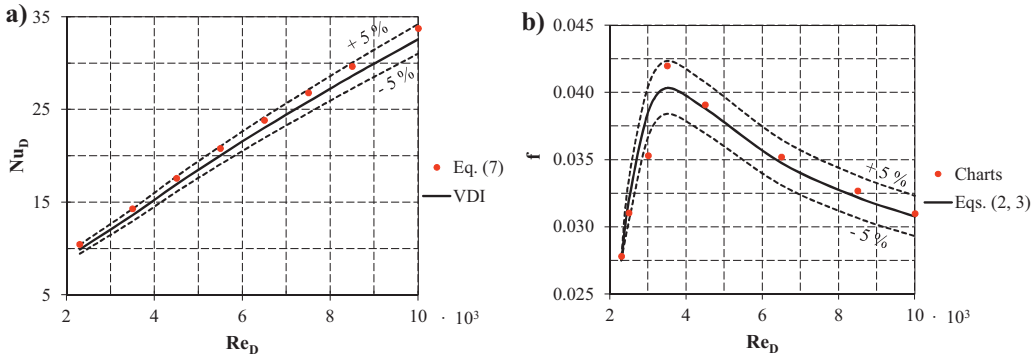

Fig. 2. (a) Variation of Nusselt-number as a function of Reynolds-number for transitional, hydrodynamically and thermally undeveloped pipe flow, $L/D = 10$. The dashed lines show a deviation of ±5% from VDI-line. (b) Variation of flow friction factor as a function of Reynolds-number for transitional pipe flow, $L/D = 10$. The dashed lines show a deviation of ±5% from VDI-line.

tube banks were used for validation. The used relations, originally developed by Žukauskas, were taken from the book of heat and mass transfer by Çengel and Ghajar [26].

A two-dimensional square in-line tube bank with equal longitudinal and transverse distance between two consecutive tubes was used as a reference. The analyzed bank consisted of four tube rows in the flow direction with four tubes in each row. The Reynolds-numbers ($Re_{d,\,max}$), in the analytical calculations were based on the outer tube diameter d and the maximum air velocity v_{max} occurring in the minimum flow cross-section between the tubes. All air properties, except Prandtl number Pr_s, were evaluated at the arithmetic mean of the air inlet and outlet temperatures as for the coil spring. The values for Pr_s were evaluated at the tube wall temperature.

2.2.1. Boundary conditions and computational mesh set-up

The CFD simulations started by reproducing a 140 mm long and 96 mm high tube bank with 16 tubes equally distributed across the length and width of the surface. The outer walls of the bank were modelled as adiabatic while the tubes inside the bank had a constant wall temperature. The surface in front of the tubes was used to specify the approach velocity while the rear end of the bank was modelled as the outlet. Since the rate of the approach velocity (velocity outside the tube bank) was changed in each simulation to achieve the desired Reynolds-number inside the bank, the height of the nearest mesh cell normal to tube walls was manually adjusted to maintain the non-dimensional wall distance y^+ around 1.0, with an average deviation of 3%. The height of the first mesh cells tube walls was gradually decreased from about 0.32 to 0.08 mm as the approach velocity was increased. The space in the regions immediately adjacent to the outer tube walls was meshed using boundary layers. Five boundary layers of fine structured mesh around the tubes were applied in all simulations. The mesh distribution within the boundary layers was performed smoothly by using a size function available in the CFD-code. The transition (growth) factor between the layers was set to 1.3. The size function was also used to transform face mesh from the boundary layers towards the outer flow regions using a growth factor 1.1. The minimum face cell was limited to 0.05 mm while the maximum face cell was set to 2.0 mm. The transition from the smallest to the largest face cells was performed smoothly in order to obtain a high-quality mesh distribution.

2.2.2. Ancillary and turbulence models

The CFD calculations were carried out applying a second-order discretization scheme for all differential equations with a pressure-based solver. The pressure–velocity coupling was handled by the Simple algorithm. The turbulence generation and convective heat transfer around the tube walls were predicted by the turbulence models and enhanced wall treatment. Three $k-\varepsilon$ turbulence models Realizable, Re-Normalization Group (RNG) and standard were tested and compared to each other and to Eqs. (8)–(10). The effect of natural convection due to internal buoyancy was predicted by the Boussinesq approximation.

2.2.3. Validation results

Validation work showed that CFD calculations performed with all three $k-\varepsilon$ turbulence models were in close agreement with each other and Eqs. (8)–(10). It was decided to persist with

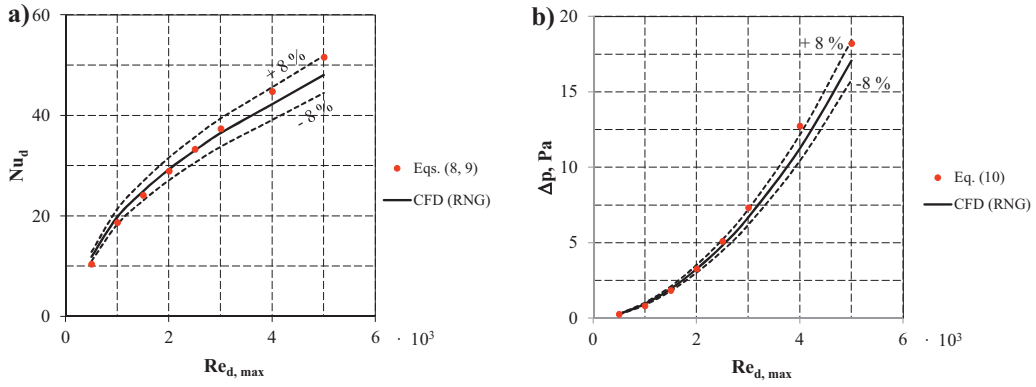

Fig. 3. (a) Variation of Nusselt-number as a function of Reynolds-number for a 4-row square in-line tube bank. The wall temperature of the tubes was set to 38 °C. The dashed lines show a deviation of ±8% from CFD-line. (b) Variation of pressure loss as a function of Reynolds-number for a 4-row square in-line tube bank. The wall temperature of the tubes was set to 38 °C. The dashed lines show a deviation of ±8% from CFD-line.

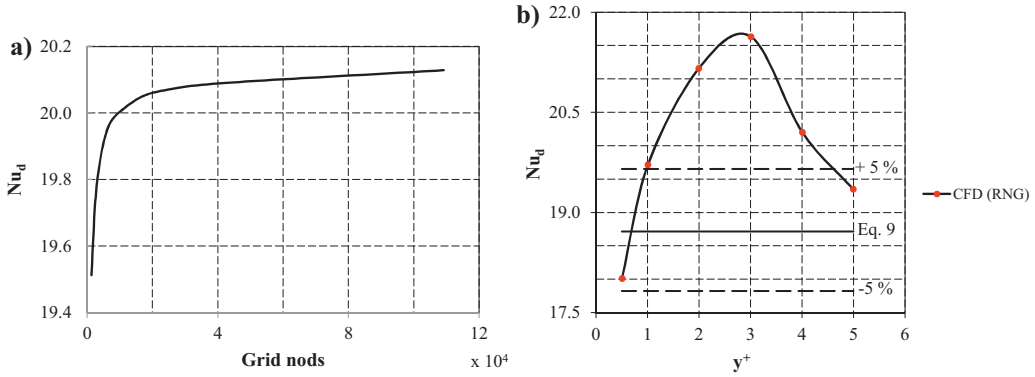

Fig. 4. (a) Change in Nusselt-number as a function of grid nods for a square in-line tube bank. The tubes' wall temperature was held constant at 38 °C and $Re_{d,max}$ was set to 1000 and $y^+ \approx 1.0$. (b) Change in Nusselt-number as a function of y^+-value for a square in-line tube bank. The tubes' wall temperature and $Re_{d,max}$ was the same as in (a). The dashed lines show a deviation of ±5% from Eq. (9) line.

$k-\varepsilon$ RNG turbulence model. The mean deviation between semi-empirical and CFD calculations for Nusselt-number in the range of $500 \leq Re_{d,max} \leq 5000$ was about ±5% and around ±8% for pressure loss, which can be seen in Fig. 3a and b. A larger disagreement of about 13% for the Nusselt-number was observed at $Re_{d,max} \approx 500$. This was regarded as acceptable since the flow in the present investigation was in the range of $1000 \leq Re_{d,max} \leq 2000$ where the deviation was ±1 to 6% for both parameters.

For consistency of testing the numerical results, the mesh (grid) independence was checked by changing the mesh density. Both coarser and finer mesh setups were tested by changing the density near the tube walls as well as in the outer flow regions. Results presented in Fig. 4a show that a change of mesh density a factor of 5 affected CFD-prediction of the Nusselt-number by less than 3%. This verified that the predictions were mesh independent. Further investigation of impact of near-wall mesh arrangement on predicted heat transfer rate have confirmed that the chosen y^+-value of around 1.0 was justified. The CFD prediction of heat transfer at $y^+ \approx 1.0$ was within ±5% agreement with Eq. (9), as is illustrated in Fig. 4b. The convergence criterion for all balance equations was set to 10^{-4} except for energy equation for which it was set to 10^{-6}. In all simulations, convergent solutions with consistent results were obtained regardless of which mesh type was used.

2.3. Heat transfer through the air-heater

The total temperature lift through the entire air-heater was calculated by an energy balance using Eq. (11). The left side of the equation stands for the rate of thermal power required to heat up the incoming airflow to a desired temperature, while the middle part represents the rate of thermal power given by hot circulating water inside the air-heater. In both parts, the thermal power Q was determined by a steady-flow energy equation. The part at far right represents the total water-to-air heat transfer.

$$Q_{air} = Q_{water} = \underbrace{A_{tube,o} \overbrace{\frac{\Delta\theta_1 - \Delta\theta_2}{\ln(\Delta\theta_1 \Delta\theta_2^{-1})}}^{\Delta\theta_{lm}}}_{\text{Water-to-air heat transfer}} \left[\overbrace{dd_i^{-1}\alpha_{water}^{-1}}^{\text{Water-to-tube wall}} + \overbrace{0.5\ d\lambda_{tube}^{-1} \ln(dd_i^{-1})}^{\text{Tube wall resistance}} + \overbrace{\alpha_{air}^{-1}}^{\text{Tube wall-to-air}} \right]^{-1} \quad (11)$$

The five variables on the right-hand side of Eq. (11) control the heat flow as follows. The α_{water} governs the rate of convective heat transfer from circulating water to the tube walls. The middle part stands for the thermal resistance of the tube wall, and the α_{air} at far right controls the convective heat transfer between hot tube walls and the cold passing airflow. $A_{tube,o}$ represents the outer heat transmitting surface area of the air-heater (entire pipe-loop) while $\Delta\theta_{lm}$ stands for the logarithmic mean temperature difference between the hot water and cold air. In $\Delta\theta_{lm}$, $\Delta\theta_1$ and $\Delta\theta_2$ represent the temperature differences between the hot and cold fluids at the two ends of the air-heater. As in the investigated case $\alpha_{water} \gg \alpha_{air}$, $\lambda_{tube} \approx 400\,W/(m\,°C)$ and $d_i \approx d$, the overall convective heat transfer inside the air-heater was dominated by α_{air}, since the inverse of large numbers is small and negligible. Therefore, the calculated overall heat transfer rate inside the air-heater was entirely based on the air-side heat transfer coefficient α_{air}. The values for α_{air} were obtained from the VDI-model and CFD predictions as described in Sections 2.1 and 2.2.

3. Results

3.1. Temperature lift inside the wall channel

In order to calculate the total temperature lift of the air supply inside the wall channel, the airflow rates passing through the coil spring (pipe passage) and in the gap (annular passage) needed to be determined. This was done by manual adjustment of the airflow rates through annular and pipe passages until the same pressure loss in both parts was achieved. Once that was accomplished, the flow velocities, air-side heat transfer coefficients and temperature lift inside the annular and pipe passages were computed. Since neither the airflow rates nor the temperature increase of the passing air inside the annular and pipe passages were the same, the total temperature lift across the entire channel was calculated using the mass-weighted mean temperature, as shown in Eq. (12). Moreover, as the cross-section of wall channel (Fig. 1c, section A-A) consisted of three coaxial circular sections, the hydraulic diameter was applied to connect two flow cross-sections into one entity. The hydraulic diameter ($D_h = 4A_c/P$) was based on total flow cross-sectional area A_c of the duct, together with the total wetted perimeter P of the flow cross-sections.

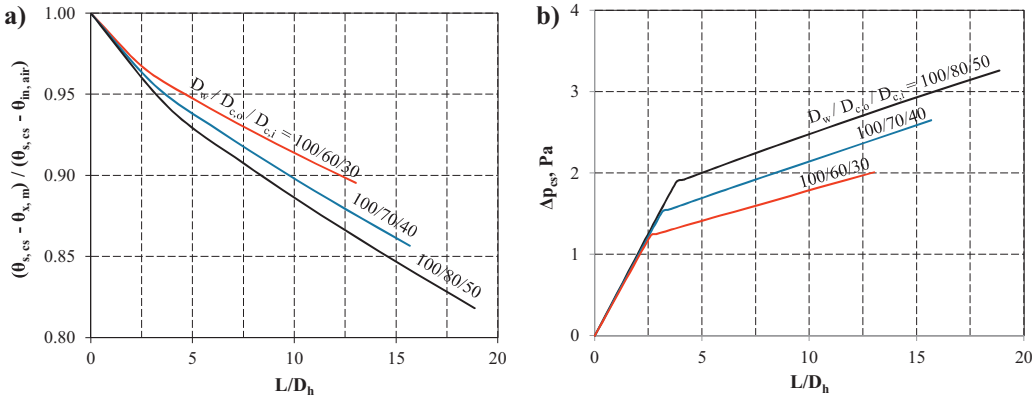

Fig. 5. (a) Variation of the dimensionless temperature with length-to-hydraulic diameter ratio along the coil spring for three different combinations at airflow of 10 l/s. (b) Variation of the pressure loss with length-to-hydraulic diameter ratio along the coil spring for three different combinations at airflow of 10 l/s.

$$\theta_{x,m} = \frac{(\theta_{x,\text{ann.}} \cdot \dot{m}_{\text{air}}/\rho_{\text{air}})_{\text{annular}} + (\theta_{x,\text{pipe}} \cdot \dot{m}_{\text{air}}/\rho_{\text{air}})_{\text{pipe}}}{(\dot{m}_{\text{air}}/\rho_{\text{air}})_{\text{annular}} + (\dot{m}_{\text{air}}/\rho_{\text{air}})_{\text{pipe}}} \quad (12)$$

In Fig. 5a and b, the change of dimensionless temperature and pressure loss as function of length-to-hydraulic diameter ratio of the coil spring is shown. In the estimation of the pressure losses both friction (major) losses and sharp-edged entrance (minor) loss were included. The temperature difference $(\theta_{s,cs} - \theta_{in,air})$ in the dimensionless temperature is constant, while $(\theta_{s,cs} - \theta_{x,m})$ decays across the coil x-axis. At $L_{cs} = 0$, the dimensionless temperature is equal to unity since $(\theta_{s,cs} - \theta_{in,air}) = (\theta_{s,cs} - \theta_{x,m})$. In practice this means that no air heating inside the wall channel has occurred. As $L_{cs} \to \infty$, the dimensionless temperature approaches zero since $\theta_{s,cs} \approx \theta_{x,m}$. This implies that airflow inside an infinitely long wall channel would be able to receive all heat from the circulating water inside the coil spring.

From the figures it can also be observed that both temperature lift and pressure loss increased with the length of the coil spring L_{cs}. This meant that the thickness of the outer wall, i.e. the length of the coil spring was a limiting factor for the temperature lift. Thus, an appropriate wall thickness needed to be selected. Janson et al. [4] presented amongst other findings also the outer walls thicknesses of 11 different residential buildings. The thicknesses given in their report ranged from 0.26 to 0.5 m, with an average value of 0.38 m, before adding a supplementary thermal insulation. Therefore in the present study the outer wall thickness of 0.3 m was used as a reference.

By some rearrangement of Fig. 5a and b it can be seen that 100/80/50 coil spring of 0.3 m was able to raise inlet air temperature of 10 l/s from −15 to −8.2 °C using 40 °C water supply at pressure loss of 2.6 Pa. Moreover, data reported in Table 2 show that the combination 100/80/50 also gave the most balanced airflow distribution through the wall channel. Approximately 53.5% of the air flowed through the annular passage and about 46.5% through the pipe passage of the coil spring. This internal flow distribution was favourable for the heat transfer because the outer surface area of the coil, which was in contact with 53.5% of the airflow, was about 2.6 times larger than inner coil surface. On the other hand, the airflow through the inner coil (pipe passage) was almost fully turbulent ($Re_{pipe} = 9625$) which contributed to high $\alpha_{air,pipe}$-values, i.e. higher temperature lift in this section. This cumulative effect of this coil spring arrangement gave thus a most favourable balance between temperature increase and pressure losses.

Table 2
Hydraulic diameter, airflow rates and Reynolds-numbers for annular and pipe passage for different spring coil combinations inside the wall channel at $L_{cs} = 0.3$ m.

Combination	D_h (mm)	$\dot{V}_{air,cs}$ (l/s)		Re (–)	
		Annular	Pipe	Annular	Pipe
100/80/50	26.5	5.35	4.65	3023	9625
100/70/40	31.9	7.46	2.54	4463	6531
100/60/30	38.4	8.84	1.16	5622	3932

3.2. Temperature lift through tube bank

Since the pipe-loop inside the tube bank was assumed to be coiled into a closed-loop single piping system without feed pipes, an appropriate bending radius for the pipes needed to be selected. According to recent manufacturer's guidelines, the minimum bending radius for the thin-walled copper tubes should be around one to one and a half outer tube diameters, i.e. $R_{bend}/d \approx 1$–1.5. Therefore in the present study the bending radius was set to $R_{bend} = 1.25d$. The magnitude of the selected bending radius limited the size of tube bank in all three (z, y and z) directions. For practical reasons the dimensionless pitches in all three directions were set to be equal, i.e. $S_x/d = S_y/d = S_z/d$.

The airflow through the tube banks was simulated by applying a fixed pressure difference Δp_{tb} between the inlet and outlet of the tube bank. At the inlet, reference pressure was set to 2.6 Pa and the air temperature to −8.2 °C. These values were the outlet boundary conditions from the wall channel. The inlet pressure and temperature were held constant in all simulations. At outlet of the tube banks, negative pressure was manually adjusted to obtain an airflow rate of approximately 10 l/s through the banks. All settings such as mesh set-up, turbulence model, near-wall treatment, y^+-value and thermal boundary conditions were the same as used during the validation process.

Many different tube bank arrangements were tested in order to find an arrangement that was able to efficiently lift the air temperature of 10 l/s from −8.2 °C to an acceptable level. In Fig. 6a and b, horizontal cross-sections of the two most relevant arrangements are presented – one without (Fig. 6a) and one with (Fig. 6b) vertical tube rows. The outer diameter of horizontal tube rows in these systems was held constant at 15 mm, while the outer diameter of the vertical tube rows was varied. The investigations showed that a tube bank without vertical tube rows, consisting of 5 consecutive tubes in x and z-direction arranged in 10 rows in y-direction gave the most favourable balance between temperature lift and pressure loss. This arrangement was able to lift the air temperature of 10 l/s from −8.2 to 18.7 °C, with tube surface temperature of 37 °C at pressure difference of 0.8 Pa. In the cases with vertical tube rows of 10 and 12 mm in diameter, 8 and 7 vertical tube rows (in y-direction) were required, to lift the inlet air temperature of −8.2 °C to the approximately same level as arrangement without

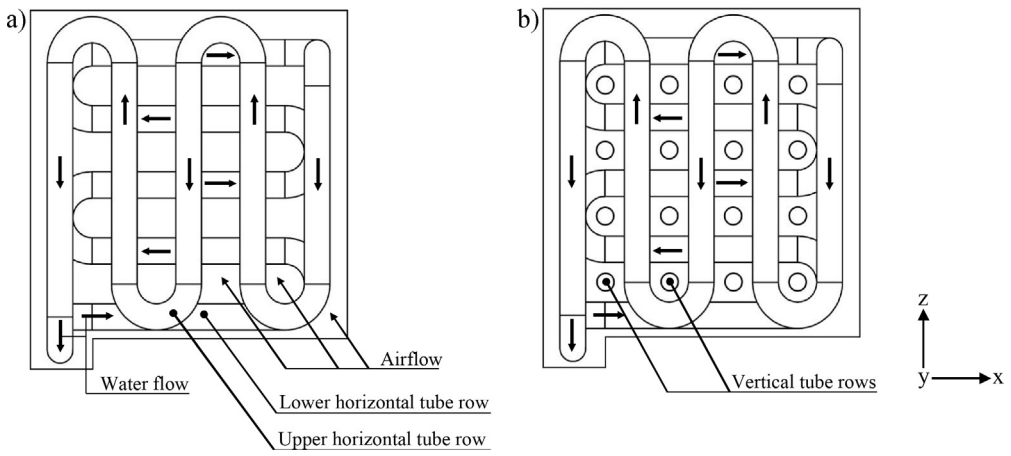

Fig. 6. (a) Tube bank arrangement without vertical tube rows. Water flow in x and z-direction. Airflow in y-direction. (b) Tube bank arrangement with vertical tube rows. Water flow in x, z and y-direction. Airflow in y-direction.

Table 3
Presentation of the results based on CFD calculations for three different tube bank arrangements.

Tube bank arrangement	$R_{bend}/d = R_{bend}/d_{vertical} = 1.25$									
	$S_x/d \times S_y/d \times S_z/d = 2.5 \times 2.5 \times 2.5$									
	$\dot{V}_{air,tb}$ (l/s)	$\theta_{in,tb}$ (°C)	$\theta_{s,tb}$ (°C)	$\theta_{out,tb}$ (°C)	d (mm)	$d_{vertical}$ (mm)	$A_{s,tb}$ (m^2)	$\alpha_{air,tb}$ (W/(m^2 °C))	N_y (number)	Δp_{tb} (Pa)
Without vertical tube rows	10.1	−8.2	37.0	18.7	15	–	0.43	27.3	10	0.8
With vertical tube rows	9.79	−8.2	37.1	18.3	15	10	0.48	22.6	8	2.2
With vertical tube rows	9.45	−8.2	37.1	18.8	15	12	0.46	23.8	7	2.4

vertical tubes. On the other hand, the flow resistance in these two cases was much higher compared to the case without vertical tubes and pressure difference of 2.2–2.4 Pa was required to obtain an airflow rate of approximately 10 l/s. More detailed results from the analyzed tube bank arrangements are presented in Table 3.

3.3. Total pressure loss of proposed air-heater

In Fig. 7, the pressure loss variation of different air-filter types for typical vent-convectors used in [20,21] at 10 l/s is given. It can be seen a medium fine filter inside a ⌀ 100 mm wall opening generates about 6.5 Pa pressure loss. This means that the tube bank arrangement without vertical tube rows and the coil spring 100/80/50 of 0.3 m are able to operate with medium fine filter. As the total pressure loss of this combined system ($\Delta p_{tb} + \Delta p_{filter} + \Delta p_{cs} = 0.8 + 6.5 + 2.6 = 9.9$ Pa) is approximately

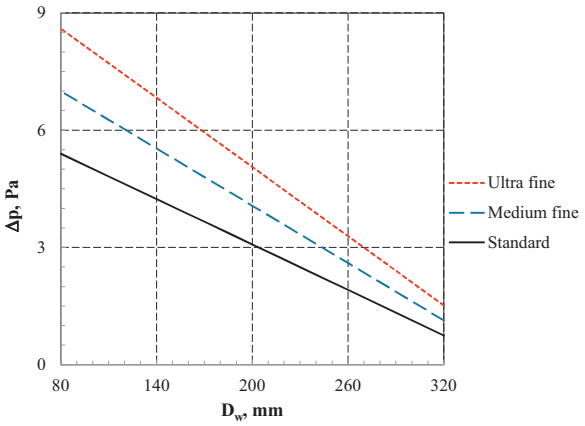

Fig. 7. Variation of pressure loss with diameter of the wall channel D_w for different air-filter types at the airflow rate of 10 l/s. Based on manufacturer's data [33].

10 Pa, which was the available pressure potential, as detailed in Section 1.3. This also means that no extra fan power is needed for running the proposed air-heater. The 100/80/50 coil spring of 0.3 m could also be combined with the tube bank arrangements with vertical tube rows, but in these systems a standard air-filter can be used only. Moreover, none of the investigated systems was able to operate with an ultra fine filter (filter class EU7/F7) since the pressure loss for $D_w = 100$ mm at 10 l/s was around 8.0 Pa, which means that about 80% of pressure potential was consumed by the filter.

3.4. Effect of combined heating-ventilation systems

The effect of combining the proposed air-heater with two different radiator systems in a 6 m long, 4 m wide and 2.6 m high room is presented in this section (Fig. 8a and b). The room space under consideration had two external walls, each having one 1.8 m by 1.8 m glazed area. The thermal transmittance (U-value) of the external walls was set to 0.17 W/(m^2 °C) and to 1.1 W/(m^2 °C) for glazing, which is close to current Swedish building practice. The external walls, and thereby the glazed areas, were exposed to outdoor temperature of −15 °C, while the indoor temperature was set to 20 °C. The rest of the walls were considered as adiabatic. The infiltration rate was estimated using American Society of Heating, Refrigerating and Air-Conditioning Engineers (ASHRAE) calculation procedure [34]. The rate was approximated for a building structure having tight-walls [34], placed in an urban area at external wind speed of 5 m/s [35,36]. The calculated heat loss per square metre floor area was 5% below field measurements performed in south-east Norway [37] and 2% below German Energy Saving Regulation EnEv 2009 [5].

Two different heating systems were analyzed. The first system consisted of two conventional double-panel radiators (Fig. 8a). The second included three radiant baseboard heaters distributed along the bottom of the room walls (Fig. 8b). In system illustrated by Fig. 8a the used double-panel radiators were of type 21, meaning

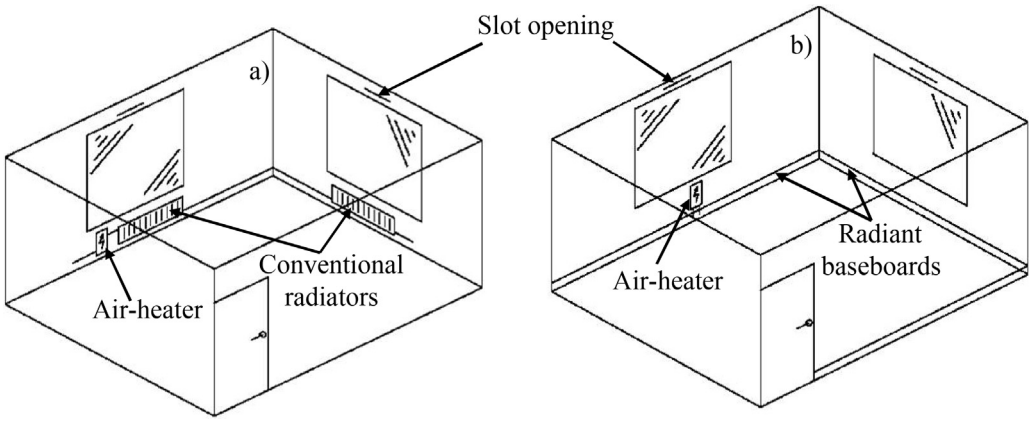

Fig. 8. (a and b) The room space with different heating-ventilation systems. The outdoor air supply of 10 l/s was the same in (a) and (b). Diagrams not to scale.

Table 4
Room heat losses and the heat outputs from the four heating-ventilation systems presented in Fig. 8a–c. The water supply (inlet) and return (outlet) temperatures used in the systems are also given below.

Heat losses from the room

Transmission heat loss		Ventilation heat loss		Total heat loss
Glazings (W)	Walls (W)	Ventilation (W)	Infiltration (W)	Q_{loss}
249	116	451	39	855

Heat supply to the room

	Two conventional radiators (Fig. 8a)					Three radiant baseboard heaters (Fig. 8b)				
Ventilation system	H (m)	L (m)	θ_{in} (°C)	θ_{out} (°C)	Q_{tot} (W).	H (m)	L (m)	θ_{in} (°C)	θ_{out} (°C)	Q_{tot} (W).
Slot openings	0.3	1.6	48	38.4	863	0.127	15	49	39.5	857
Proposed air-heater	0.3	1.6	40	30.6	858	0.127	15	40	30.7	849

that the entire rear surface of the front panel was covered with convection fins. The heat outputs from conventional radiators were estimated using a calculation code based on manufacturer's heat emission data [38], while the thermal power from the radiant baseboards was calculated using a diagram presented by Siegenthaler [39]. The total length of the baseboards was adjusted to cover three of four room walls.

Two different ventilation types in combination with radiator systems were also analyzed. One was rather traditional with slot openings above the windows, and another incorporated the proposed air-heater investigated in current study. In cases with slot openings, the outdoor air supply of 10 l/s at −15 °C was brought directly into the room space without any pre-heating. In the cases with air-heater, the outdoor air was pre-heated as described in previous sections. Four different heating-ventilation systems (cases) were analyzed and compared.

Case 1: Room a) – two conventional radiators in combination with slot openings.
Case 2: Room a) – two conventional radiators in combination with proposed air-heater.
Case 3: Room b) – three radiant baseboard heaters in combination with slot openings.
Case 4: Room b) – three radiant baseboards heaters in combination with proposed air-heater.

In all cases considered, the heat outputs Q_{tot} were adjusted to cover both transmission and ventilation heat losses Q_{loss} of the room space. The heat outputs presented in Table 4 were estimated under the assumption that all thermal units (air-heater, baseboards and radiators) in all four cases were connected by a single-pipe circuit, i.e. the outlet temperature from one unit was the inlet temperature to the next lying behind. This was done so that all five systems could be assessed at same water mass flow rate of approximately 77.6 kg/h. This rate of water flow together with d_i = 13 mm generated a pressure loss of roughly 40 Pa/m which is much lower than 100 Pa/m, that is usually used as guideline value for dimensioning of heating pipe network. The θ_{in} in Table 4 represents the supply (inlet) water temperature to the first thermal unit and θ_{out} stands for outlet (return) water temperature from the last unit in the circuit.

Results presented in Table 4 show that both conventional and baseboard radiators needed to operate at almost the same water supply temperatures to cover the space heat loss of the room. The effect of forcing the cold incoming air through the air-heater, instead of taking it directly from outside without any pre-heating was obvious. In cases when unheated outdoor air was brought directly to the room, the supply water temperatures of the both radiator systems needed to be 48–49 °C to compensate for the heat loss. On the other hand, both systems in combination with the proposed air-heater covered the space heat loss at a water temperature of 40 °C. This implied that supply water temperature in the combined system could be lowered by 20–22.5%.

4. Discussion

Results from present study showed that it would be fully possible to meet the space heat demand of a modern room with analyzed heating-ventilation systems, with supply water temperature similar to that currently used in floor heating systems. The results clearly highlight the advantage of local air pre-heating instead of taking air directly from outside without pre-heating. Calculations showed that supply water temperature in radiator systems equipped with the proposed air-heater could be

significantly lowered without decreasing the total heat output of the systems. As a consequence of this, the efficiency (COP) of the heat pumps installed in these combined hydronic systems will be higher than in systems without air-heating. Earlier studies performed on different heating-ventilation systems served by heat pumps indicated that lowering of supply water temperature by 1 °C would increase the heat pump efficiency by approximately 2% [40], 1.5–1.7% [17], and 1% [41]. By combining these findings with results from the present study it can be concluded that local air pre-heating could improve heat pump efficiency by approximately 8–18%. Moreover, in modern buildings outer wall thicknesses tend to be increasingly larger, due to addition of supplementary thermal insulation. Thicker outer walls give more space for the instalment of a larger heat exchanger (coil spring) inside the wall and thus enable the design of the wall-mounted unit (tube bank) to be even more compact. This should be appreciated by most architects.

In order to fully utilize the potential of the proposed air-heater, in common with ventilation-radiator and vent-convector, they should be installed in rather air-tight buildings. All three preheaters also require regular maintenance to operate optimally. For example, major clogging of the air-filter or surface fouling would greatly decrease their heat output, and thereby the entire advantage of forced airflow through them could be lost. In addition, if the analyzed heating-ventilation systems (Fig. 8a and b) or some other hydronic systems are to be combined with a heat pump, the heat pump should operate with so-called floating condensation (i.e. condensation temperature follows the changes in heat demand) to fully utilize the advantage of the low-temperature water supply. Otherwise, if the heat pump works with so-called fixed condensation (maintaining maximum temperature) the entire benefit of the low-temperature water supply could be lost. Finally, one important subject remains to be explored – to find the method to reduce air-filter resistance in the air-heater.

5. Conclusions

The best known and most thoroughly investigated low-temperature heating system has until recently been floor heating. In the present article authors have investigated possibilities of improving the efficiency of the existing radiator systems so that they can operate at similar supply temperatures as floor heating systems. The first part of the study focused on finding the design requirements for the proposed air-heater and the second part focused on analyzing the effects of combining the proposed air pre-heater with two different radiator systems. Based on the results obtained by the analytical (semi-empirical relations) and numerical (Computational Fluid Dynamics – CFD) calculations in this study, following conclusions can be drawn:

- At given conditions, the proposed air-heater is able to preheat airflow of 10 l/s from −15 to 18.7 °C using 40 °C water supply, at a pressure loss of approximately 10 Pa.
- Radiator systems equipped with the proposed air-heater are able to cover a space heat loss of 35.6 W per square meter floor area, with water temperatures 20–22.5% lower than conventional radiator systems.
- Also, results from present study, in combination with earlier findings by others, indicate that heat pump efficiency in hydronic systems with proposed air-heater would be 8–18% higher than in systems without air-heater.
- In total, the findings from present study support the results from earlier investigations and further enhance our understanding of the benefits of local air-heating.

Acknowledgements

Financial support from the Swedish Energy Agency and Swedish Construction Development Fund (SBUF) is gratefully acknowledged. The authors also wish to thank Heather Robertson for language correction and Aida Ploskić for her help with CAD modelling.

References

[1] Swedish Energy Agency, Heat Pumps, Successful Intervention in Energy Research: Sweden – The Leader in Heat Pumps, ET 2009:23, 2009 (in Swedish).
[2] F. Karlsson, M. Axell, P. Falén, Heat Pump System in Sweden – Country Report for IEA HPP Annex 28, SP AR 2003:01, 2003.
[3] J.M. Moran, H.N. Shapiro, Fundamentals of Engineering Thermodynamics, 5th ed., 2006, pp. 196, 472–473, ISBN-10 0-470-03037-2 (Chapters 5 and 10).
[4] U. Janson, B. Berggren, H. Sundqvist, Improving the Energy Efficiency of Residential Buildings by Retrofitting, Report Number EBD-R-08/22, 2008, pp. 65–88, ISBN 978-91-85147-32-8 (in Swedish).
[5] Radson, The Guide to Radiators for Low Temperature Heating Systems, Technical Note, DM023030150602-02/2012, 2012, pp. 25–33.
[6] A. Boerstra, P.O. Veld, H. Eijdems, The health, safety and comfort advantages of low temperature heating systems: a literature review, in: Proceedings of the 6th International Conference on Healthy Buildings, vol. 2, 2000, pp. 629–634.
[7] J. Babiak, B.W. Olesen, D. Petras, Low Temperature Heating and High Temperature Cooling, REHVA Guidebook, 2007, pp. 14–21, 64–70, ISBN 2-9600468-6-2 (Chapters 3 and 6).
[8] S. Frederiksen, S. Werner, District Heating – Theory, Technique and Functionality, Lund, Studentlitteratur, 1993 (in Swedish).
[9] J.A. Myhren, S. Holmberg, Flow patterns and thermal comfort in a room with panel, floor and wall heating, Energy and Buildings 40 (2008) 524–536.
[10] A. Ploskic, S. Holmberg, Heat emission from thermal skirting boards, Building and Environment 45 (2010) 1123–1133.
[11] S.M.B. Beck, S.C. Grinsted, S.G. Blakey, K. Worden, A novel design for panel radiators, Applied Thermal Engineering 24 (2004) 1291–1300.
[12] A.K.A. Shati, S.G. Blakey, S.B.M. Beck, The effect of surface roughness and emissivity on radiator output, Energy and Buildings 43 (2011) 400–406.
[13] S.B.M. Beck, S.G. Blakey, M.C. Chung, The effect of wall emissivity on radiator heat output, Building Services Engineering Research and Technology 22 (2001) 185–194.
[14] S.I. Gustafsson, Optimisation of insulation measures on existing buildings, Energy and Buildings 33 (2000) 49–55.
[15] S.A. Al-Sanea, M.F. Zedan, Improving thermal performance of building walls by optimizing insulation layer distribution and thickness for same thermal mass, Applied Energy 88 (2011) 3113–3124.
[16] O. Wallin, Computer Simulation of Particle Deposition in Ventilating Duct Systems, Building Services Engineering, Royal Institute of Technology, 1994, ISSN 0284-141X (Doctoral Thesis).
[17] J.A. Myhren, S. Holmberg, Design considerations with ventilation-radiators: comparisons to traditional two-panel radiators, Energy and Buildings 41 (2009) 92–100.
[18] J.A. Myhren, S. Holmberg, Improving the thermal performance of ventilation radiators – the role of internal convection fins, International Journal of Thermal Sciences 50 (2011) 115–123.
[19] A. Ploskic, S. Holmberg, Low-temperature baseboard heaters with integrated air supply – an analytical and numerical investigation, Building and Environment 46 (2011) 176–186.
[20] A.A. Elmualim, H.B. Awbi, D. Fullford, L. Wetterstad, Performance evaluation of a wall mounted convector for pre-heating naturally ventilated spaces, Journal of Ventilation 3 (2003) 213–222.
[21] E. Mundt, M. Gustavsson, P. Leksell, Vent-convector – an experimental study, in: Proceedings of 8th International Conference on Indoor Air Quality and Climate. Indoor Air 99, vol. 5, 1999.
[22] Swedish Meteorological and Hydrological Institute, Data Sheet No. 22, 2004, Available from: http://www.smhi.se/sgn0102/n0205/faktablad_variationer_och_trender.pdf (accessed 01.06.11) (in Swedish).
[23] Verein Deutscher Ingenieure, VDI-Gesellschaft Verfahrenstechnik und Chemieingenieurwesen (GVC), VDI Heat Atlas, 2nd ed., Springer-Verlag, Berlin Heidelberg, 2010, pp. 693–708, ISBN 978-3-540-77876-9.
[24] V. Gnielinski, New equations for heat and mass transfer in turbulent pipe and channel flow, Journal of International Chemical Engineering 16 (1976) 359–368.
[25] J.P. Abraham, E.M. Sparrow, W.J. Minkowycz, Internal-flow Nusselt numbers for the low-Reynolds-number end of the laminar-to-turbulent transition regime, International Journal of Thermal Sciences 54 (2011) 584–588.
[26] Y.A. Çengel, A.J. Ghajar, Heat and Mass Transfer – Fundamentals and Applications, 2010, pp. 439–444, 488–489, ISBN 978-0-07-339812-9 (Chapters 7 and 8).
[27] S. Kakaç, L. Hongtan, Heat Exchangers – Selection, Rating and Thermal Design, 2002, pp. 89, 99–112, ISBN 0-8493-0902-6 (Chapters 3.2.3 and 3.5).
[28] N.S. Cheng, Formulas for friction factor in transitional regimes, Journal of Hydraulic Engineering, ASCE 134 (9) (2008) 1357–1362.
[29] P.L.C. Lage, J.F. Mitre, L.M. Santana, R.B. Damian, J. Su, Numerical study of turbulent heat transfer in 3D pin-fin channels: validation of a quick procedure to

estimate mean values in quasi periodic flows, Applied Thermal Engineering 30 (2010) 2796–2803.
[30] C. Suárez, P. Joubert, J.L. Molina, F.J. Sánchez, Heat transfer and mass flow correlations for ventilated facades, Energy and Buildings 43 (2011) 3696–3703.
[31] S.H. Hashemabadi, F.S. Mirhashemi, Experimental and CFD study of wall effects on orderly stacked cylindrical particles heat transfer in a tube channel, International Communications in Heat and Mass Transfer 39 (2012) 449–455.
[32] A.K. Sharma, N.S. Thakur, CFD based fluid flow and heat transfer analysis of a v shaped roughened surface solar air heater, International Journal of Engineering Science and Technology 4 (2012) 2115–2121.
[33] Exhausto, Vent-convectors TK 35, TK 100, Product Information – Release 2. 3002478 – 12.2005, 2005 (in Swedish).
[34] C.Y. Shaw, G.T. Tamura, The calculation of air infiltration rates caused by wind and stack action for tall buildings, ASHRAE Transactions 83 (2) (1977) 145–158.
[35] P. Walgren, Good Examples of Airtight Building Design Solutions, SP Technical Research Institute of Sweden, SP Rapport 2010:09, Borås, 2010, ISBN 978-91-86319-45-8 (in Swedish).
[36] W.R. Chan, P.N. Price, A.J. Gadgil, Sheltering in buildings from large-scale outdoor releases, in: Air Infiltration and Ventilation Centre, Ventilation Information Paper LBNL-55575, 2004.
[37] J. Rekstad, M. Meir, A.R. Kristoffersen, Control and energy metering in low temperature heating systems, Energy and Buildings 35 (2003) 281–291.
[38] Radiator Heat Output Calculator, Manufacturer's data, 2013, Available from: http://www.purmo.com/se/ladda-hem-filer/effektsimulering.htm (accessed 26.01.12).
[39] P.E.J. Siegenthaler, Modern hydronic heating for residential and light commercial buildings, 2nd ed., 2004, pp. 241, ISBN-10 0-7668-1637-0.
[40] D. Schmidt, Design of low exergy buildings-method and a pre-design tool, International Journal of Low Energy and Sustainable Buildings 3 (2004) 1–47.
[41] A. Ploskic, Low-temperature baseboard heaters in built environments, in: Licentiate Thesis in Technology, KTH Royal Institute of Technology, Stockholm, 2010, pp. 8, ISBN 978-91-7415-744-4.

Applied Thermal Engineering 62 (2014) 382–389

Contents lists available at ScienceDirect

Applied Thermal Engineering

journal homepage: www.elsevier.com/locate/apthermeng

Performance evaluation of radiant baseboards (skirtings) for room heating – An analytical and experimental approach

Adnan Ploskić*, Sture Holmberg

KTH Royal Institute of Technology, School of Architecture and the Built Environment, Fluid and Climate Technology, Brinellvägen 23, 100 44 Stockholm, Sweden

HIGHLIGHTS

- Thermal performance of radiant baseboards (RBs) used for space heating was analyzed.
- The proposed heat output equation can be used with confidence for RBs heaters.
- The heat transfer ability of RBs was 50% higher than that of panel radiators.
- The heat emission from RBs increased by roughly 2.1% per centimeter of height.
- The RBs of maximum height should be used for water supply temperatures below 45 °C.

ARTICLE INFO

Article history:
Received 19 June 2013
Accepted 27 September 2013
Available online 8 October 2013

Keywords:
Baseboard (skirting) heating
Radiator heating
Space heating
Energy efficiency
Measurements
Curve fitting

ABSTRACT

The aim of this study was to investigate the thermal performance of the hydronic radiant baseboards currently used for space heating in built environments. The presently available equations for determination of heat outputs from these room heaters are valid for a certain height at a specific temperature range. This limitation needed to be addressed as radiant baseboards may be both energy and cost efficient option for space heating in the future. The main goal of this study was therefore to design an equation valid for all baseboard heights (100–200 mm) and excess temperatures (9–60 °C) usually used in built environments.

The proposed equation was created by curve fitting using the standard method of least squares together with data from previous laboratory measurements. It was shown that the predictions by the proposed equation were in close agreement with reported experimental data. Besides, it was also revealed that the mean heat transfer coefficient of the investigated radiant baseboards was about 50% higher than the mean heat transfer coefficient of five conventional panel radiators of different types.

The proposed equation can easily be used or programed in energy simulation codes. Hopefully this will help engineers to quantify more accurately the energy consumption for space heating in buildings served by radiant baseboards.

1. Introduction

Different types of hydronic and electric systems are currently used for space heating in the Swedish residential sector [1]. In hydronic systems, heat is usually distributed by conventional hot-water radiators while in electrical systems various distribution arrangements are used. Between 1960 and 2010 electrical systems were predominantly used for space heating in Swedish single-family dwellings. Accordingly, approximately 70% of the country's single-family houses either used or could use electricity for space heating in 2001. By that time, around 34% of 1.6 million Swedish single-family houses were heated by direct-acting electricity and water-based electric heating [2]. In addition to these 34%, another 36% had electric heating as an alternative heating system [2]. This means that about 1.12 million of country's single-family houses used electricity either as sole or as a supplementary heating system in 2001.

In order to reduce the electrical peak loads and energy consumption during the heating season, the Swedish government has undertaken a number of measures over the last decades. Thus, during the period between 2006 and 2010 the homeowners could have been refunded with up to 30% of their conversion costs, when

* Corresponding author. Tel.: +46 (0) 8 790 48 86; fax: +46 (8) 790 48 00.
E-mail address: adnan.ploskic@byv.kth.se (A. Ploskić).

1359-4311/$ – see front matter © 2013 Elsevier Ltd. All rights reserved.
http://dx.doi.org/10.1016/j.applthermaleng.2013.09.053

Nomenclature

Latin letters

A	area m^2
a	constant in Eq. (3) -
b, c and d	exponents in Eq. (3) -
c_p	specific heat capacity, J/(kg °C)
d	diameter, m
H	baseboard height, m
h	height of waterway, m
f	flow friction factor between water and waterways
K	heater constant, W/°C^n
k	equation number
L	length, m
$\dot{m}$	mass flow, g/s
n	temperature exponent or number of samples
P	heat output/thermal power, W
q	heat output per m, W/m
Re	Reynolds number
SEE	standard error of estimate, W/m
U	total heat transfer coefficient, W/(m^2 °C)
v	velocity of water, m/s
w	width of waterway, m

Greek letters

ε	absolute inner surface roughness, m
θ	temperature, °C
Δ	percentage difference, %
$\Delta\theta$	excess temperature = mean temperature difference between room heater and room air, °C
Δp	pressure loss, Pa

Subscripts

ave	average
calc	calculation by Eq. (9)
eq	equivalent
max	maximum
ref	reference value
room	room
rtn	Return
supp	supply

conventional radiator types

10	single panel
11	single panel + single convector plate
21	two panels + single convector plate
22	two panels + two convector plates
33	three panels + three convector plates

converting from electric to alternative heating systems [3]. As a result of conversions between 2006 and 2010, the electrical energy consumption for space heating in the residential sector has been decreased by 476 GWh/year. It was estimated that about 34% of this total saving could be directly attributed to the government's financial support [4].

In addition to the above-mentioned, the installation of heat pumps in Sweden increased greatly between 1994 and 2011. As a result of this the one-millionth heat pump was put in operation in single-family houses in 2010 [5]. The Swedish Heat Pump Association has estimated that by that time approximately half of the installed heat pumps were of the air-to-water and closed-loop types [6]. By 2010, these two heat pump types stood for approximately 490 MW of installed nominal power in Sweden [7].

As is generally known, the efficiency of the heat pump in a heating system is strongly dependent on the supply water temperature of the system. The lower the supply water temperature, the higher the efficiency of the heat pump. Up to now, the supply temperature of the heating system in Swedish single-family houses was usually decreased by increasing the number of room heaters. Although various types of the room heaters were available on the market at that time, conventional radiators were mainly used for heat distribution in dwellings heated by heat pumps. Similarly, conventional radiators were also predominantly used when converting from direct-acting electricity to hydronic heating. Despite the fact that perhaps some other types of room heaters could have been more appropriate option, especially for homes served by heat pumps.

It should also be noted that Sweden is not alone in making efforts to improve the efficiency of the heating systems. Different research groups in several European countries are also currently working on finding methods to improve thermal efficiency of the heating systems in residential buildings. Meir et al. [8] presented a new method for temperature control in buildings with floor heating. The presented control method decreased the response time and resulted in closer follow of changes in outdoor temperature. Consequently, this control method was more energy efficient than the traditional one with conventional thermostats. The joint influence of the enhanced emissivity and the surface roughness of a wall behind a hot radiator was studied by Shati et al. [9]. They found that the total heat output from the radiator could be increased by 26% through the use of a high emissivity saw-tooth wall surface. Pinard et al. [10] studied the possibility to enhance the heat output from a room heater using induced stack effect. Reported results suggested that this method could improve the total heat output by approximately 24%, at maximum. Badescu [11] investigated the potential of using active solar heating in a passive house. He found that 62% of the total annual heat demand could be met by this system. Hewitt et al. [12] analyzed performance of an air-source heat pump connected to a radiator system. Not surprisingly, they concluded that low-temperature radiators would increase the heat pump efficiency.

In conclusion, findings from the presented studies clearly suggest that the need for efficient and flexible heating systems is broad.

1.1. Potential of radiant baseboard heaters

A hydronic heating system that is still limitedly used in Swedish residential sector is radiant baseboards (Fig. 1a). The radiant baseboards usually have two waterways. One supply and one return pipe, which are attached to the enclosing metal plate (Fig. 1b). The waterways are also connected by a 180° u-bend at the opposite end of the circuit. The typical height of the radiant baseboards is between 120 and 180 mm, and their length is normally ranging from 8 to 15 m per room. Since enclosing plates have no openings at the front side, the adjacent room air is prevented from passing over the inner part of the unit. Consequently, a large portion of the emitted heat is transferred by thermal radiation [13]. An additional example of radiant baseboards placement in a real-life room is given by Fig. 1c.

Due to their low height, the transferred convective heat flux from radiant baseboards to the room air is high [15]. Also, since radiant baseboards are installed at the base of the walls they are

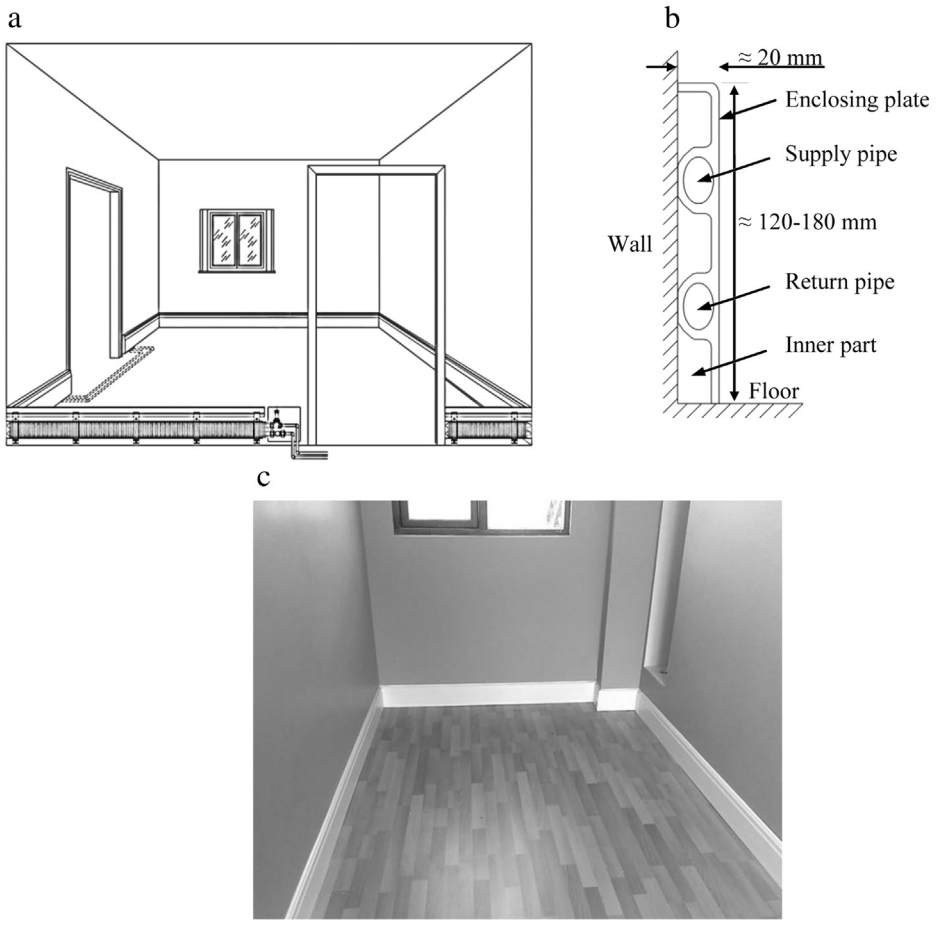

Fig. 1. a. Illustration of the placement of radiant baseboards along the inner periphery of a room [14]. b. The typical dimensions and vertical cross-section of a radiant baseboard heater. c. The installation of radiant baseboards under real-life conditions.

exposed to colder room air along their entire length. This increases the thermal gradient and thus their ability to transfer heat to the room. The cumulative effect of these two characteristics of the radiant baseboards is illustrated in Fig. 2a. As can be seen, the mean heat transfer coefficient of the radiant baseboard is much higher than that of conventional panel radiators. The average heat transfer coefficients of the panel radiators ranged from 7.4 to 9.7 W/m^2 °C, with a joint mean value of 8.4 W/m^2 °C. On the other hand, the mean heat transfer coefficient of the used radiant baseboard arrangement was 12.6 W/m^2 °C. This means that the heat transfer ability of the used radiant baseboard was about 50% higher than that of the selected radiator types.

The total heat output as a function of the length of a 0.185 m high radiant baseboard is shown in Fig. 2b. In the same figure the outputs from two panel radiators of different geometries and types are also shown. It can be seen that 12 m long and 0.185 m high radiant baseboard, gave the same heat output (≈890 W) as a 1.2 m long and 0.5 m high panel radiator of type 22. This means that in a 5 m by 3.5 m room space, the selected radiant baseboards installed along three walls would be able to give the same amount of heat as the above-mentioned radiator type. With these water temperatures the used radiant baseboard arrangement is also powerful enough to cover the heat loss of the considered room space at an outdoor temperature of −17 °C [8]. This temperature level presently corresponds to the design outdoor temperature for buildings with time constants between 24 and 72 h, placed in the central part of Sweden [16].

1.2. Previous studies on radiant baseboard heaters

In contrast to most conventional hydronic room heaters, reliable heat emission data from radiant baseboards is still limited. Usually the data provided by the radiant baseboard manufacturers is both limited and often poorly presented. Consequently, the traceability of the presented data is very difficult or impossible and therefore the validity might be questioned. According to the authors' present knowledge, four reliable reports dealing with heat emission from radiant baseboards have been reported in the recent past. In a previous study [15] we estimated heat emission from 0.15 m high radiant baseboards using well-known relations for natural convection and thermal radiation for a vertical flat plate. Russell [18,19] reported the measured heat outputs from 0.185 and 0.13 m high radiant baseboards. Siegenthaler [20] in his book presented a diagram with heat emission from a 0.127 m high radiant baseboard heater.

Summarizing the findings from previous studies presented in Sections 1–1.3 the following can be concluded:

- There is a need for efficient and flexible hydronic heating systems that can either be used as an alternative or as a complement to existing room heaters.
- The heat transfer ability of radiant baseboards is much higher than that of conventional panel radiators. Radiant baseboards may therefore play an important role for space heating both in new-built and retrofitted buildings.

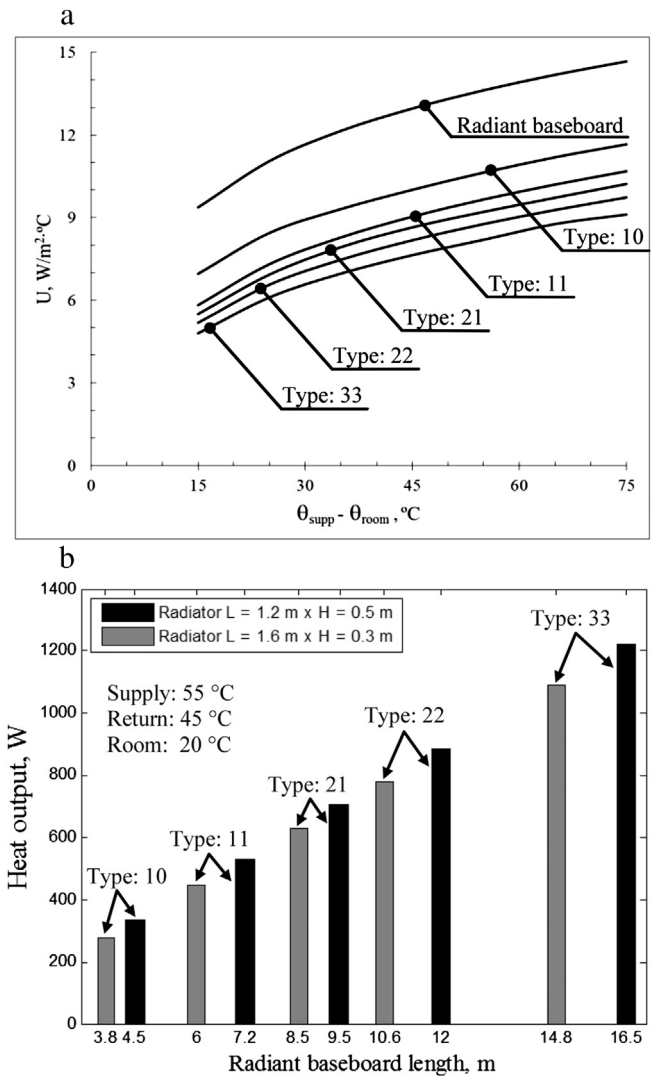

Fig. 2. a. The variation of the mean heat transfer coefficient *U* for considered room heaters [17,18]. The heights for used radiant baseboards and conventional radiators were 0.185 m and 0.3 m, respectively. b. The required lengths of a 0.185 m high radiant baseboard [18] to produce the same heat outputs as the different radiator types of 1.6 m length and 0.3 m height, and 1.2 m length and 0.5 height [17].

- In the previous investigations, the heat emission from radiant baseboards was either measured or calculated at a certain baseboard height.

1.3. Objectives

Therefore, the main objective of this study was to design a reliable equation for estimation of heat output from radiant baseboards. The aim was to design an equation that would be applicable for all baseboard heights (0.1–0.2 m) and excess temperatures (9–60 °C) usually used for radiant baseboards in built environments.

2. Method

2.1. Laboratory measurements

The experimental data reported by Russell [18,19] was used as base for designing the aimed equation. In these two reports, the heat outputs from 0.13 and 0.185 m high radiant baseboards operated at different water temperatures were reported. The heat outputs were measured in a testing chamber of 4 m (1ength) × 4 m (width) × 3 m (height). The tested radiant baseboards consisted of a 3 m long aluminum extrusion with two integral horizontal waterways. The hot-water inlet and outlet were at the same end of the baseboards, and connected with a return bend at the opposite end. Since the radiant baseboards were tested at different water temperatures, all chamber walls except the wall behind the baseboards were also water-cooled. By doing so, the mean indoor air temperature in the chamber was kept at 20 °C. The air temperature was monitored at 0.75 m above the floor level at the center of the chamber. The wall behind the baseboards was also well insulated to prevent heat losses.

The steady-state condition inside the chamber was maintained for at least 30 minutes before starting the measurements. After reaching steady state, the measurement data was automatically logged at 100 second intervals. The heat outputs from the baseboards were determined by measuring: 1) the change of water temperature between inlet and outlet, 2) the water mass flow rate through the baseboards and 3) the air temperature inside the chamber. The water and air temperatures were measured by resistance thermometers, while the water flow rate was measured by a mass flow meter. The air thermometer also had a protecting shield to minimize the influence of thermal radiation from the surrounding walls. All used measuring instruments were calibrated with probes of higher accuracy before testing, see Table 1. The dates of testing for both radiant baseboards were within the time range of calibration validity for all instruments.

It should be noted that the outputs were measured according to European norm EN 442-2 from 1997. This norm defines procedures for determining the thermal power of the heating appliances fed with water or steam at temperatures below 120 °C. In order to hold the license for testing according to EN 442-2, the total precision of the performed measurements in the testing laboratory must be within ±2% deviation of results obtained by other certificated laboratories [21]. Since 2003, this precision level is regularly controlled by a round-robin test at least once a year without prior notice. The precision and the accuracy levels of measurements performed by the Building Services Research and Information Association (BSRIA) testing laboratory was checked regularly according to the above described method. The precision and the accuracy of data used for this study lay within the above-specified range and as shown in Table 1.

2.1.1. Operating water flow rate

The thermal outputs of the radiant baseboards were measured at three water flow rates, 10.6 g/s, 56.0 g/s and 112.5 g/s. In order to decide which flow rate was the most appropriate for the present study, the Reynolds number and linear pressure loss for all three water flow rates were calculated and compared to each other. The

Table 1
The ranges, uncertainties and calibration accuracies of instruments used for measurements in the testing chamber [18,19].

Item	Instrument	Range	Uncertainty	Calibration accuracy
Water temperature	Resistance thermometer	30–90 °C	±0.05 °C	±0.02 °C
Air temperature	Resistance thermometer	19–21 °C	±0.04 °C	±0.02 °C
Mass flow rate	Mass flow meter	10–113 g/s	±0.02–0.04%	±0.02–0.04%
Pressure	Barometer	900–1066 mbar	±1 mbar	±0.02%

calculations were based on the equivalent diameter d_{eq} of an oval cross section, as the waterways of the tested baseboards were elliptical.

From Table 2 it can be seen that the water flow at 10.6 g/s was laminar and generated a pressure loss of 3 Pa/m per waterway. At 56.0 and 112.5 g/s the flow was turbulent and the pressure loss per waterway was 54 and 180 Pa/m, respectively. Based on this, the heat outputs at 10.6 g/s were excluded from further consideration as this flow was not turbulent and thus should be avoided when designing baseboard heating systems [13,14]. Similarly, the heat outputs at the flow rate of 112.5 g/s were also excluded as this flow generated a pressure loss 1.8 times higher than 100 Pa/m per waterway. As this value is presently used as a guideline in dimensioning heating pipe networks [16]. Thus for the current study the heat outputs produced by the water flow of 56.0 g/s were used as reference in designing the aimed equation.

2.2. Equations for estimation of the heat output

In general, heat output from hydronic room heaters is mostly controlled by three parameters: the temperature of the heater surface, the size of the heater surface area and the temperature of the room air. The total influence of these three parameters is normally summarized by a global energy balance, as shown by Eq. (1).

$$P = \dot{m} c_p (\theta_{supp} - \theta_{rtn}) = UA \overbrace{\frac{\theta_{supp} - \theta_{rtn}}{\ln[(\theta_{supp} - \theta_{room})/(\theta_{rtn} - \theta_{room})]}}^{\Delta\theta} \quad (1)$$

The magnitude of the heat transfer coefficient U is affected by several factors, such as the material, design, height and operating water temperatures of the heater. Due to this, the theoretical calculation of the U value is normally laborious. For room heaters with a constant surface area, the heat output becomes a function of the heater constant and excess temperature only. Accordingly, the complexity of the right-hand side of Eq. (1) can be reduced to Eq. (2) [13]. In this expression, P represents the total heat output, K is the heater constant and n is the temperature exponent. The values for K and n are not universal and they apply to a certain heater dimension only. Normally they are determined using an experiment-based approach together with regression analysis. For hydronic baseboard heaters, Eq. (2) was also used for estimation of the heat output per linear meter (W/m) for a fixed height [14].

$$P(\Delta\theta) = K\ \Delta\theta^{n} \quad (2)$$

Since the aim of this study was to design an equation that would be valid for all heights and excess temperatures usually used for radiant baseboards in built environments, Eq. (2) needed to be generalized. According to norm EN 442 the heat emission from conventional radiators can also be estimated by Eq. (3) [22]. In this equation, q stands for heat output per meter length (=P/L), H for radiator height and a, b, c and d are polynomial coefficients. Also here, the coefficients are not universal and they apply for a certain radiator design only. As in case with Eq. (2), the values of the coefficients are determined by measurements and regression analysis.

$$q(H,\ \Delta\theta) = a\ H^{b}\Delta\theta^{c\pm d\cdot H} \quad (3)$$

In the present study, the form of Eq. (3) was used to design the aimed equation. The adaptation of Eq. (3) occurred in two steps. In the first step, the heat output data for baseboard heights 0.1, 0.15 and 0.2 m was extrapolated and interpolated linearly from the experimental data obtained for heights 0.13 and 0.185 m [18,19]. This was considered as acceptable since the baseboard heights of 0.1, 0.15 and 0.2 m are sufficiently close to the heights of 0.13 and 0.185 m, respectively. In the second step, values of coefficients in Eq. (3) for baseboard heights of 0.1–0.2 m and excess temperatures of 9–60 °C were determined using least squares method, as follows. First, the polynomial expression in Eq. (3) was linearized as shown by Eq. (4).

$$\ln(a) + b\ln(H_k) + c\ln(\Delta\theta_k) + d\,H_k\ln(\Delta\theta) = \ln(q_k),\ \text{where } k = 1,\ldots,55. \quad (4)$$

In a following step, the measured, extrapolated and interpolated heat output values (q_k) for the corresponding H_k and $\Delta\theta_k$ were substituted into Eq. (4). This resulted in a system of 55 equations. The generated equation system had the matrix form of $\mathbf{AX} = \mathbf{B}$, where $\mathbf{A}$ was a 55×4 matrix with rows [1, ln (H_k), ln ($\Delta\theta_k$), H_k ln ($\Delta\theta_k$)], $\mathbf{B}$ was a 55×1 column matrix with entries ln (q_k) and $\mathbf{X}$ was the column vector with elements to be determined. The elements of vector $\mathbf{X}$ are shown below.

$$\mathbf{X} = \begin{bmatrix} \ln(a) \\ b \\ c \\ d \end{bmatrix}$$

Generally, vector $\mathbf{X}$ is a least squares solution of the system $\mathbf{AX} = \mathbf{B}$ if and only if it is a solution of the associated normal system $\mathbf{A^T AX} = \mathbf{A^T B}$. As in our case $\mathbf{A^T A}$ (4×4) was invertible, the solution for $\mathbf{X}$ was thus obtained by Eq. (5).

$$\mathbf{X} = \left(\mathbf{A^T A}\right)^{-1}\mathbf{A^T B} \quad (5)$$

2.3. Statistical comparison

The calculated heat outputs obtained by the modified Eq. (3) were also statistically compared with the measured, extrapolated and interpolated values. For simplicity, these three types of values are in continuation collectively termed as reference values. In total, three equations have been used. Eqs. (6) and (7) were applied to quantify the absolute mean and maximum difference between the calculated and reference values, and Eq. (8) was used to calculate the Standard Error of Estimate (SEE) for the entire data set-up. The SEE is a standard statistical tool for rating the standard deviation of the residuals (differences). Ideally, the SEE = 0. In that case there would be no difference between the reference and calculated values. However, in reality, this is never the case. Therefore, in practice, the goal is always to minimize the SEE.

Table 2
The geometries of a single waterway of the tested radiant baseboards, together with flow parameters. The calculations were performed at a mean water temperature of 50 °C.

Item	$\dot{m}$(g/s)	h (mm)	w (mm)	d_{eq} (mm)	v (m/s)	$Re_{d_{eq}}$	ε/d_{eq}	f	$\Delta p/L$ (Pa/m)
I	10.6	20	15	17.4	0.05	$1.43\cdot10^{3}$	$8.6\cdot10^{-5}$	0.045	3
II	56.0	20	15	17.4	0.24	$7.53\cdot10^{3}$	$8.6\cdot10^{-5}$	0.033	54
III	112.5	20	15	17.4	0.48	$1.51\cdot10^{4}$	$8.6\cdot10^{-5}$	0.028	180

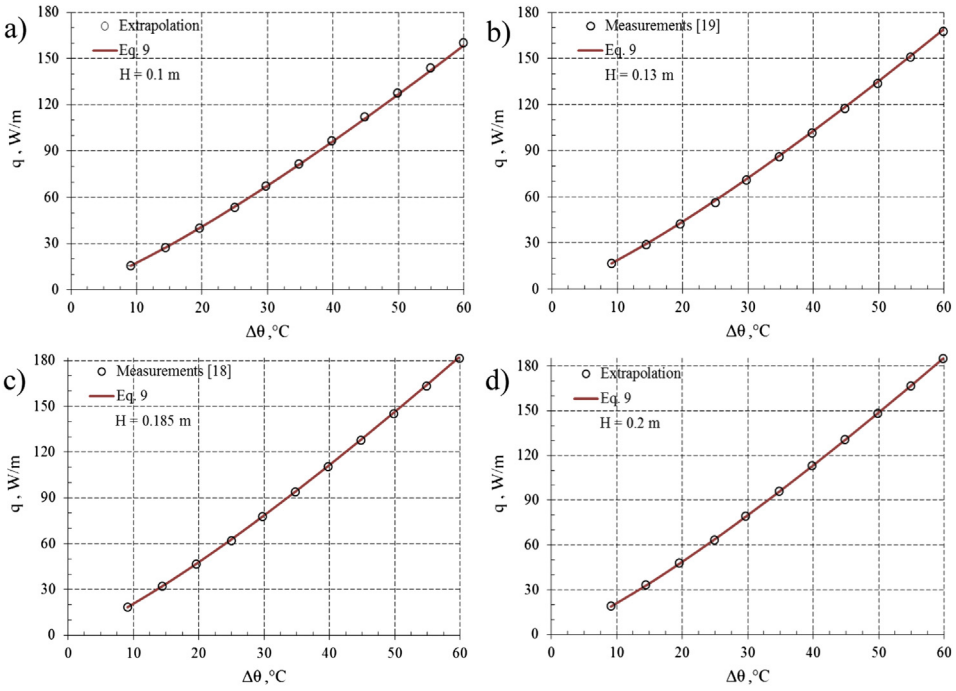

Fig. 3. a–3d. Comparative plots of the measured, extrapolated and calculated heat outputs by Eq. (9). a) shows the plot for a baseboard height of $H = 0.1$ m, b) for $H = 0.13$ m, c) for $H = 0.185$ m and d) for $H = 0.2$ m. The range of excess temperatures was the same for all four cases, i.e. $\Delta\theta = 9$–60 °C.

$$\Delta_{ave} = \frac{1}{n}\sum_{i=1}^{n}\frac{\left|q_{calc,\ i} - q_{ref,\ i}\right|}{q_{calc,\ i}} \tag{6}$$

$$\Delta_{max} = \max\left(\frac{\left|q_{calc,\ i} - q_{ref,i}\right|}{q_{calc,\ i}}\right) \tag{7}$$

$$SEE = \sqrt{\frac{\sum_{i=1}^{n}\left(q_{ref,\ i} - q_{calc,\ i}\right)^2}{n}} \tag{8}$$

3. Results

In general, the best curve fit in the least squares sense is obtained by minimizing the sum of squared differences between the reference and the calculated (fitted) values. Practically this means that in the present study the values of the elements in vector **X** were determined so that the absolute differences between the reference and the calculated values were the smallest possible. The obtained values for elements in vector **X**, applying the conditions and the calculation steps described at the end of Section 2.2, are presented below.

$$\mathbf{X} = \begin{bmatrix} 0.747 \\ 0.313 \\ 1.246 \\ -0.147 \end{bmatrix}$$

Accordingly, $\ln(a) = 0.747 \Leftrightarrow a = 2.110$, $b = 0.313$, $c = 1.246$ and $d = -0.147$ are the values of the constant and exponents for Eq. (3), respectively. Finally, the final form of the modified Eq. (3) is shown by Eq. (9).

$$q(H,\ \Delta\theta) = 2.110 \cdot H^{0.313} \cdot \Delta\theta^{1.246 - 0.147 \cdot H} \tag{9}$$

The comparative plots between the reference values and those calculated by Eq. (9) are demonstrated in Fig. 3a–d. The rings represent the reference values and the solid lines show the calculated values. The plots confirm that the proposed Eq. (9) is applicable for all baseboard heights from 0.1 to 0.2 m and excess temperatures from 9 to 60 °C. In that height and temperature range, the mean and maximum absolute differences between the reference and calculated values were less than 0.8 and 1.6%, respectively (Table 3). The dispersion (SEE) between the values for $\Delta\theta = 9$–60 °C and $H = 0.1$ m was 1.09 W/m, and ≤0.65 W/m for $H = 0.13$–0.2 m. It should be noted that dispersion for $H = 0.1$ m and $\Delta\theta = 9$–46.6 °C was also ≤0.65 W/m. Practically this means that for supply water temperatures between 35 and 71.5 °C and baseboard heights between 0.1 and 0.2 m, the maximum uncertainty of the prediction by Eq. (9) is ±0.65 W/m.

Furthermore in Fig. 4a, the increase of relative heat output for five different baseboard heights between 0.1 and 0.2 m is shown. It can be observed that heat emission on average increases by approximately 2.1% per centimeter of height. The increase for heights between 0.1 and 0.15 m is somewhat higher than average, i.e. around 2.25%/cm, and for heights 0.15–0.2 m it is slightly lower than average, about 2.0%/cm. The increase for $H = 0.1$–0.15 m and $\Delta\theta = 9$–60 °C is also approximately linear and constant, while between $H = 0.15$ m and $H = 0.2$ m the increase is exponential. In

Table 3
Overview of the absolute mean and maximum differences and SEE between the reference and values calculated by Eq. (9) for $\Delta\theta = 9$–60 °C.

Item	H (mm)	Δ_{ave} (%)	Δ_{max} (%)	SEE (W/m)
I	100	0.78	1.35	1.09
II	130	0.78	1.21	0.64
III	185	0.32	0.72	0.42
IV	200	0.57	1.60	0.35

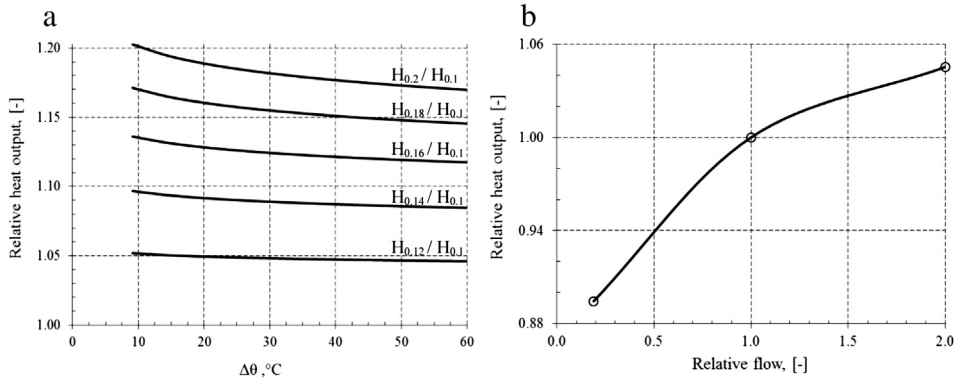

Fig. 4. a. The increase of relative heat output as a function of excess temperature for five baseboard heights between 0.1 and 0.2 m. b. The measured relation between the relative heat output and relative water flow [18,19].

particular for the range $\Delta\theta = 9–20$ °C, or more precisely for supply water temperatures 35–45 °C. Therefore, if radiant baseboards are to be operated at water supply temperatures lower than 45 °C their height should be the maximum possible in order to maximize the thermal output of the system.

Moreover, according to measurements the heat outputs at a water flow of 112.5 g/s were on average 4.5% higher than the outputs at 56.0 g/s, which were about 10.5% higher than the outputs at 10.6 g/s [18,19]. This finding is also illustrated in Fig. 4b. In other words, a doubling of the water flow through the radiant baseboards would increase their total heat output by about 4.5%. On the other hand, the pressure loss on the water-side generated by the doubling of the flow would increase by approximately 230% (Table 2). This means that for the case considered, the hydraulic power loss due to increased water flow would be roughly 6.4 times higher than the heat power gain due to increased heat emission. This relation between power loss and gain is not universal and applies for a certain baseboard design at certain water flows only. However, this gives an indication of at which water flow rates radiant baseboards should be operated.

4. Discussion

Despite their potential and flexibility, the use of radiant baseboards for space heating in Sweden is still very limited. Besides, until now the linear heat outputs from radiant baseboards were predicted by expressions valid for a certain baseboard height. As this heating system may play an important role for space heating in the future, this limitation needed to be addressed. The main aim of the present study was therefore to design a reliable equation for prediction of linear heat output for baseboard heights between 0.1 and 0.2 m and excess temperatures in range of 9–60 °C. For this purpose, the recently reported measurements performed in the United Kingdom's leading independent laboratory (BSRIA) were used [18,19]. The proposed equation (Eq. (9)) is an adaptation of the expression given by the European norm EN 442, and is a function of both baseboard height and excess temperature. It was shown that the predictions of linear heat outputs by the proposed equation were in close agreement with experimental data obtained in the laboratory.

The laboratory measurements also revealed that doubling the water flow through the radiant baseboards will only slightly increase the heat emission. It is therefore recommended to use the current guideline value of 100 Pa/m for water-side pressure loss for system design, for two reasons. Firstly, to keep the energy usage for pumping at a moderate level and secondly to ensure an acceptable temperature drop across each baseboard heating circuit.

As also confirmed in this study, the basic advantage of the radiant baseboards lies in their placement along the bottom of the room walls. The room air in these parts of the heated space is usually the coldest. Therefore, the heat transfer ability of the radiant baseboards is much higher compared to other conventional radiator types. Since radiant baseboards are installed along the base of the walls, they are also suitable for homes without basements where cold floors are common [13]. In addition, due to their installation flexibility they can both operate as a sole heating system or be combined with already existing heating systems in the buildings. Due to this characteristic, the radiant baseboards might be an alternative when converting from electric to hydronic heating as well as for use in homes served by a heat pump. Other characteristics of the radiant baseboards are: I) elegant and discrete design, II) minimal interference with furniture placement, and III) the heat distribution near the floor.

The penultimate statement is ambivalent – since placing furniture close to baseboard heaters may degrade their heat output. In order to avoid this, a minimum of 150 mm of free space should be available in front of any baseboard heater [20]. The last characteristic creates a floor-to-ceiling temperature difference of about 1–2 °C, and thus produces a uniform temperature distribution across the entire heated space [15]. However, in the same study it was found that draught discomfort could occur at supply temperatures lower than 45 °C in a room with high glass surfaces.

Beside the operating water temperatures and the height, the heat emission from the radiant baseboards is strongly influenced by the free wall perimeter of the room. These room heaters should not therefore be installed in rooms with limited perimeter and high heating demand. A good practice guideline is that installed length of radiant baseboards per room should be around 12 m and not exceed 15 m. In this study it has been revealed that 12 m long and 0.185 m high radiant baseboards were able to give the same amount of heat as a 0.5 m high and 1.2 m long panel radiator of type 22. This means that radiant baseboards with this arrangement are able to replace most common radiator types used in built environments. However, it was also observed that a radiator of large dimensions and more compact design, such as type 33, was able to give more heat than the investigated radiant baseboards under the same conditions.

The proposed equation can easily be used and programed in energy simulation codes. In the future it would be interesting to simulate energy consumption for space heating in a given building served by radiant baseboards. This would further deepen the knowledge about advantages and limitations of this heating system. Another important subject remains to be explored. This is whether the heat emission from radiant baseboards can further be

enhanced by an additional supply waterway (pipe), as a compliment to the existing one.

5. Conclusions

In this study the authors have investigated the thermal performance of hydronic radiant baseboards. The main goal was to design a reliable equation for prediction of heat output per unit length of the baseboard. Based on the obtained results the following can be concluded:

- The heat outputs predicted by the proposed equation (Eq. (9)) were in close agreement with the previous experimental investigation. Therefore the proposed equations can be used with confidence for system design in practice.
- A doubling of the water flow through the investigated baseboards would increase the total heat emission by only 4.5%. It was therefore recommended to use the current guideline value of 100 Pa/m for water-side pressure loss for the system design.
- Calculations showed that heat emission per unit length from radiant baseboards increased by approximately 2.1% per centimeter of height. It is therefore suggested to use radiant baseboards of maximum possible height if this heating system is to be operated at supply water temperatures below 45 °C.
- Because of their installation flexibility and discreet finish, radiant baseboards can be used both in new-built and in retrofitted buildings. Either as the sole or as an additional heat-distributing system.
- Radiant baseboards should not be used in rooms with small wall perimeter and high heating demand.

Acknowledgements

Financial support from the Swedish Energy Agency and Swedish Construction Development Fund (SBUF) is gratefully acknowledged. The authors also wish to thank Armin Halilović for his help with mathematical modeling and company DiscreteHeat for the technical support.

References

[1] F. Karlsson, M. Axell, P. Falén, Heat Pump Systems in Sweden – Country Report for IEA HPP, 2003. Annex 28, SP AR 2003:01.
[2] M. Sandberg, Conversion of Electrically Heated Houses – an Overview of Different Configurations for Heating Systems. report number 2003:03, 2003, ISBN 91-7848-951-2 (in Swedish).
[3] M. Heymowska, L. Aspelin, Conversion of Direct-acting Electric Heating in Residential Buildings, County Administrative Board of Stockholm County, 05.03.2012 (in Swedish).
[4] Swedish National Board of Housing, Building and Planning, Evaluation of Support for the Conversion from Direct-acting Electric Heating in Residential Buildings. ISBN: 978-91-868271-59-5, report number 2011:20, 2011 (in Swedish).
[5] Swedish Heat Pump Association, More than 1 million heat pumps in Sweden, press release from 01.20.2011, available from: http://www.svepinfo.se/aktuellt/nyhetsarkiv/2011/fler-an-1-miljon-varmepumpar-i-sverige/, (accessed 18.07.2012). ((in Swedish))
[6] Swedish Heat Pump Association, Sales of Heat Pumps in Sweden, 2002, 2011 available from: http://www.svepinfo.se/usr/svep/resources/filearchive/10/diagram_forsaljning_2002_2011.pdf (accessed 18.07.2012). (in Swedish).
[7] Swedish Heat Pump Association, Heat Pump Sales Expressed in Nominal Output for the Years 1982–2011, available from: http://www.svepinfo.se/usr/svep/resources/filearchive/10/varmepumpsforsaljning_1982_2011.pdf, (accessed 18.07.2012). (in Swedish)
[8] M. Meir, J. Rekstad, A.R. Kristoffersen, Control and energy metering in low temperature heating systems, Energy Build. 35 (2003) 281–291.
[9] A.K.A. Shati, S.G. Blakey, S.B.M. Beck, The effect of surface roughness and emissivity on radiator output, Energy Build. 43 (2011) 400–406.
[10] S. Pinard, G. Fraisse, C. Ménézo, V. Renzi, Experimental study of a chimney enhanced heat emitter designed for internal renovation of buildings, Energy Build. 54 (2012) 169–178.
[11] V. Badescu, Simulation analysis for the active solar heating system of a passive house, Appl. Therm. Eng. 25 (2005) 2754–2763.
[12] N.J. Hewitt, M.J. Huang, M. Anderson, M. Quinn, Advanced air source heat pumps for UK and European domestic buildings, Appl. Therm. Eng. 31 (2011) 3713–3719.
[13] American Society of Heating, Refrigerating and Air-Conditioning Engineers (ASHRAE), HVAC Systems and Equipment, 2008, ISBN 0-910110-86-7, p. 33.4 (chapter 33).
[14] Thermodul Hekos, Skirting Board Heating System, Technical Manual, 2007, pp. 8 and 10.
[15] A. Ploskic, S. Holmberg, Heat emission from thermal skirting boards, Build. Environ. 45 (2010) 1123–1133.
[16] C. Warfvinge, M. Dahlblom, Design of HVAC Installations, first ed.:2, 2010, ISBN 978-91-44-05561-9 (chapter 4), pp. 4:5 and 4:6. (in Swedish).
[17] Radiator heat output calculator, manufacturer's data, available from: http://www.purmo.com/se/ladda-hem-filer/effektsimulering.htm, (accessed 26.01.2012).
[18] A. Russell, Thermal Tests on a Skirting Board Heater, Building Services Research and Information Association (BSRIA), November 2007 report number 513828.
[19] A. Russell, Radiator Tests, Building Services Research and Information Association (BSRIA), August 2006 report number 40079/1.
[20] J.P.E. Siegenthaler, Modern Hydronic Heating for Residential and Light Commercial Buildings, second ed., 2004. http://www.google.se/search?tbo=p&tbm=bks&q=inauthor:%22John+Siegenthaler%22. ISBN 10: 0-7668-1637-0, (chapter 8), p. 241 and 282.
[21] TÜVRheinland, DIN CERTCO, Certification Scheme DIN-geprüft, Radiators and Convectors According to DIN EN 442, August 2008, pp. 1–27.
[22] Thermopanel, Technical Manual, Design Brochure 11-2010, 2010, p. 5 (in Swedish).

Clima 2010, Ref. Nr: 0572

Low-temperature heat emission with integrated ventilation air supply

Sture Holmberg, Jonn Are Myhren and Adnan Ploskic

Fluid and Climate Technology, Department of Civil and Architectural Engineering,
Royal Institute of Technology, KTH
Marinens väg 30, SE-13640 Haninge-Stockholm, Sweden
sture.holmberg@sth.kth.se

Keywords: heat emission, energy efficiency, thermal comfort and health, CFD, exhaust ventilation

SUMMARY

Sustainable energy sources are most often regarded as including renewable sources and usually also technologies that improve energy efficiency. Various techniques which combines heat emission and ventilation air supply have here been used to improve energy efficiency of heat emitters. The idea is to boost convective heat transfer by leading cold ventilation supply air through the heat emission device before it enters the room. As a result, a lower water temperature in the heat emitter is sufficient to provide the required heat output. Decreased supply water temperature to heat emitters results in energy savings in production and distribution of warm water for heating purposes. In heat pumps, for example, the condensation temperature can be lowered, which results in an increased Coefficient of Performance (COP) value. Results of this evaluation show that it is possible to lower the system supply temperature from 55 °C to 45 °C. Two different systems, i.e. a modified ventilation radiator and a thermal baseboard, were evaluated with Computational Fluid Dynamics (CFD) calculations, analytical models and measurements. Correct design parameters are critical for heat transfer conditions but also for the ventilation and thermal comfort conditions in the room. This study shows that combined heat emission and ventilation supply can provide a better overall performance compared to most conventional systems. Thermal radiation from enlarged heat emission surfaces (baseboard) can contribute to decreased room air temperature levels with constant operative temperature (comfort) levels. A lower room air temperature means energy savings both by decreased heat transmission through the building shell and by losses related to outgoing ventilation air. A correlation between sustainability and exergy is discussed in the report as well as the influence of indoor air quality and thermal comfort on health and work productivity.

INTRODUCTION

The primary focus with an ongoing research projects at the division of Fluid and Climate Technology (KTH, Stockholm) is to improve heat emission from different types of hydronic thermal units. The goal is to find heating systems that are able to operate at sufficiently low supply temperature to justify heat pump systems. The lower the supply temperature is the higher the Coefficient of Performance (COP) for the heat pump will be resulting in a more energy efficient and environmental friendly solution. Apart from the energy efficiency good thermal comfort should also be provided for the occupants. Floor heating is by far the most common and investigated system where the thermal energy is distributed at low supply-water temperature. Its large heat emitting surface, the entire floor area, makes it possible to operate at low-temperature supply conditions. In addition to energy savings warm floor areas are popular and thermal comfort conditions are in general acceptable. However, complicated installation work, reported moister problems, restrictions in choosing appropriate floor material and a slow thermal response when using floor heating are reasons enough to try to find alternative low-temperature heating solutions.

It is well-known that forced air movements along a heated plate or inside a heat emitting channel improve heat transfer. By using this technique, the supply flow temperature to the heat emitting unit can be decreased with constant or even increased heat output. Forced convection is therefore used to improve the function of existing heat emitters. Such units are particularly of interest in exhaust ventilated spaces, where the fresh ventilation air is supplied directly from outdoors to the room. By forcing the cold ventilation air between radiator plates or throughout a baseboard heater its thermal output will automatically increase. At the same time a high ventilation rate will be guaranteed with positive effect on health, work productivity and the wellbeing of occupants. Also, strong convection stream form the heat emitting devices can perfectly be used to meet cold draught from windows. By these means a high quality indoor thermal environment can be achieved.

Hydronic supply temperature levels between 55-90 °C are used in Europe [1]. In order to create more sustainable and energy efficient conditions for a heat pump based system, the supply temperature should be lower the 50 °C. Hydronic panel and section radiators are the most common type of thermal units used for heat emission inside buildings. Traditionally, these thermal units are designed to operate at high-temperature supply. For good function at low-temperature water supply a different design should be applied. A ventilation radiator is a combined heat emitter and ventilation supply system with forced heat convection into the room, i.e. higher driving force between radiator panels compared to traditional radiators. Enlarged heat transferring surfaces to improve thermal efficiency can therefore be used. Figure 1 shows the principle of a ventilation radiator. Cold air enters a vent in the building wall, passes trough a wall channel and a filter before entering a channel formed by the radiator panels. Here the air is pre-heated to room air temperature by warm supply water in the radiator. The driving forces of ventilation air are buoyancy forces and pressure differences between outdoors and indoors created by an exhaust ventilation system in the building. The filter prevents contaminants in the incoming air from reaching the indoor environment.

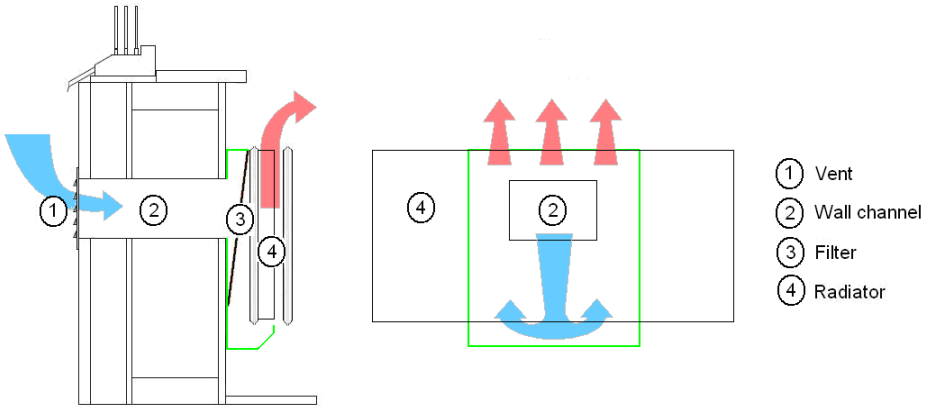

Figure 1. The principle of a ventilation-radiator system. Cross-section below window (left); Front view from the room (right). Blue arrows denote cold inlet air, red arrows warm air entering the room.

Another efficient heat-emitting device is the baseboard radiator. This low profile radiator type is placed just above the floor level along the inner periphery of the room, see Figure 2. A typical baseboard radiator, like the one presented here, is about 150 mm high and 20 mm wide. This heat emitter can also be combined with ventilation air supply as shown in Figure 3. Ventilation supply inlets (below vertical arrows in Figure 3) should be installed underneath glazed surfaces and the rest of the heat-emitting panels along internal walls.

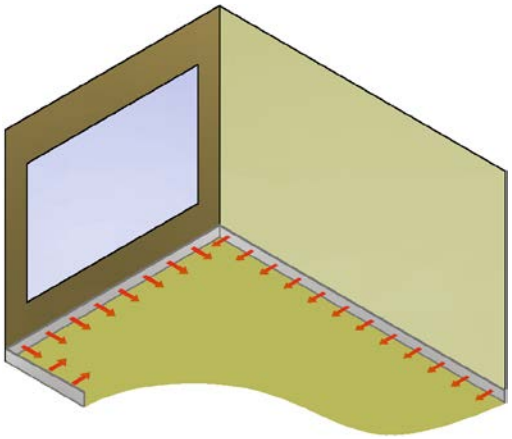

Figure 2. Placement of the baseboard radiators inside the room, [2]

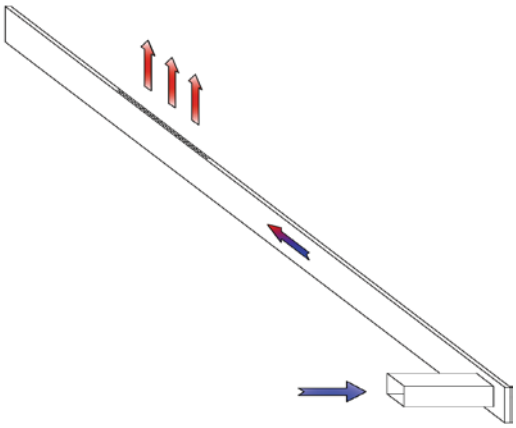

Figure 3. Baseboard radiator with a forced ventilation air flow through the supply channel

Both the ventilation radiator and the baseboard radiator are heat emitters integrated with supply of ventilation air direct from outdoors. The short duct systems used here are easy to keep clean from contaminants. This hygienic aspect is very important and difficult to realize with conventional central air supply duct systems. Both systems are designed to increase ventilation flow and thermal efficiency in buildings. Health conditions and conditions for work productivity are expected to be improved, see Figure 4.

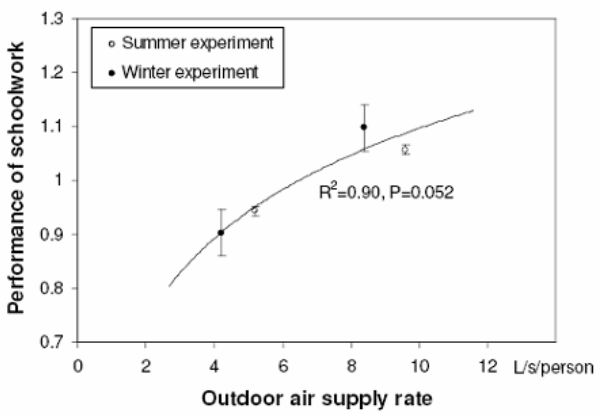

Figure 4. Improved performance of school work with increased ventilation rates, [3]

METHOD OF LOW-TEMPERATURE SYSTEM DEVELOPMENT

Air supply to the room is controlled by an under pressure in the room and buoyancy forces. Heat transfer versus pressure loss through the heat emitter can be controlled in different ways. This is either by variation of heat transferring areas, roughness of the areas or by controlling the speed and turbulence levels in the supply air. An upper limit for forced convection through the heat emitter is set by pressure drop, noise and draught requirements. Design work, research and development still remain to find optimal design parameters for ventilation and baseboard radiator systems.

The main goal with the baseboard radiator study is to evaluate whether the suggested concept is powerful enough to raise the temperature of the incoming ventilation air from – 6 to 21 °C by water supply temperatures lower than 50 °C. The cold supply air is first brought via a duct through the room wall to the baseboard radiator. Then the ventilation air is pre-heated in the horizontal baseboard channel before it enters the room via an opening at the top of the channel. Since the cross section of the baseboard radiator is relatively small the air velocity inside the channel will be high. This will create a turbulent flow and forced convection inside the channel, which will enhance the total heat transfer. Heat transfer between heated channel walls and three different ventilation flows (7.0, 8.5 and 10 l/s) was analytically analyzed. Following well-known Equations (1-2) were used.

$$(\dot{m} \cdot c_P \cdot \Delta\theta)_{water} = (\dot{m} \cdot c_P \cdot \Delta\theta)_{air} = (h_C \cdot A_S \cdot \Delta\theta_m)_{heat\ transfer\ \ water-air} \qquad (1)$$

Where $\dot{m}$, c_p and $\Delta\theta$ symbolize the mass flow rate, specific heat capacity and the temperature difference between inlet and outlet for the air and water side, respectively. While h_C represent the convective heat transfer coefficient inside the channel, A_S channel transmitting surface area, and $\Delta\theta_m$, the logarithmic mean temperature difference between water and air side.

$$Nu = \frac{h_C \cdot D_H}{\lambda_{air}} = \frac{(f/8) \cdot \mathrm{Re} \cdot \mathrm{Pr}}{1.07 + 12.7 \cdot \sqrt{(f/8)} \cdot (\mathrm{Pr}^{2/3} - 1)} \cdot \left[1 + \left(\frac{D_H}{L}\right)^{2/3}\right] \cdot \left(\frac{T_{MBT}}{T_W}\right)^{3/8} \qquad (2)$$

The temperature dependent properties such as Nusselt number Nu, Reynolds number Re, Prandtl number Pr and air conductivity λ_{air} are evaluated at mean fluid bulk temperature $(\theta_{air,\ inlet} + \theta_{air,\ outlet}) / 2$. The Reynolds number is also calculated using the hydraulic diameter $D_H = 4 \cdot A_C \cdot P^{-1}$, where A_C and P represent cross sectional area and perimeter of the channel.

Above presented Nusselt correlation was develop by Petukhov [4] and is applicable for fully developed turbulent flow for both smooth and rough tubes. This equation is the most used expression for evaluation of forced convective heat transfer inside tubes and channels. The correlation is accurate and reliable over a wide flow range, which is confirmed by many experimental investigations. The equation can be used both for constant wall temperature and constant wall heat flux [5]. The friction inside the channel was predicted by Equation 3:

$$f = \left(1.82 \cdot \log\left(\mathrm{Re}\right) - 1.64\right)^{-2} \qquad (3)$$

This friction factor was also developed by Petukhov and can be applied for friction evaluation of turbulent flows inside smooth tubes and channels. The second part of the Nusselt equation is recommended to be used for more accurate heat transfer prediction inside short ducts. While the third part is used for correction of the temperature variation between wall temperatures T_W and the fluid temperature at the channel centre (mean fluid bulk temperature) T_{MBT}. Temperatures in this ratio are evaluated at thermodynamic (absolute) temperature.

RESULTS

Figures 5 and 6 show how the heat output and pressure loss inside the baseboard channel vary with its length. The diagonal lines in Figure 5 show the variation of the thermal energy produced inside the channel while the horizontal lines illustrate the heat output needed to warm the ventilation air from – 6 to 21 °C. The supply and return water flow temperature levels used here are set to 45 and 40 °C, respectively. Straight lines in the diagrams demonstrate the system performance at 7.0 l/s (2.3 m/s), dashed lines at 8.5 l/s (2.8 m/s) and dash-point-dash lines at 10 l/s (3.3 m/s). The intersection between diagonal and horizontal lines in Figure 5 shows the point where the heat output and demand is in equilibrium. The mean channel length for all three cases that is needed to raise the temperature of ventilation air from – 6 to 21 °C is about 1.45 m. The pressure loss due to friction inside the channel is illustrated in Figure 6 and amounts to about 5.2 Pa for 7.0 l/s, 7.3 Pa for 8.5 l/s and 9.6 Pa for 10 l/s. Although heat transfer inside the baseboard channel increases with higher air velocity, too high air speed levels should be avoided due to rapid increase in pressure loss. This should particularly be noticed in exhaust ventilated spaces were the indoor and outdoor pressure difference (around 10 Pa) is the driving force for the ventilation flow.

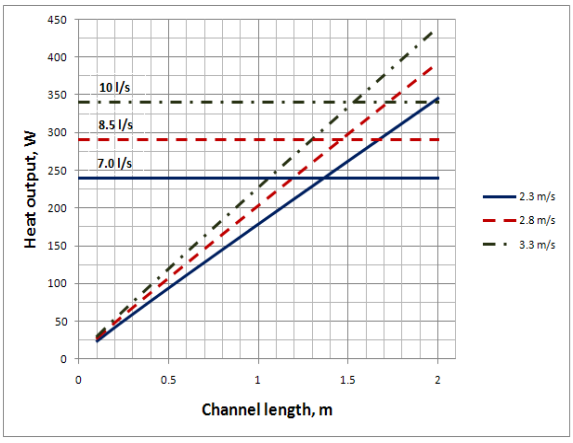

Figure 5. Heat output as function of channel length

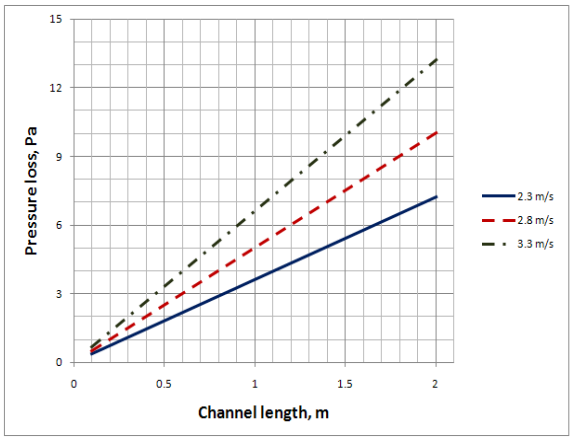

Figure 6. Pressure losses as function of channel length

In the next a study on how to improve the heat gain from an existing ventilation radiator is reported. Results from this study show that heat transfer can be increased in the section where ventilation air is brought into the room by slightly changing the geometry of the fins, decreasing the fin to fin distance and cutting off a middle section of the fin array. This change in internal design could mean considerable increase in thermal efficiency for the ventilation radiator as a whole and allow a lower water inlet temperature in the heating system with an unchanged heat output. The investigations were partly done by Computational Fluid Dynamics (CFD) simulations, while analytical calculations were used for verification of different flow and heat transfer mechanisms. Finally a prototype of a modified ventilation radiator was made and tested in a lab to validate and confirm the results.

Thermal comfort with ventilation radiators was investigated in a previous study by Myhren and Holmberg [6]. Figure 7 shows predicted thermal comfort distribution in a room with a ventilation radiator, a traditional radiator of the same size and a floor heating system (for comparison). Notice that the surface temperature of the ventilation radiator could be set lower than that of the traditional radiator with the same comfort temperature in the middle of the room.

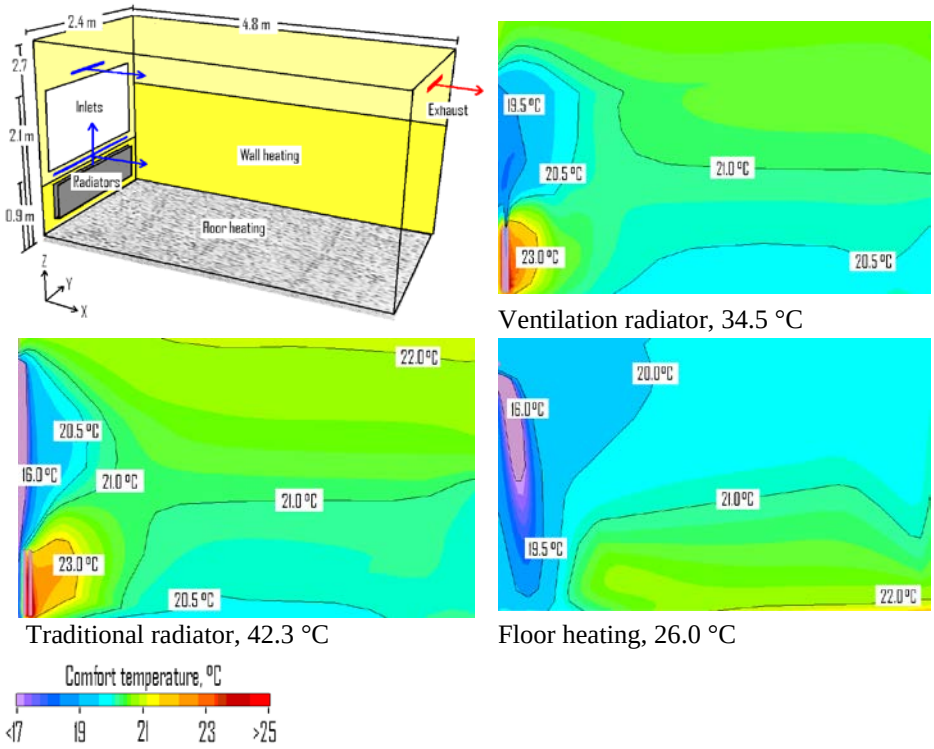

Figure 7. Upper left: room geometries with dimensions, including ventilation openings and positions of heat emitters. Blue lines indicate positions of air inlets and directions of incoming air. Red lines indicate where air was sucked out through the exhaust unit.
Upper right and below: Simulated comfort temperature sections, vertical plane at Y = L/2. Note that the comfort temperature, a measure of the perceived temperature, was the same in the middle of the room in every case.

For additional improvement of thermal efficiency low-temperature heat emitters are recommended to be a part of a heat-pump based heating system. Two examples where a heat pump has been integrated into the heating system design have been investigated by Schmidt [7]. In the first system solution, an electrically driven ground source heat pump was the heat generator and high temperature radiators were the heat emission system. The radiators regarded were designed with a supply temperature of 70 ºC. Because of this unfortunately high temperature level, the heat pump worked with a moderate COP of only 2.5. A better system design used the combination of a heat pump with a low temperature emission system. The same ground source heat pump was coupled with a low temperature floor heating system with a supply temperature of 35 ºC and had, therefore, an increased COP of 4.3. Extraction of heat from the surrounding was now more efficient.

Flow of exergy can be estimated by Equation (4) below [7, 8],

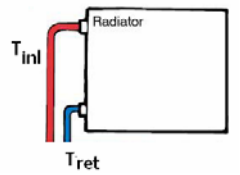

$$\Delta Ex = \frac{P}{(T_{inl} - T_{ret})}\left\{(T_{inl} - T_{ret}) - T_0 \cdot \ln\left(\frac{T_{inl}}{T_{ret}}\right)\right\} \quad (4)$$

where ΔEx, P, T_{inl}, T_{ret} and T_0 are flow of exergy (W), heating power P, inlet, return and outdoor temperatures (K) respectively. By analyzing Equation 4 one can find out that a low-temperature heat emitter is not only an energy efficient choice it also means less generation of exergy than a traditional heating system. This means that the low-temperature system is more environmental friendly and sustainable.

CONCLUSIONS

Based on the results of this study it can be concluded that baseboard radiators and ventilation radiators showed a good ability in combining heat emission with ventilation supply air. Analytical studies confirmed that this technology is capable to heat outside air from – 6 °C to 21 °C using a supply water temperature of 45 °C in a baseboard radiator. To be able to achieve this, the baseboard channel length must be around 1.45 m long. Furthermore, the air velocity inside the channel should not exceed 2.8 m/s due to high pressure loss. Both presented heating systems are able to operate at low temperature levels in the heat emitting system, which makes the combination with heat pumps energy efficient and sustainable. It has been concluded that the surface temperature of a ventilation radiator can be set lower than that of the traditional radiator with the same comfort temperature in the room. In addition to this Boerstra [9] has in a review article identified health advantages with low-temperature heat emission.

REFERENCES

1. Nilsson PE (Editor). Achieving the Desired Indoor Climate. ISBN 91-44-03235-8; 2003, Chapter 9; pp. 468-484
2. Ploskic A, Holmberg S. Heat emission from thermal skirting boards. Journal of Building and Environment 2010;45:1123-1133
3. Wargocki P, Ventilation and performance of school work, Proceedings, International REHVA Conference Clima 2005
4. Petukhov BS. Heat transfer and friction in turbulent pipe flow with variable physical properties. Advanced in Heat Transfer. Academic, New York; 1970, pp. 504-564
5. Sunden B. Värmeöverföring (Heat Transfer). ISBN 91-44-00087-1; 2006, Chapter 9, pp. 182-183.
6. J. A. Myhren, S. Holmberg, Design considerations with ventilation radiators: Comparisons to traditional two-panel radiators, Energy and Buildings 41 (2009), pp. 92–100
7. Schmidt, D, *Design of Low Exergy Buildings Method and a Pre-Design Tool*, International Journal of Low Energy and Sustainable Buildings, Vol. 3, 2003
8. Holmberg S, *Modelling of low-temperature heating systems in buildings*, World Renewable Energy Conference, WREC 2008, 19-25 July, Glasgow, 2008
9. Boerstra A, Veld PO and Eijdems H, The health, safety and comfort advantages of low temperature heating systems: A literature review, Proceedings, Healthy Buildings, 2000

Heat emission from skirting boards – an analytical investigation

Adnan Ploskić and Sture Holmberg

Fluid and Climate Technology, School of Technology and Health, KTH,
Marinens väg 30, SE-13640 Haninge-Stockholm, Sweden
E-mail address: adnan.ploskic@sth.kth.se
Phone number: + 46 - 8 - 790 48 41

Abstract

Thermal insulation of buildings has greatly improved over past decades and thermal power needed to cover heat losses through the building envelope has markedly decreased. This means that powerful heating appliances are not always needed in modern buildings. Low-temperature thermal emitters can often replace conventional heating devices. Different studies have shown that people living in buildings with low-temperature heating systems were very satisfied with ambient indoor conditions. In particular; thermal comfort levels were considered to be higher than in buildings with a traditional heating system. Low-temperature heating systems distribute mainly radiant heat with small temperature differences and minimal air movement. This means less spread of allergens and pollutants in the room air and a healthier indoor environment. The general conclusion from this research is that low-temperature heating systems give not just energy savings but may also improve indoor conditions. A combination of low-temperature heating systems and low-valued energy sources, such as heat pumps, give a higher coefficient of performance (COP). This means an environmentally friendly alternative.

The primary aim of this study was to investigate heat transport through a skirting board. An analytical model for total heat transfer including governing equations and boundary conditions is presented. The goal was also to find out whether L-shaped aluminium skirting convectors were powerful enough to warm up an office room with a large thermal requirement. The skirting convectors consisted of one long supply pipe, and a vertical and horizontal plate attached perpendicularly to each other. These thermal emitters were placed along the inner periphery of the room instead of traditional wooden skirting boards. This study presents comparison of the thermal requirement of an office room and the heat generated from skirting convectors inside the room, at different supply temperatures.

The total heat power needed to cover heat losses through envelope of the office room at an outside temperature of -16 °C was calculated to be about 1390 W. Skirting boards supplied by 55 °C and 35 °C hot water gave a heat output of 2710 W and 1470 W, respectively. This means that the skirting convectors were powerful enough to produce the required thermal power at low supply temperature. General conclusion of this analysis is that the skirting convectors investigated in this study can be used as a low-temperature heating system in office rooms. Furthermore, in modern well-insulated office rooms where thermal requirement is low a horizontal heat emitting plate may not be needed. Low surface temperature makes these emitters suitable for use where safety of children or the elderly is needed. Skirting convectors may also be useful in rooms where wall space is limited.

Keywords: Heat requirement, Heat transfer, Low-temperature heating, Skirting heating, Thermal power

Nomenclature

Latin letters

A_C	Cross-section area	[m^2]
A_j	Wall surface area in office room	[m^2]
$c_{p\ (air)}$	Specific heat capacity of indoor air	[J/(kg·°C)]
h_{plate}	Plate height	[m]
k	Combined heat transfer coefficient	[W/(m^2·°C)]
L	Plate length	[m]
P	Perimeter	[m]
T_x	Plate surface temperature at certain distance from heat source	[K]
T_{RS}	Mean room surfaces temperature	[K]
t_∞	Mean indoor air temperature	[°C]
$Q_{leakage}$	Uncontrolled ventilation flow (leakage)	[m^3/s]
$Q_{ventilation}$	Controlled ventilation flow	[m^3/s]
U_j	Heat transfer coefficient through room envelope	[W/(m^2·°C)]
$\bar{u}$	Mean laminar sub-layer velocity	[m/s]
x	Distance from heat source	[m]

Greek letters

α_C	Convective heat transfer coefficient	[W/(m^2·°C)]
α_R	Radiative heat transfer coefficient	[W/(m^2·K)]
δ	Insulating sub-layer thickness	[m]
ε	Emissivity, 0.9 used in study	[-]
θ_B	Base temperature in crossing between plates	[°C]
θ_{indoor} , θ_∞	Mean indoor air temperature	[°C]
$\theta_{outdoor}$	Mean outdoor air temperature	[°C]
θ_x	Plate surface temperature at certain distance from heat source	[°C]
λ	Thermal conductivity, 220 for aluminum	[W/(m·°C)]
$\rho_{(air)}$	Density of indoor air	[kg/m^3]
σ	Stefan–Boltzmann constant	[W/(m^2·K^4)]
Φ_{calc}	Calculated heat output	[W]
$\Phi_{required}$	Heat requirement of office room	[W]

Introduction

Modern buildings have relatively air-tight construction and are thermally well insulated. This means that thermal power needed to cover heat losses through building envelope has considerably decreased. This also means that powerful radiators or convectors are not always needed in such buildings. Low-temperature heat emitters can now replace conventional heating devices. Different studies have shown that people living in buildings with low-temperature heating systems were very satisfied with ambient indoor conditions. Thermal comfort conditions in particular were considered better than in buildings with a traditional heating system [1]. Low-temperature heating is also beneficial with regard to distribution losses and efficiency of the generated heat [2]. Low-energy heating systems utilize low-valued thermal energy, which can be delivered by sustainable energy sources such as heat pumps [3]. It has been established, both theoretically and in practice, that a combination of low-temperature heating systems and heat pumps give higher coefficient of performance (COP). This is an environmentally friendly alternative and can also lead to lower energy costs for the building owner.

Thermal power from different kinds of heat emitters was analyzed in several separate studies at the Royal Institute of Technology, School of Technology and Health in Stockholm [4-7]. The main focus in these studies was to investigate possibilities of improving thermal efficiency of different heat emitters. Another important goal of ongoing research is to develop hydronic low-temperature heating systems that are powerful enough to cover heat requirements and provide sufficient levels of thermal comfort. Floor, wall and ceiling heating have so far been commonly used in low-energy heating systems. However, sometimes there are reasons to use other solutions. In rooms where the heat requirement varies during the day or where the wall space is a limiting factor, the use of skirting convectors could be appropriate. Skirting convectors are thermal emitters placed along inner periphery of the room instead of traditional wooden skirting boards. The heat transferring unit often consists of one long supply pipe and heat transmitting plates.

Molin (2005) has analytically analyzed performance of radiators in low-temperature system. He concluded that heat transfer with natural convection was higher for low profile heat emitters, especially when supply temperature was decreased from 55 °C to 35 °C. Air flow pattern along a vertical heated plate is affected by several different factors such as air velocity near the plate, its height and surface temperature. When buoyancy-driven air flow rises up along a heat transferring plate it forms an insulating laminar sub-layer. A high plate will result in a ticker insulating sub-layer. In order to increase the convective part of the total heat transfer this sub-layer must be reduced. Figure 1 shows propagation of this sub-layer next to the heated wall. Stålberg (2007) has investigated heat transfer from an L-shaped aluminium skirting board installed in an office. Below presents the results of the study.

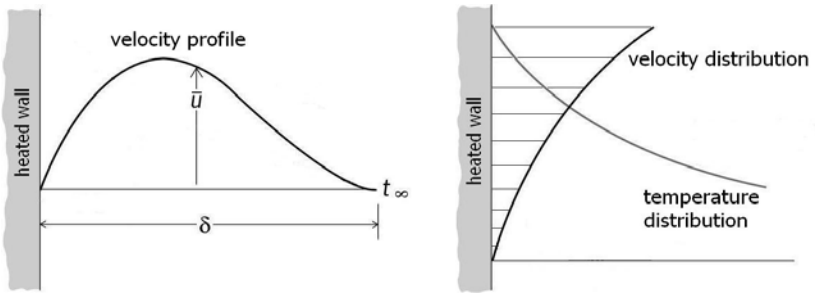

Figure 1. Picture on left side shows velocity profile along a heated wall (plate). Hatched area on right side picture illustrates propagation of insulating sub-layer. This picture also shows velocity and temperature distribution alongside of heated wall.

Aim of study

The goal of this study was to investigate heat transport through a skirting board; in particular to find out whether skirting heating is powerful enough to suit an office room with large thermal requirement, such as winter in northern Sweden. Finally a general discussion on the use of skirting convectors in low-temperature heating system is given.

Method

Description of the office model

Performance of skirting heating was analytically investigated in an office room with dimensions 4.0 m x 3.0 m x 2.4 m. The office room is regarded as an artificial climate chamber. Thus, all external walls are assumed to be exposed to outdoor environment which represents a normal day during winter season in north Sweden. Office model has one wall with two large windows. The main characteristics of the office model are presented in Table 1. A constant air supply flow rate of 4.8 l/s was used for ventilation. The incoming ventilation air had a temperature of - 16 °C which corresponded to outside air temperature. Heat amount required for warming up the office room was calculated using Equation 1.

$$\Phi_{required} = [(\sum U_j \cdot A_j) + (Q_{leakage} \cdot c_{p\,(air)} \cdot \rho_{(air)})] \cdot (\theta_{indoor} - \theta_{outdoor}) + [(Q_{ventilation} \cdot c_{p\,(air)} \cdot \rho_{(air)}) \cdot (\theta_{indoor} - \theta_{outdoor})] \quad (1)$$

Table 1. Mail characteristics of the office room

Enclosing elements	Dimensions [m x m]	Heat transfer coefficient [W/(m²·°C)]	Air supply [ACH]		Properties of indoor air	
Window wall	3.0 x 2.4	0.25	Ventilation	0.5	Density	1.2 kg/m³
Back wall	3.0 x 2.4	0.25	Leakage	0.1	Specific heat	1000 J/(kg·°C)
Side walls	4.0 x 2.4	0.25			Temperature	22 °C
Ceiling	4.0 x 3.0	0.25				
Floor	4.0 x 3.0	0.35				
Window	1.5 x 1.2	2.0				
Door	0.9 x 2.1	0.55				

Heat transfer from a skirting board

The office room was heated by L-shaped (200 mm x 200 mm x 5 mm) aluminium skirting boards that were placed along the inner periphery of the office room. A pipe for heat distribution with circulating warm water was placed in the cross-point between the vertical and horizontal plate segments (skirting panels). Thermal energy carried by supply flow was directly transported to the aluminium plates. Heat was distributed via conduction through both plates and finally was transported by convection and radiation to the indoor air.

Heat conduction through the thin plate is described by second-order ordinary differential equation for $\theta = \theta(x)$.

$$\frac{d^2\theta}{dx^2} - \frac{k \cdot (\theta - \theta_\infty)}{A_C \cdot \lambda} = 0 \qquad (2)$$

The analytical solution of Equation 2 is given by Equation 3.

$$\frac{\theta_X}{\theta_B} = \frac{\cosh\,(\beta \cdot (L - x))}{\cosh\,(\beta \cdot L)}, \qquad \text{where} \qquad \beta = \sqrt{\frac{k \cdot P}{A_C \cdot \lambda}} \qquad (3)$$

From Equation 3, the following expression for thermal power can be deduced. Thermal power was generated by heat emitting skirting plates.

$$\Phi_{calc} = \sqrt{(k \cdot P \cdot \lambda \cdot A_C)} \cdot \theta_B \cdot \tanh\,(\beta \cdot L), \qquad \text{where} \qquad (4)$$

$$k = \alpha_C + \alpha_R \qquad (5)$$

Expression 5 gives the combined of convective and radiative heat transfer coefficient. Expression for convective heat transfer coefficient for the vertical and horizontal plate is given by Equations 6 and 7, respectively. Contribution by radiation is given by Equation 8.

$$\alpha_C = a \cdot \left(\frac{\theta_X - \theta_\infty}{h_{plate}} \right)^n, \qquad \text{where } a = 2.2 \qquad (6)$$

$$\alpha_C = b \cdot \sqrt[3]{\theta_X - \theta_\infty}, \qquad \text{where } b = 1.5 \qquad (7)$$

$$\alpha_R = \varepsilon \cdot \sigma \cdot \left(T_X{}^2 + T^2{}_{RS} \right) \cdot \left(T_X + T_{RS} \right) \qquad (8)$$

The following assumptions were made for analytical calculation of total heat transfer.

- The temperature of the plate edge connected to the pipe was the same as supply flow temperature.
- Heat transmission (losses) through the walls and floor next to the skirting boards was assumed to be zero.
- Plate edges towards the room were regarded as adiabatic.

The governing equations were implicitly solved. The starting point for all calculations was set at the point of intersection of the vertical and horizontal plates. Since the temperature of the skirting boards decreased with distance from the heat source, an average value was calculated. Heat emitting plates were considered as divided into 10 equal parts. For each part a mean value for surface temperature, convective and radiant heat transferring coefficient was calculated. Calculated values were then used for final computation of total heat release to the room. Vertical and horizontal plates were treated separately regarding calculation of total thermal power, but summarized afterwards. Figure 2 shows typical L-shaped skirting panels placed in a room.

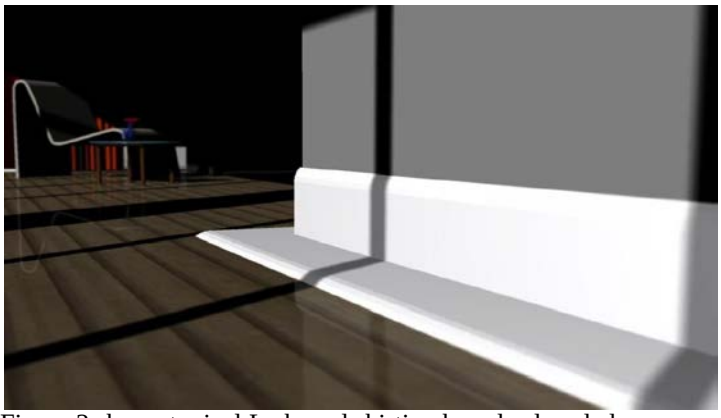

Figure 2 shows typical L-shaped skirting boards placed along inner periphery of an office room.

Result and discussion

The heating power needed for warming up the office room was calculated by Equation 1 and was about 1390 W. Skirting boards heated by 55 °C supply temperature gave a heat output of 2710 W. This means that the skirting boards discharged nearly twice as much heat power that required. This also means that temperature of supply flow could be decreased. After some optimization it was found that a supply temperature of 35 °C gave a heat output of 1470 W. This is clear evidence that the heat emitting skirting boards used in this study could be successfully used in a low-temperature system.

One drawback with L-shaped thermal panels could be limited furnishing of the room, due to the horizontal emitting plate. Further, single-pipe hydronic heating systems often requires more complex technical solutions. However it should be emphasized that these analytical calculations were made for an artificial climate chamber, where all walls were exposed to the outdoor environment. Regardless of this it was still possible to adequately warm the office room using low-temperature supply flow. Usually office rooms are placed with most walls adjacent to other indoor spaces. Thus, the spaces next to, below and above are assumed to have same thermal conditions as those of the room. In modern better sealed and insulated office spaces, heat power needed to cover transmissions losses is about 500 W. This is considerably lower than used in present study. However, heat losses through the outer walls are usually quite small compared to the transmission through windows. Figure 3 presents different heat requirements and outputs as results of this study.

The benefits of using well-insulated glazing units in order to reduce thermal requirements have already been shown in different studies [8-12]. Here it is concluded that these units provide better thermal climate for occupants and may also give energy savings. In some cases by employing well-insulating glazing, heating devices may not even be needed. All this indicates that horizontal heat emitting plate may not be needed in modern well-insulated office rooms. For single-family homes it could be an advantage to install thermal skirting boards for many different reasons. For example, a conversion from electrical to radiator heating could be very costly. A relatively simple and fast installation of hydronic thermal skirting boards may reduce this cost, especially if a heat pump is used as the thermal source. Furthermore, the low surface temperature makes these emitters suitable for use where safety of children or the elderly is needed. Skirting convectors may be also useful in rooms where wall space is limited.

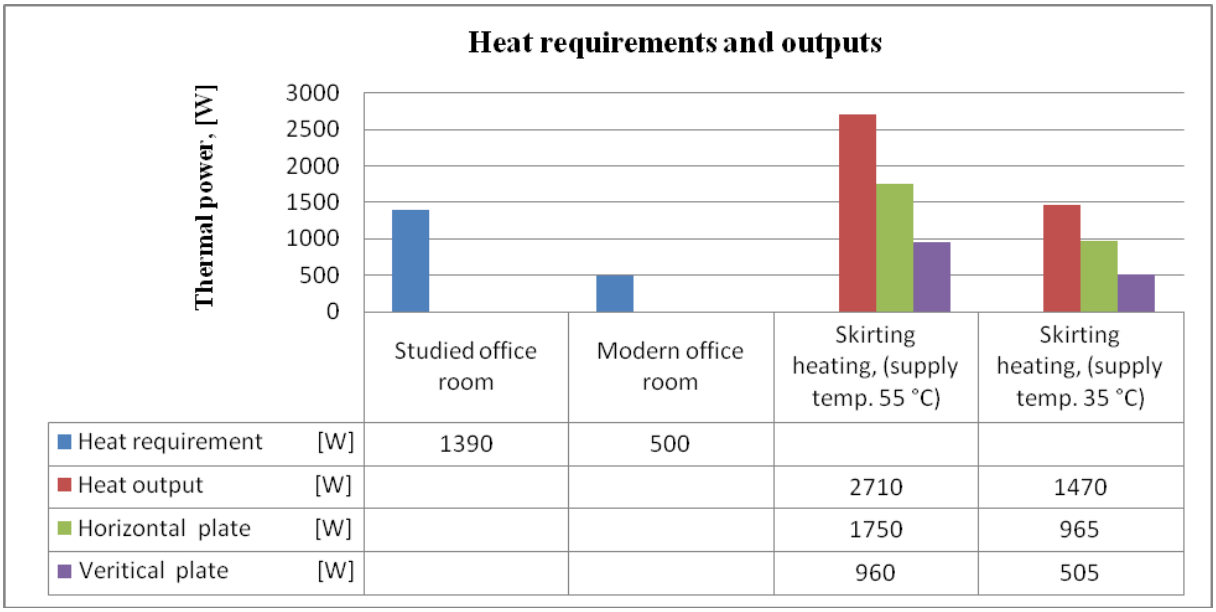

Figure 3. Illustration of different heat outputs and requirements

Future work

This study showed that it is fully possible to heat up an office room using L-shaped skirting panels. The next step is to evaluate how indoor thermal environment is affected by skirting heating. Computational Fluid Dynamics – CFD will be employed to map indoor thermal climate and to optimize heat output from the skirting convectors. Different heating arrangements, including skirting heating, will be compared to each other in a mechanically ventilated office room.

Acknowledgement

Part of this work was done in a project degree work by Andreas Stålberg. His contribution is gratefully acknowledged. Authors also want to acknowledge Dr Heather Robertson for language correction.

Reference

[1] M. A. Juusela (Ed.), Heating and Cooling with Focus on Increased Energy Efficiency and Improved Comfort, Guidebook to IEA ECBCS, Annex 37, (2004)
[2] S. Frederiksen, S. Wener, District Heating – Theory, Technique and Functionality (in Swedish), Studentlitteratur, Lund, (1993)
[3] J. Babiak, B. W. Olesen, D. Petras, Low temperature heating and high temperature cooling, Chapter 6, REHVA Guidebook, (2007)
[4] J. A. Myhren and S. Holmberg, Flow patterns and thermal comfort in a room with panel, floor and wall heating, Energy and Buildings (2007)
[5] J. A. Myhren and S. Holmberg, Design considerations with ventilation-radiators: Comparisons to traditional two-panel radiators, (2008)
[6] F. Molin and S. Holmberg (supervisor), Radiators in low-temperature heating systems, Bachelor project, (in Swedish), Royal Institute of Technology, School of Technology and Health in Stockholm, (2004)
[7] A. Stålberg and S. Holmberg (supervisor), Ledges for building heating, Bachelor project, (in Swedish), Royal Institute of Technology, School of Technology and Health in Stockholm, (2007)
[8] B. Moshfeg and U. Larsson, Experimental investigation of downdraught from well-insulated windows, Energy and Buildings (2002)
[9] B. Moshfeg, U. Larsson, M. Sandberg, Thermal analysis of super insulated windows (numerical and experimental investigations), Energy and Buildings, (1999)
[10] T. Rueegg, V. Dorer, U. Steinemann, Must cold down draughts be compensated when using high insulating windows, Energy and Buildings, (2001)
[11] H. Ge, P. Fazio, Experimental investigation of cold draft induced by two different types of glazing panels in metal curtain walls, Energy and Buildings (2004)
[12] A. Jurelionis and E. Isevicius, CFD predictions of indoor air movement induced by cold window surfaces, Journal of Civil Engineering and Management (2008)
[13] Long A Christopher, Essential Heat transfer, Pearson Education Limited, Edinburgh (1999)
[14] Warfvinge Catarina, HVAC Technique for Civil Engineers, (in Swedish), The Faculty of Engineering at Lund University, (2000)